UNIVERSIDAD DE MURCIA

ESCUELA INTERNACIONAL DE DOCTORADO

TESIS DOCTORAL

Study of accommodation dynamics and defocus fluctuations in the human eye

Estudio de la dinámica de la acomodación y las fluctuaciones del desenfoque en el ojo humano

D. Vahid Pourreza Ghoushchi

2023

UNIVERSIDAD DE MURCIA
ESCUELA INTERNACIONAL DE DOCTORADO

TESIS DOCTORAL

Study of accommodation dynamics and defocus fluctuations in the human eye

Estudio de la dinámica de la acomodación y las fluctuaciones del desenfoque en el ojo humano

Autor: D. Vahid Pourreza Ghoushchi

Director/es: D. Pablo Artal Soriano y Pedro María Prieto Corrales

DECLARACIÓN DE AUTORÍA Y ORIGINALIDAD
DE LA TESIS PRESENTADA PARA OBTENER EL TÍTULO DE DOCTOR
Aprobado por la Comisión General de Doctorado el 19-10-2022

D. Vahid Pourreza Ghoushchi

doctorando del Programa de Doctorado en

Ciencias de la visión

de la Escuela Internacional de Doctorado de la Universidad Murcia, como autor/a de la tesis presentada para la obtención del título de Doctor y titulada:

Study of accommodation dynamics and defocus fluctuations in the human eye

Estudio de la dinámica de la acomodación y las fluctuaciones del desenfoque en el ojo humano

y dirigida por,

D. Pablo Artal Soriano

D. Pedro María Prieto Corrales

DECLARO QUE:

La tesis es una obra original que no infringe los derechos de propiedad intelectual ni los derechos de propiedad industrial u otros, de acuerdo con el ordenamiento jurídico vigente, en particular, la Ley de Propiedad Intelectual (R.D. legislativo 1/1996, de 12 de abril, por el que se aprueba el texto refundido de la Ley de Propiedad Intelectual, modificado por la Ley 2/2019, de 1 de marzo, regularizando, aclarando y armonizando las disposiciones legales vigentes sobre la materia), en particular, las disposiciones referidas al derecho de cita, cuando se han utilizado sus resultados o publicaciones.

> *Si la tesis hubiera sido autorizada como tesis por compendio de publicaciones o incluyese 1 o 2 publicaciones (como prevé el artículo 29.8 del reglamento), declarar que cuenta con:*
> - *La aceptación por escrito de los coautores de las publicaciones de que el doctorando las presente como parte de la tesis.*
> - *En su caso, la renuncia por escrito de los coautores no doctores de dichos trabajos a presentarlos como parte de otras tesis doctorales en la Universidad de Murcia o en cualquier otra universidad.*

Del mismo modo, asumo ante la Universidad cualquier responsabilidad que pudiera derivarse de la autoría o falta de originalidad del contenido de la tesis presentada, en caso de plagio, de conformidad con el ordenamiento jurídico vigente.

En Murcia, a 22 de febrero de 2023

Fdo.: Vahid Pourreza Ghoushchi

Esta DECLARACIÓN DE AUTORÍA Y ORIGINALIDAD debe ser insertada en la primera página de la tesis presentada para la obtención del título de Doctor.

To my parents

Habib and Setareh

Contents

Resumen

El proceso de la visión que finaliza con la sensación de ver algo, es decir, con la percepción de un estímulo visual, comienza con la formación de la imagen del mundo sobre la retina. Esto hace que, aunque pueden surgir múltiples complicaciones a distintos niveles que empeoren la calidad visual, la calidad de la imagen retiniana impone un primer límite físico a nuestra capacidad de distinguir detalles y extraer información de lo que vemos. El desenfoque es la causa más importante y a la vez más común de emborronamiento de la imagen en la retina. Esta borrosidad reduce la calidad de imagen, disminuyendo su resolución y contraste y haciendo que se pierdan detalles. La nitidez de la imagen depende de la interrelación entre la longitud axial del ojo, su potencia óptica y la distancia al objeto. Hasta que se vuelve rígido con la edad, el ojo es capaz de modificar la forma del cristalino para ajustar su potencia óptica, un proceso que se denomina acomodación. De esta forma el sistema visual puede enfocar sobre la retina las imágenes de objetos situados a distintas distancias. Aunque este proceso no es instantáneo, la acomodación es un mecanismo rápido y bastante preciso en la mayoría de los sujetos jóvenes, que da como resultado una visión clara del mundo tridimensional. Sin embargo, se ha sugerido que la aparición y/o progresión de la miopía podría estar relacionada con alteraciones en el proceso acomodativo que podrían alterar el proceso de emetropización.

Por otro lado, incluso cuando se mira fijamente un objeto a una distancia determinada, la potencia óptica del ojo fluctúa de forma más o menos aleatoria. No está claro si esta inestabilidad es un resultado no deseado de la incapacidad del ojo para mantener un enfoque constante o puede ser parte integrante del proceso de acomodación con un propósito concreto, por ejemplo, aumentando la velocidad de respuesta. Sea como fuere, considerando el fenómeno desde un punto de vista óptico, sería de esperar que la imagen retiniana sufriera algún tipo de degradación al verse sometida a una fluctuación de foco, perdiendo nitidez. En esas circunstancias, un tiempo de integración corto podría permitir que el sistema visual percibiera una secuencia instantáneas con distintos niveles de emborronamiento, y que empleara la más nítida para extraer información sobre el objeto, maximizando la calidad visual.

En este contexto, esta tesis estudia los efectos de distintos tipos de variaciones de enfoque, tanto discretas como progresivas, con el objetivo de analizar cómo son manejados por el sistema visual. Para ello se llevaron a cabo dos experimentos separados empleando un sensor Hartmann-Shack (HS) de campo abierto, que mide tanto la refracción como las aberraciones de alto orden de ambos ojos en tiempo real. En primer lugar, se analizó la dinámica de la respuesta acomodativa en condiciones realistas de visión binocular, tanto en sujetos emétropes como miopes, cuando cambiaban su fijación abruptamente de un objeto lejano a otro cercano. Posteriormente, en un segundo experimento estudiamos el efecto sobre la sensibilidad al contraste de oscilaciones rápidas de desenfoque con diferentes amplitudes y frecuencias temporales, generadas con una lente sintonizable acoplada al sistema para este propósito.

En el primer experimento, se midió la dinámica en tiempo real de las tres componentes de la respuesta acomodativa binocular (acomodación, convergencia y miosis pupilar) en emétropes y sujetos con distintos grados de miopía. El aparato empleado, un sensor de frente de onda de campo abierto, se desarrolló en nuestro laboratorio en un trabajo anterior en el que se utilizó para medir sujetos sin error refractivo únicamente. En él se pueden distinguir tres ramas: de iluminación, de medición y de calibración. Como iluminación se emplea luz infrarroja invisible de 1050 nm, de forma que el sujeto no percibe el haz de medida y no le afecta en su tarea visual. El sistema consta de un único sensor HS conjugado con el plano pupilar de ambos ojos a través de periscopios gemelos, con el que es posible medir simultáneamente la dinámica de la acomodación, las aberraciones de alto orden, el tamaño de las pupilas y la convergencia (en forma de distancia interpupilar). Un espejo dicroico de gran tamaño, colocado a 45º de la horizontal, refleja en vertical la luz infrarroja, de forma que el láser de iluminación y el sensor quedan en un nivel inferior y no entorpecen la mirada del sujeto, que tiene una línea de visión despejada a través del espejo, ya que este transmite la luz visible proveniente de los estímulos visuales. En el marco de esta tesis, se construyó una nueva versión de sensor portátil de HS, montado en una placa independiente que se puede desacoplar del sistema para facilitar su calibración, y dotado de una nueva matriz de microlentes de mayor resolución y menor distancia focal, lo que para mejora el rango dinámico del sistema y permite realizar medidas en miopes de más alta graduación. Además, el software de control se actualizó con la incorporación de un paquete de procesado basado en un algoritmo de computación paralizada en una tarjeta gráfica (GPU) de altas prestaciones, lo que permite acelerar el cálculo de

aberraciones, de forma que la dinámica de la acomodación se obtiene en tiempo real y no a posteriori como en la anterior generación de instrumento.

El mecanismo de acomodación no solo conlleva el cambio de potencia óptica del cristalino sino que además incluye una rotación coordinada de los globos oculares para hacer que las líneas de mirada converjan sobre el objeto observado y una reducción del tamaño (miosis) de las pupilas. Existe una extensa literatura sobre estos procesos y sus combinaciones, pero relativamente pocos estudios los miden simultáneamente en visión binocular. Hasta donde sabemos, este es el primer estudio de la dinámica combinada de las tres componentes de la respuesta acomodativa se mide de forma precisa, en tiempo real y en condiciones realistas de observación. Además, se realizaron medidas tanto en miopes como emétropes, con el objeto de analizar las posibles diferencias de comportamiento entre ellos.

En el estudio participaron 18 sujetos jóvenes, con un error refractivo promedio de -2.3 D en un rango de 0 D a -7.5 D, todos ellos con valores de cilindro por debajo de 2 D. Con su mejor corrección, que portaron durante las medidas en caso necesario, todos los sujetos alcanzaron una agudeza visual decimal por encima de la unidad y ninguno presentó antecedentes de enfermedades oculares o problemas visuales. Tanto el estímulo cercano, ubicado a 2.8 D, como el lejano, a 0.36 D, consistieron en cruces de Malta negras sobre un fondo blanco, con una anchura angular de 1.3° en ambos casos. Cada sujeto se sometió a 3 ciclos de 6 cambios de distancia de fijación (lejos-cerca-lejos-cerca-lejos-cerca). Para el análisis de datos se empleó un método de umbralización consistente determinar los instantes en los que se alcanza el 10% y se supera el 90% del rango de variación entre los estados inicial y final para cada variable estudiada. A partir de los datos experimentales se calcularon varios parámetros relacionados con el cambio de fijación de lejos a cerca, incluyendo las amplitudes de acomodación, convergencia y miosis pupilar, las duraciones de estos tres procesos y sus velocidades medias, el retraso acomodativo, el RMS total de las aberraciones de alto orden y la magnitud de la aberración esférica, y se analizaron los coeficientes de correlación de todas estas variables con el error refractivo y con la velocidad de acomodación.

El análisis de correlación de la refracción (en forma de equivalente esférico) con los parámetros dinámicos de la respuesta acomodativa sugiere que la miopía afecta levemente o se ve afectada por la acomodación. Se encontró una relación de proporcionalidad entre el retraso acomodativo y el error refractivo (R = -0.57, p = 0.01), así como una correlación apreciable entre la velocidad de constricción pupilar y la refracción del sujeto (R = -0.49, p = 0.04), en ambos casos con

valores de p por debajo de 0.05. En otras palabras, la acomodación en los miopes parece tender a ser menos precisa y la contracción de su pupila a ser más lenta. Los coeficientes de correlación entre el equivalente esférico y el resto de parámetros relacionados con la respuesta acomodativa fueron en general pequeños, con valores de p muy por encima de 0.05. Por otro lado, se encontró una correlación sustancial, con valor de p bajo, entre la velocidad de acomodación y la velocidad de convergencia (R = 0.48, p = 0.04), una asociación que no hemos encontrado mencionada en la literatura previa. Y todavía más fuerte fue la correlación la velocidad de acomodación y la duración de la convergencia (R = 0.57, p = 0.01), lo que puede reflejar las diferencias entre las dinámicas de estos dos procesos. Además, parece haber una correlación entre la velocidad de acomodación y la amplitud de la miosis pupilar, ya que el valor de p fue inferior a 0.05 (R = 0.47, p = 0.049). En resumen, el análisis de correlación de la velocidad de acomodación sugiere que una acomodación lenta puede estar asociada a una convergencia lente y a una constricción pupilar más evidente.

Para la segunda parte de esta tesis se construyó un sensor HS más rápido, con una frecuencia de actualización de 60 Hz, y con mayor sensibilidad a la luz infrarroja de 1050 nm de longitud de onda. Este sensor se empleó para caracterizar una lente sintonizable, no solo para la producción en modo estático de valores fijos de desenfoque sino también, por primera vez que sepamos, en modo dinámico para la generación de variaciones sinusoidales de desenfoque. Después de la calibración, la lente sintonizable se utilizó para provocar oscilaciones periódicas de desenfoque, de distintas amplitudes y frecuencias, a 5 jóvenes emétropes mientras realizaban una tarea de sensibilidad al contraste. Todos los sujetos alcanzaron agudeza visual unidad o mejor y carecían de antecedentes de problemas visuales. El estímulo visual fue un test de Gabor de 1º de diámetro angular y una frecuencia espacial de 12 c/grado, ubicado a 3 m de distancia del observador. Las franjas se inclinaron aleatoriamente 10º hacia la izquierda o la derecha de la vertical y se utilizó un protocolo de elección forzada de dos opciones para determinar el umbral de contraste para cada condición de oscilación. Las medidas se tomaron monocularmente con el ojo derecho. En total se estudiaron 24 casos de fluctuación sinusoidal de desenfoque presentados en orden aleatorio, correspondientes a las combinaciones de 3 frecuencias temporales (5, 15 y 25 Hz) y 8 valores de pico-valle de desenfoque entre un mínimo de 0,15 D y 3 D de máximo. No se ha encontrado literatura previa analizando el efecto de este tipo de fluctuaciones rápidas de desenfoque en la calidad visual.

Los resultados de este estudio indican que la calidad visual, cuantificada mediante el umbral de contraste, es resistente a las oscilaciones de desenfoque inducidas. Solo se encontró una

reducción notable de la sensibilidad al contraste para las variaciones más grandes y rápidas (25 Hz, ± 1,5 D) consideradas. Este hecho se puede tomar como una indicación de que el ojo humano solo necesita que la imagen retiniana esté enfocada durante un periodo corto de tiempo para poder percibir claramente los estímulos visuales.

Como complemento a las medidas experimentales, en la última sección de esta tesis se desarrolló un modelo cuantitativo para predecir el deterioro en la calidad de imagen retiniana que puede producir una fluctuación periódica de desenfoque. Para las amplitudes y frecuencias de oscilación utilizadas en el experimento, se calculó la PSF promedio para varios tiempos de integración. A partir de ellas se evaluó la MTF compuesta para 12 c/grado y se comparó con la MTF limitada por difracción a dicha frecuencia, con el objeto de determinar la pérdida de modulación inducida por las variaciones de enfoque. La comparación entre los resultados experimentales y los datos simulados sugiere que el ojo puede estar integrando el emborronamiento causado por desenfoque en intervalos de 10 a 20 ms, y que una instantánea más o menos enfocada en una secuencia muy emborronada resulta suficiente para que el sistema visual extraiga información relevante para percibir el estímulo.

Summary

The quality of the retinal image is the first, physical limiting factor of visual quality. Defocus is the most common source of blur leading to retinal image quality loss. It depends on the interrelationship between the eye's axial length, optical power, and distance to the object. Until it is lost with age, the eye has the ability to modify its optical power (i.e., to accommodate) to produce focused retinal images. Although this process is not instantaneous, accommodation is a fast and fairly accurate mechanism in most young subjects, that results in a clear vision. However, it has been suggested that myopia onset and/or progression may be related to alterations in the accommodative process that could upset the emmetropization process.

On the other hand, even when steadily looking at an object at a fixed distance, the optical power of the eye fluctuates more or less randomly. It is unclear if this fluctuation is an undesired inability of the eye to keep a constant focus or may serve a purpose in the accommodative process. In any case, from an optical point of view, fast fluctuations of defocus would be expected to produce some kind of blurring in the retinal images. In those circumstances, a short integration time may allow the visual system to select the best focused position in the sequence to maximize visual quality.

In this context, this thesis studies the effects of changes in focus, both discrete and progressive, aiming to discern how the visual system copes with them. Two separate experiments were carried out with an open-view Hartmann-Shack sensor measuring refraction and high-order aberrations in real time. First, the dynamics of the accommodative response was analyzed in realistic binocular viewing conditions, both for emmetropic subjects and myopes, when the fixation abruptly changed from far to near. In a second experiment, we studied the effect on contrast sensitivity of fast oscillations of defocus with different magnitudes and temporal frequencies, generated with a tunable lens attached to the system.

In the first experiment, the real-time evolution of the three components of the binocular near response (accommodation, convergence, and pupil miosis) was measured in emmetropes and myopes. The apparatus employed was previously reported and used to measure emmetropic subjects. Three branches can be distinguished in the system: illumination, measurement, and calibration arms. Invisible, 1050 nm light was used for illumination. The single HS sensor was conjugated with both eyes' pupil planes through twin periscopes for simultaneous measurement of the dynamics of accommodation, aberrations, pupil sizes, and convergence (quantified by interpupillary distance). A large dichroic mirror pointing downwards shuttles the infrared beams for illumination and sensing from and to a lower level where the sensor is positioned while transmitting the visible light to allow the subject an open view of the field in front. For this thesis, a new portable HS sensor was developed with a new microlens array (lenslet pitch = 192 µm, focal length = 3.17 mm) to improve the dynamic range of the system in order to measure higher myopes. Also, a previously developed software package using GPU computation was successfully implemented into the system, allowing the HS sensor to measure the accommodation dynamics in real time with no need for post-processing.

During the accommodation mechanism, convergence of the eyeballs and miosis of the pupils accompany the change in optical power of the crystalline lens. There is extensive literature on these processes but relatively few studies simultaneously measuring all three of them in binocular vision. To the best of our knowledge, this is the first study of their combined dynamics in real time under realistic viewing conditions. Furthermore, it was performed in both myopic and emmetropic young individuals.

Eighteen young subjects participated in the first experiment, with an average refractive error of -2.3 D and a range from -7.5 D to 0 D. Cylinder was below 2 D in all cases. Excluding refractive errors, no subject had a history of visual problems and all of them reached 20/20 VA or better in both eyes. They were corrected during the measurements. The near stimulus, located at 2.8 D, and far target, at 0.36 D, were both black-on-white Maltese crosses with 1.3° width. Each subject underwent 3 cycles of 6 target switching (far-near-far-near-far-near). The data was analyzed with a threshold method consisting of calculating the initial and final states for each studied variable and considering the central 80% of the variation. Several far-to-near response parameters were calculated, including accommodation speed and amplitude, convergence speed and amplitude, pupil miosis speed, and amplitude, high-order aberration

xix

RMS, spherical aberration, lag of accommodation, and duration of accommodation, convergence, and pupil miosis. Correlation analysis between refractive error and accommodation speed and of these two variables with various far-to-near response parameters was performed.

The correlation analysis of refraction (spherical equivalent, SE) with accommodation dynamics parameters suggests that myopia mildly affects or is affected by accommodation. The lag of accommodation was found to be linked to refractive error (R = -0.57, p = 0.01). Moreover, the correlation between miosis speed and refractive error also had a p-value below 0.05 (R = -0.49, p = 0.04). In other words, myopes may tend to have less precise accommodation and slower pupil constriction. The correlation coefficients between SE and the rest of accommodation-related parameters were small, with p-values well above 0.05. A substantial, low-p-value correlation was found between accommodation speed and convergence speed (R = 0.48, p = 0.04). To the best of our knowledge, this finding has not been previously reported. Furthermore, the correlation was stronger between accommodation speed and convergence duration (R = 0.57, p = 0.01), which may reflect the differences in the dynamics of these two processes. In addition, there may be a correlation between accommodation speed and miosis amplitude since the p-value was below 0.05 (R = 0.47, p = 0.049). These analyses showed that slower accommodation might be a function of slow convergence and more evident pupil miosis.

For the second part of the thesis, a faster HS sensor with a refresh rate of 60 Hz and higher sensitivity to 1050 nm IR light was developed. This sensor was employed to characterize an optically tunable lens both in the typical static mode and, for the first time to our knowledge, in dynamic mode. After calibration, the tunable lens was used to apply defocus oscillations during contrast sensitivity measurements. Different amplitudes and frequencies were induced in 5 young emmetropes with 20/20 or better VA and no previous history of visual troubles. The visual stimulus was a 12 c/deg Gabor patch of 1° angular diameter located at 3 m. It was tilted 10 degrees left or right and a two-choice forced-choice protocol was used to determine the contrast threshold for each oscillation condition. The measurements were carried out in monocular mode, and the subjects viewed the stimulus through the tunable lens with their right eye. The sinusoidal waves induced included combinations of 3 temporal frequencies, 5, 15, and 25 Hz, and 8 peak-to-valley defocus values, ranging from 0.15 to 3 D, presented in fully random

order. To the best of our knowledge, the effect of this kind of fast fluctuations of defocus on visual quality has not been previously studied.

Visual performance, in the form of contrast threshold, was found resilient to induced defocus oscillations. The data showed that only for fast, large variations (25 Hz, ± 1.5 D), there was a noticeable reduction in contrast sensitivity. This indicates that for the eye to clearly perceive visual stimuli, the retinal image only needs to be in focus for a short time.

A quantitative model was developed for predicting the deterioration in retinal image quality due to periodic defocus fluctuations. For the amplitudes and frequencies of oscillation used in the experiment, the average PSF was calculated for several integration times and the loss in the ensuing MTF was computed. Comparison between experimental results and simulated data suggests that the eye may be integrating defocus blur at 10 to 20 ms intervals.

List of abbreviations

HS	Hartmann-Shack
WA	Wave aberration
PSF	Point spread function
MTF	Modulation transfer function
CSF	Contrast transfer function
VA	Visual acuity
AMF	Accommodation microfluctuations
RMS	Root mean square
SE	Spherical equivalent
CYL	Cylinder
HOA	High-order aberration
AR	Augmented reality
VR	Virtual reality
FOV	Field of view
OTF	Optical transfer function
ACT	Adjustment contrast threshold
ISO	International Organization for Standardization
ANSI	American national standards institute
SCT	Subjective contrast threshold
Cpd	Cycles per degree
IPD	Interpupillary distance
OS	Oculus sinister, left eye
OD	Oculus dexter, right eye
AE	Artificial eye
GPU	Graphical processing unit

"We should not overthink. The moment we start to move our fear will disappear."

Samad Behrangi, The little black fish

Chapter 1

"Life is not easy for any of us. But what of that? We must have perseverance and above all confidence in ourselves. We must believe that we are gifted for something and that this thing must be attained."

Marie Curie

Chapter 1.   Introduction

This thesis studies the effects of changes in focus, both discrete and progressive, aiming to discern how the visual system reacts to them. In the first experiment, the dynamics of the accommodation response were analyzed under realistic binocular conditions, both for emmetropic and myopic subjects, when the fixation target abruptly moved from far to near. Later, we studied the effect on contrast sensitivity of fast oscillations of defocus with different magnitudes and at diverse temporal frequencies.

The open-view optical setup and the algorithm for HS image processing were previously reported [Chirre et al., 2014; Prieto et al., 2000]. However, the system has been improved both computationally and optically for this study [Ghoushchi et al., 2021; Mompeán et al., 2019]. We investigated the relationship between refractive error and accommodation speed with various far-to-near response parameters and provided a novel correlation analysis. In addition, a new 60 Hz HS sensor, was developed for real-time measurements of the ocular aberrations. This sensor was utilized to calibrate a focus tunable lens to introduce defocus both in static and dynamic modes. By inducing rapid periodic defocus oscillations, we tested the human eye's contrast sensitivity with an unstable retinal image [Ghoushchi et al., 2022]. To the best of our knowledge, the effect of rapid defocus oscillation on contrast sensitivity is explored experimentally and theoretically for the first time. Parts of this thesis were conducted within the MYFUN (Myopia Fundamental Understanding Needed) [MYFUN, n.d.] Marie Curie network. This comprised fourteen early-stage researchers from seven universities and research centers in Europe in order to gain new insights into myopia development and onset.

In this chapter, some history of vision science is covered, and the human eye's anatomy is described. The aberration theory, high-order-aberrations (HOA), and Hartmann-Shack aberrometry are also presented. The ocular accommodation's theory, anatomy, and cues are explained. The binocular vision, convergence, and pupillary response are briefed. An overview of refractive errors and their effects on our vision and the myopia epidemic is discussed. Finally, the contrast sensitivity function and its measuring methods are presented.

1.1. A brief history

The visual system is the most important sensory system for obtaining information about the surrounding world. Humans use their vision to search for food and defend themselves; therefore, it has played a vital role since ancient times. Ophthalmology is one of the oldest practices, dating back to 4270 years. The oldest record about the vision science is the Babylonian code of Hammurabi, King of Babylon in 2250 BC [Prince, 1904] (*Figure 1.1*). The code mentions "a surgeon who saves an eye would be awarded ten shekels of money". In Ancient Egypt, medical practices concerning eye care were documented in Eber Papyrus [Major, 1930]. This was the first known ophthalmology document in which, over nine pages, they discussed the eye and related diseases like staphyloma, cataract, pterygium, and trichiasis in detail.

Figure 1.1. *The code of Hammurabi is the oldest record of vision science (Image adapted from [Randall S. Barton, n.d.]).*

In ancient Greece, eye care was a main concern, but the theory of visual perception was a controversial issue among philosophers and physicians. In the sixth century B.C., Alcmaeon of Croton was the first physician to study the eye and claim that it has two layers. [Retief et al., 2008]. In his model, the inner layer consisted of the pupil containing liquid in the center, and the outer layer included the cornea and sclera. In the Hippocratic Corpus [Craik, 2014] which refers to a work of sixty ancient Greek physicians collected by Hippocrates II (460 BC–370 BC) the eye was thought to have three layers: a thick outer layer, a middle layer, and a fragile inner layer that is the thinnest and most vulnerable to damage. In the fourth century B.C. Plato (428 BC–347 BC) and later Theophrastus (371 BC-287 BC) believed in emission or extramission theory (*Figure 1.2*), which claimed that visual perception is due to some rays emitted from the eye that shine on the objects [Reymond, 1927]. However, Aristotle (384 BC–322 BC) supported the intromission theory [Finger, 1994]. On the contrary, the intromission theory postulated that the eye sees objects because of the light rays emanating from them, not from the eye.

In Roman times one of the first thorough manuscripts about the eye was written by Aulus Cornelius Celsus (5 BC–50 AD), who was the first to describe cataract surgery. [Bieganowski, 2004]. In his work "De Medicina," which was part of a wider encyclopedia, Celsus compiled all the ancient Greek physicians' knowledge; he described ocular pathologies, eye physiology, and ophthalmic treatments. Galen (129–216), a pioneer physician and surgeon in the Roman Empire in the second century A.D., adhered to the extramission theory [King, 1969]. He thought this theory was well aligned with his belief in spirituality, in which the rays come from the brain through hollow optical nerves and pass through the crystalline lens. Galen provided much information regarding the physiology and anatomy of the eye, such as the cornea, iris, retina, crystalline lens, aqueous humor, vitreous humor, and uvea. He performed cataract surgery and attempted to remove the crystalline lens [Keele, 1963] which he thought was the primary part of the vision and located in the center of the eye [Leffler et al., 2016].

Figure 1.2. The concept of the emission theory is depicted in"System der visuellen Wahrnehmung beim Menschen" (1687)" (Image adapted from [Wikipedia, n.d.]).

Muslims excelled in philosophy, optics, astronomy, and medicine throughout the Islamic Golden Age, which lasted from the eighth to the fourteenth centuries [Renima et al., 2016]. In this era, oculists were highly respected in Muslim culture. Hunayn ibn Ishaq, also known as Johannite, was a renowned ophthalmologist and surgeon who translated Greek medical manuscripts and authored numerous innovative works in a variety of fields. His book "Ten Treatises on the Eye" was one of the earliest texts taught in medical schools, in which he methodically covered the eye's anatomy, abnormalities, diseases, cures, and surgical

procedures. One of the legends of that era was Ibn al-Haytham (or Alhazen), who lived in the 10th century in Iraq and is regarded by some as the father of modern optics [Tbakhi & Amr, 2007]. The year 2015 has been named the International Year of Light [Unesco, n.d.] in memory of the 1000th anniversary of his masterwork "Book of Optic" (i.e. Kitab al-Manazir in Arabic) (*Figure 1.3*). In his book, Ibn al-Haytham was the first scholar who scientifically explained that vision was due to the reflection of light rays from objects that later enter the eyes [Adamson, 2016] and due to the subjective experience, the final image was perceived in the brain. [Baker, 2012].
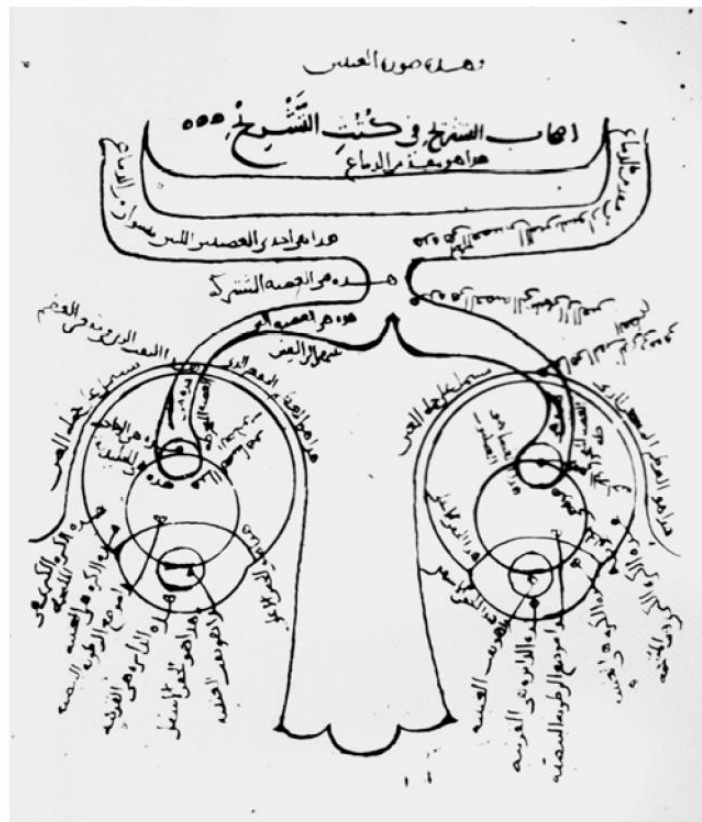

Figure 1.3. *The visual system described by Ibn al-Haytham from a copy of his book titled "Book of Optic" (i.e. Kitab al-Manazir in Arabic) at Süleymaniye Library, Istanbul (image adapted from [Falco, 2007]).*

Another important figure whose writings influenced many scientists and physicians was the 11th-century Iranian physician Avicenna, or Ibn Sina. In his book "The Canon of Medicine," he covered a wide range of topics, including ophthalmology. He performed cataract surgery and claimed that cataracts can be treated in their early stages, offering a variety of medications to alleviate the condition [Nejabat et al., 2012]. He followed many of Galen's practices, such as the idea that optic nerves are hollow ducts or that crystalline lenses are the primary part of the vision, but he adhered to Aristotle's intromission theory.

Ibn al-Haytham's works, in which he described the function of lenses, were translated in Europe from Arabic to Latin and provided the seed for the invention of eyeglasses. It is debatable who invented the first spectacles, as they were used by Italian monks and Chinese people in the 13th century. However, Roger Bacon (1214–1294) was the first person to write about correcting old people's vision by employing convex lenses in 1268 [Rosen, 1956]. In the 14th century using spectacles became popular and northern Italy was the lens making center in Europe.

Leonardo da Vinci (1452–1519), the great inventor, scientist, and artist of the 15th century, was fascinated by light and visual perception during the Renaissance. He first supported the extramission theory of vision but later reversed it to intromission. Leonardo sketched a drawing of the crystalline lens in the center of the eye and was the first person to compare the eye with a pinhole camera, "camera obscura," which has been used for centuries to model the human eye [Berggren, 2001]. His most ambitious plan was to construct an artificial eye using a water-filled glass globe with a tiny lens attached to a box placed above the person's head (*Figure 1.4*).

Achillini (1463–1512) disputed the crystalline lens's role as the principal component of the visual system [Tombran-Tink & Barnstable, 2007] and Andreas Vesalius in the 16th century rejected the notion that optic nerves were hollow ducts and suggested the retina's role as the "the seat of vision". Later, anatomist and medical professor at the University of Basel Felix Platter (1536-1614) developed theories about vision based on his observations of a posterior vitreous detachment in his left eye and a patient with a cranial tumor that crushed the optical nerves and caused blindness. He was the first physician to suggest the pure optical function of the crystalline lens, describe the retina as a sensor in the eye, and attribute the primary function of vision to optical nerves. [Koelbing, 1990].

The precise location of the crystalline lens remained unknown until 1600 when Hieronymus Fabricius (1533–1619) discovered that the crystalline lens was positioned after the pupil in the eyeball. The German astrophysicist Kepler (1571–1630) was the first scientist to clearly propose that the retina is at the image plane in the eye in 1604 [A. Mark Smith, n.d.]. He postulated that the light is guided by the pupil, and reaches the crystalline lens, i.e., a convex lens, and the inverted images of the objects were formed on the retina, reinforcing the "camera obscura" concept.
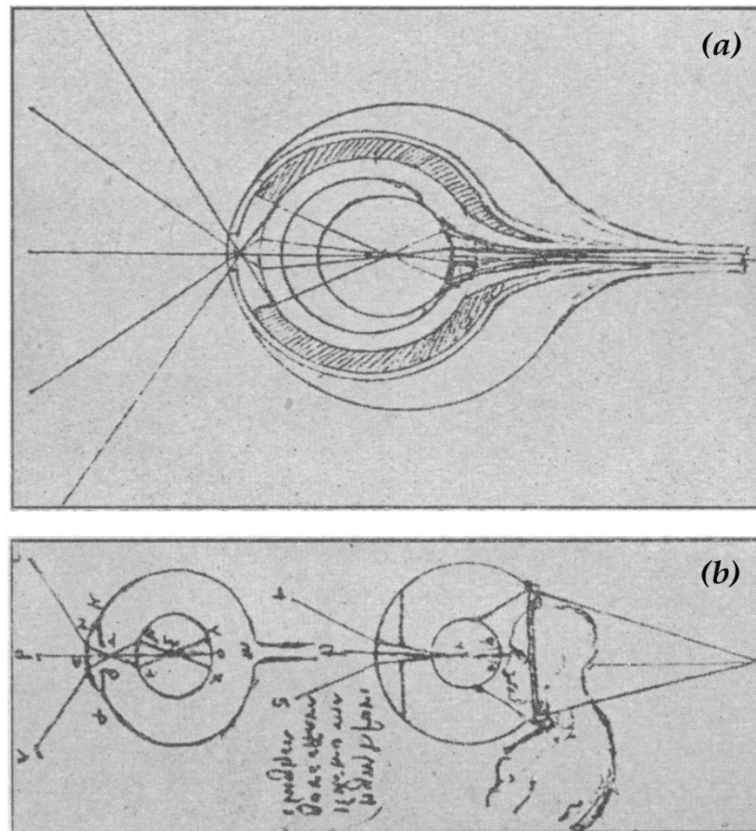
Figure 1.4. *The schematics of the eye by Leonardo Da Vinci, a) Light enters the eye two times first in the pupil and later in the crystalline lens, circle in the middle, and then the final image forms in the optic nerve b) Da Vinci's futuristic artificial eye experiment (Figure adapted from* [Keele, 1955]*).*

In 1637, Descartes published "La Dioptrique," in which he explained Snell's law of refraction for the first time. He also noticed the change in the curvature of the crystalline lens during accommodation [Atchison et al., 2000]. Later, Christian Huygens (1629-95) developed the first actual eye model. Sir Isaac Newton (1642–1727), conducted his famous prism experiment and found that white light is composed of distinct colors. Therefore, the refraction of light depends on wavelength, with the first refracted wavelength being blue and the last being red which explains the chromatic aberration (*Figure 1.5).*

During this era, the publications of two scientists had a significant impact on the understanding of ocular anatomy and ophthalmology. George Bartisch (1535–1607), widely regarded as a pioneer of modern ophthalmology, wrote his groundbreaking book titled "Ophthalmodouleia," in which he discussed eye illnesses, ophthalmological surgery, and instruments, in 1583. The other trailblazing book in eye anatomy was written by German anatomist Johann Gottfried Zinn (1727–1759), who is considered the father of ocular anatomy [Tower, 1956]. In his book, "Descriptio anatomica oculi humani," he provided a detailed and comprehensive description of

ocular anatomy and the layer-by-layer structure of the eye. As a result of his significant contributions, many ocular structures are named after him, e.g., the annulus of Zinn, the zonule of Zinn, and the circle of Zinn.

Figure 1.5. *Isaac Newton's prism experiment (Image adapted from [Biographyonline.net, n.d.]).*

There were many great inventions in vision science during the 1800s, which are regarded as the "golden age" of ophthalmology. In 1801, Tomas Young (1773-1829) in his paper, "mechanism of the eye" discussed many topics about ocular optics [Young, 1801]. He investigated the accommodation and postulated that the source of accommodation is the change in the crystalline lens, not the axial length of the eye or the shape of the cornea (*Figure 1.6*) [Atchison & Charman, 2010]. He designed an optometer to measure refraction and noticed astigmatism in his eye. He also reported some optical values, which correspond to modern values, such as the refractive index of water and lens, which were 1.333 and 1.44, respectively. [Atchison et al., 2000].

Moser was the first to develop a schematic eye in 1844, but his model was hypermetropic due to the extremely low refractive index of the lens. Listing is known for developing the first "precise" schematic eye. In 1851, he described a schematic eye with three refracting surfaces,
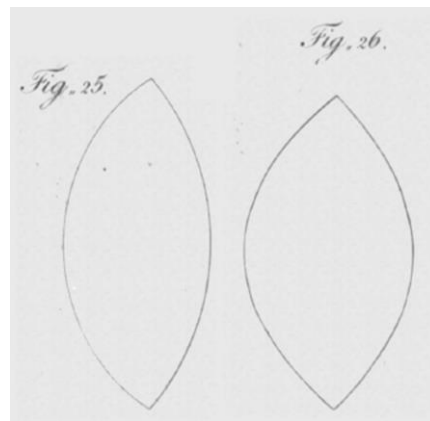
Figure 1.6. Thomas Young's drawings of unaccommodated (left) and accommodated crystalline lens (right) (The image adapted from [Atchison & Charman, 2010]).

a single-surface cornea, a uniform lens, and so small aperture stop in front of the lens [Atchison et al., 2000]. Helmholtz (1821–1894) proposed a model for ocular accommodation, which is the most accepted theory for ocular accommodation and will be discussed in detail in the accommodation section [Bharadwaj, 2017]. He invented the direct ophthalmoscope in 1851 [Keeler, 2002] (*Figure 1.7*) and altered the positions of the crystalline lens surfaces on Listing's model [Atchison et al., 2000]. In 1862, the Dutch ophthalmologist Hernan Snellen developed a chart named after him, the "Snellen chart," He employed optotypes in the chart, which soon became the standard method for measuring visual acuity (VA).

Figure 1.7. The early model of the direct ophthalmoscope was invented by Helmholtz in 1851 (Image adapted from [Keeler, 2002]).

In the modern age, there have been many advances in ophthalmology and vision science including the first corneal transplant in 1905, the invention of the slit lamp in 1911 [Gellrich, 2014], the first cataract surgery utilizing intraocular lenses by Harold Ridley [Apple & Sims, 1996; Ridley, 1952], laser-assisted in situ keratomileusis (LASIK) surgery in 1989 by Gholam A. Peyman [Alió & El Bahrawy, 2017; Reinstein et al., 2012], and invention of Optical

Coherence Tomography (OCT), based on low-coherence interferometry [Fercher et al., 2003; D. Huang et al., 1991].

1.2. The human eye anatomy

The human eye is an exceptional visual detector with unique characteristics. As was discussed in detail in the previous section, throughout history, our knowledge of the human eye's optics, morphology, and image perception got deeper thanks to a great deal of effort by physicists, physicians, ophthalmologists, and psychologists. Recently, with advancements in technology, we have a much better understanding of the eye's interior structure (*Figure 1.8*). The eye consists of three distinct layers: the outer fibrous layer, the middle vascular layer (uvea), and the inner nervous layer (retina) [Atchison et al., 2000].

The eye can be divided into anterior and posterior segments. The anterior segment of the eye is the frontmost part of the eye and includes the cornea, aqueous humor, iris, a portion of the ciliary body, and the crystalline lens. The posterior segment, which comprises approximately 66% of the eyeball, borders the rear portion of the crystalline lens. It contains the vitreous humor, retina, choroid, and optic nerve [Choh & Sivak, 2017].
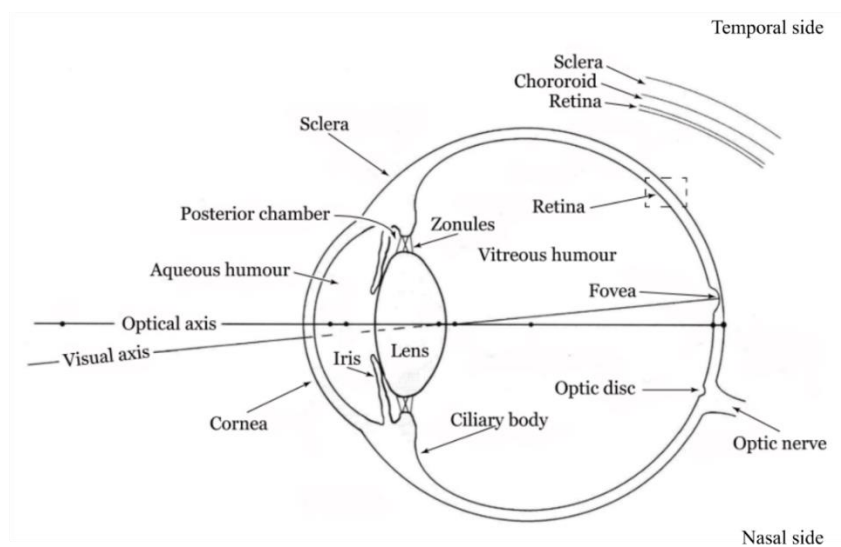

Figure 1.8. *The schematic of the human eye (Figure adapted from* [Atchison et al., 2000]*).*

Alternatively, the eye can be divided into three compartments: anterior, posterior, and vitreous chambers. The anterior chamber of the eye is the space between the cornea and iris and contains a fluid called aqueous humor. The posterior chamber of the eye is the location of the crystalline

lens and also contains aqueous humor [Atchison et al., 2000; Choh & Sivak, 2017]. The vitreous chamber, which contains the vitreous humor, is located between the lens and the retina.

1.2.1. *The outer layer*

The outer layer includes the posterior sclera and anterior cornea. Sclera is the opaque, protective white layer of the eye consisting of collagen and fiber [Cassin et al., 1990]. In comparison to almost all primates, the human eye has the greatest ratio of visual sclera extended horizontally [H. Kobayashi & Kohshima, 1997] making it a distinct feature, so the direction of gaze can easily be distinguished [Morris, 1985].

The cornea has a central radius of curvature between 7.7 and 7.9 mm and a mean thickness of 535 µm [Doughty & Zaman, 2000; Read et al., 2006]. The cornea resembles a prolate ellipse, and its radius of curvature decreases from the center to the periphery. It consists of six layers: the epithelium, Bowman's layer, stroma, Dua's layer, Descemet's layer, and endothelium [Choh & Sivak, 2017]. The first outer layer of the cornea is the epithelium, 52 µm thick, followed by Bowman's layer. [Li et al., 2012]. The cornea's main component is the stroma, which is composed of collagen floating in an extracellular matrix. The consequent layers are Dua's and Descemet's layers. Finally, endothelium, a single layer of cells, borders the anterior chamber of the eye. The boundary of the sclera and cornea is known as the limbus, and it protects the visible portion of the sclera [Dogru et al., 2009].

1.2.2. *The middle layer, Uvea*

The uvea is the middle layer of the eye. It is composed of the iris, choroid, and ciliary body. The Choroid has a mean thickness of 300 µm, forming the posterior part of the uvea. It is highly vascular and supplies the eye with oxygen and blood. It joins the ciliary body internally and is sandwiched between the sclera and the retina posteriorly. [Miller, 2008]. The Iris is the anterior part of the uvea. It plays a significant role in vision by regulating the amount of light entering the retina which affects the image quality [Campbell & Green, 1965b; Campbell & Gubisch, 1966]. The Iris controls the size of the pupil and its diameter changes from around 1.5 mm in high luminance conditions to 8.0 mm in low luminance. [Choh & Sivak, 2017]. When the iris contracts due to intense light or accommodation, or other factors (e.g., drugs, fear, or concentration, etc.) this is known as pupil miosis, and when it dilates due to disaccommodation and low light, or other factors this refers as pupil mydriasis. Individuals have different iris colors due to melanin pigments, which make the iris opaque. The ciliary body is essential

during ocular accommodation, which is the process of changing the focus of the crystalline lens by changing its shape and radius of curvature. [Fisher, 1986]. The capability of changing the crystalline lens's focus declines and eventually disappears with age [Heron et al., 2002].

1.2.3. *The retina*

The retina is the eye's innermost layer and is connected to the brain via the optic nerve so it can be thought of as an extension of the nervous system [Atchison et al., 2000]. As mentioned before, for centuries it was misunderstood as vascular tissue until Kepler discovered its role as the image plane. The retina is transparent, with a mean thickness range between 100 and 300 μm. It borders the choroid and is composed of layers and six types of cells: Rod, cones, horizontal, bipolar, amacrine, and ganglion cells (*Figure 1.9*) [Choh & Sivak, 2017; Mahabadi & Al Khalili, n.d.].

The first two are photoreceptors in the retina that convert the light into electrical signals. Horizontal, bipolar, and amacrine cells, are secondary neurons and process the electrical signals produced by photoreceptors. Finally, ganglion cells, stream the processed signals to the brain.
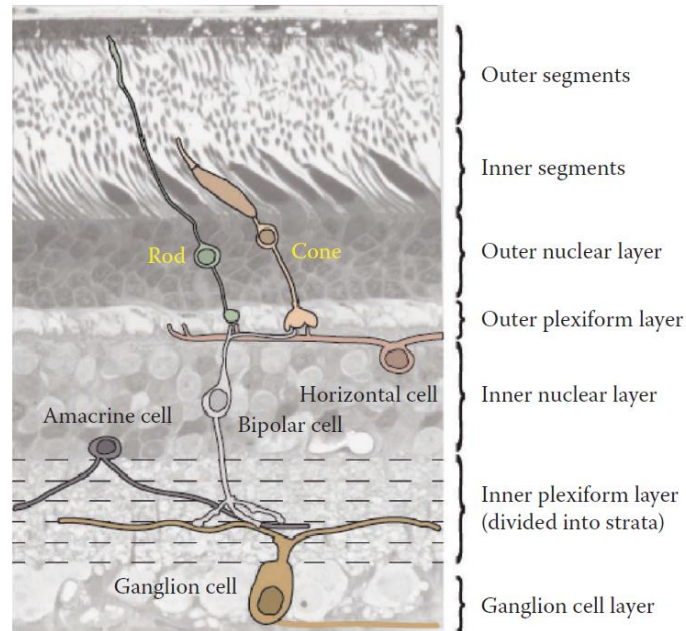

Figure 1.9. *Anatomy of the retina. Rods, cones, horizontal bipolar, amacrine, and Ganglion cells are depicted in the image (Figure adapted from [Choh & Sivak, 2017])*

The retina itself is divided into peripheral and central parts. The macula is the central retina; it is 5.5 mm in diameter and covers 18 degrees of field of view (FOV) (*Figure 1.10*) [Yanoff &

Sassani, 2018]. The fovea is the central part of the macula and produces the best visual acuity. It is 1.5 mm in diameter and accounts for 5 degrees of FOV. [Hendrickson & Yuodelis, 1984; Williams, 1985]. The optic disc corresponds to a small blind spot in the eye positioned roughly 15 nasal to the fovea, 3 to 4 mm away from the fovea [Quigley et al., 1990]. It is the place where the optic nerve exits the eye and spans 5 degrees horizontally and 7 degrees vertically.

There are two kinds of photoreceptors: cones and rods. The majority of the photoreceptors in the eye (95%) are rods [Lamb, 2016]. Rods function in low light levels called scotopic conditions, providing black-and-white sensory information. The fovea does not have any rod cells, but they predominate in the peripheral retina. The rods have a slow reaction time and produce poor spatial acuity and low contrast sensitivity. [Lamb, 2016].
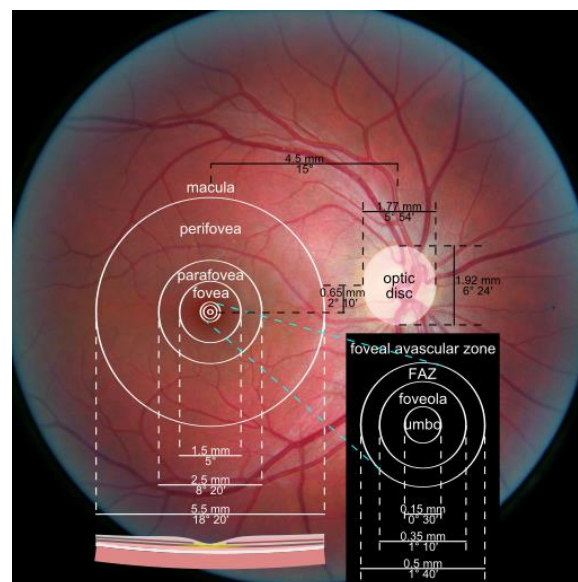

Figure 1.10 *Central part of the retina. The macula, optic disc, and fovea positions are depicted in the image (The figure adapted from [Hope, n.d.]).*

The colors are seen because there are three types of cones with different spectral sensitivities, i.e. 380 to 700 µm. There are approximately 4.5 million cones in the human eye, accounting for 5% of photoreceptors and located primarily in the central retina and macula. [Purves et al., 2019]. Therefore humans have poor color vision in peripheral vision [Johnson, 1986]. In our foveal vision, where visual acuity is most relevant, there are one hundred thousand cones. The cons are most effective in bright light (photopic conditions). L cones (long wavelength), account for 64% of all cons; M cones (medium wavelength), contribute to about one-third of all cons; and S cons (short wavelength), account for only 2% of all cons [Hunt, 1995; Wyszecki & Stiles, 1982]. The S-type cones are the most sensitive and are mostly populated outside of

the fovea. Contrary to rods, cones have a quick reaction time, and provide excellent spatial acuity, and high contrast sensitivity.

1.2.4. *The crystalline lens*

The crystalline lens, or the lens, has an oblate spheroid shape and is located in the posterior chamber of the eye after the iris (*Figure 1.11*). The crystalline lens can simply be considered a biconvex lens that focuses light on the retina and has a critical role in the optics of the eye. However, in reality, the crystalline lens is a more complex optical component. It is an aspheric, inhomogeneous, and Gradient-index lens. [Choh & Sivak, 2017]. It is also an active optical component since Its shape can be changed by the ciliary muscles to adjust its focus during the ocular accommodation process [D. Goss, 1995] This ability to change its focus is gradually lost with age, leading to presbyopia, as the aging lens becomes stiffer [Hodge et al., 1995]. It also grows, changing its curvature and mean refractive index. Finally, it progressively becomes more opaque [Philipson, 1973], and the ensuing increase in scattering can lead to age-related cataracts, which are common health issues in the elderly population.
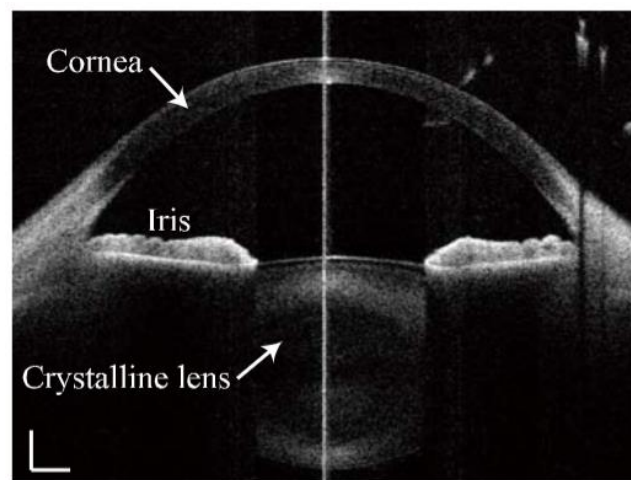

Figure 1.11. An OCT image of the anterior part of the eye in relaxed accommodation. The cornea, iris, and crystalline lens are depicted in the image [Furukawa et al., 2010].

1.3. *Aberrations*

In a perfect optical system, the wavefront coming from a point source at infinity becomes concentric spherical sectors in image space. They result in an Airy pattern and produce the sharpest-possible (diffraction-limited) image (*Figure 1.12*, *left*). However, real optical systems, such as the eye, typically exhibit misalignments and irregularities in surfaces and refractive indexes, distorting the wavefront. The difference between real and ideal wavefronts is known

as wave aberration (WA) [Hecht, 2017; Smith, 2008]. Although the wavefront distortions can happen at different positions along its path, it is typical to consider the overall lead or lag for each portion as occurring at a single plane, usually the pupil plane, and the WA can be defined as the point-by-point optical path difference (OPD) across the pupil, between the real wavefront and the ideal one. In an aberrated system, the image of a point source is an extended pattern or point spread function (PSF) and the image of an extended object is blurred (*Figure 1.12, right*).
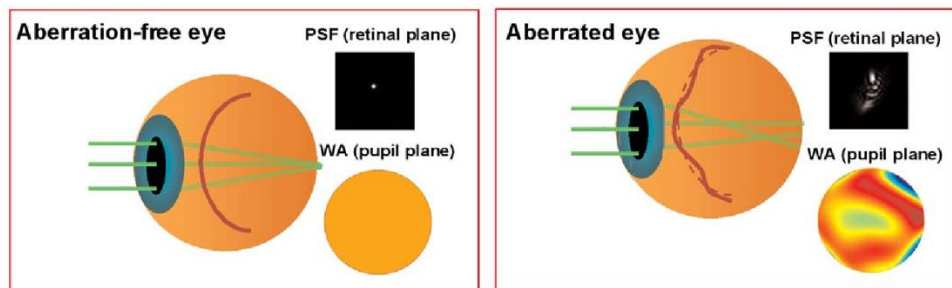

Figure 1.12. *Schematics of aberration-free (left) and real (right) eyes, and corresponding wave aberration (as a color map denoting lag in blue and lead in red at each pupil point), and point spread function (image of a point source). (Image adapted from [Marcos, 2001]).*

1.3.1. *Zernike polynomials*

Instead of expressing the WA in terms of the point-by-point OPD, it is typical to use a modal description consisting of the coefficients, C_i, of a linear combination of a set of orthonormal functions, $Z_i(\rho, \theta)$:

$$WA(\rho, \theta) = \sum_i C_i Z_i(\rho, \theta) \qquad (1.1)$$

where (ρ, θ) represent polar coordinates.

The standard set of functions used for this modal description are Zernike polynomials, named after Dutch physicist and Nobel laureate Frits Zernike (1888–1966), who first used them, albeit in a non-normalized form. Zernike polynomials are radial polynomials with an angular modulation characterized by two integer numbers: radial degree (n) varying from 0 to ∞; and azimuthal number (m) from –n to +n with the same parity as n.

It is important to note that Zernike polynomials are defined over a unit circle. That is, the radial coordinate, ρ, is normalized from 0 at the pupil center to 1 at the rim.-This feature effectively removes pupil size information from the Zernikes and has advantages from a mathematical point of view, but makes it impossible to evaluate the optical impact of the aberrations expressed as Zernike coefficients unless the pupil size is provided.

Several normalizations and ordering schemes and notations have been used in the past and are still in use in some fields. However, in Visual Sciences the standard form was established by Optica (formerly OSA) taskforce in 2002 [Thibos et al., 2002], and is regulated by ANSI [ANSI, 2004] and ISO standards [ISO, n.d.]. Zernike polynomials are composed of a normalization constant, a radial polynomial, and a sinusoidal component:

$$Z_n^m(\rho, \theta) = \begin{cases} N_n^m \, R_n^{|m|}(\rho) \; cos(m\theta), & m \geq 0 \\ -N_n^m \, R_n^{|m|}(\rho) \; Sin(m\theta), & m < 0 \end{cases} \qquad (1.2)$$

where the radial polynomial is defined as

$$R_n^{|m|}(\rho) = \sum_{s=0}^{(n-|m|)/2} \frac{(-1)^s(n-s)!}{s! \left(\frac{(n+|m|)}{2} - s\right)\left(\frac{(n-|m|)}{2} - s\right)!} \rho^{n-2s} \qquad (1.3)$$

and the normalization factor is

$$N_n^m = \sqrt{\frac{2(n+1)}{1+\delta_{m0}}} \, , \qquad and \qquad \delta_{mo} = \begin{cases} 1 & m = 0 \\ 0 & m \neq 1 \end{cases} \qquad (1.4)$$

δ_{m0} being Kronecker delta function.

Table 1.1 shows the mathematical expression of Zernike polynomials up to 6th order and their shape can be seen in *Figure 1.13,* where the typical pyramid arrangement has been used to present the false-color elevation maps.

Table 1.1. *Zernike polynomials up to 6th order.*

	index (j)	Order (n)	Frequency (m)	Polynomial $\left(Z_n^m(\rho,\theta)\right)$	Classical names
Lower-order Aberrations	0	0	0	1	Piston
	1	1	-1	$2\rho\sin\theta$	Tilt Y (vertical tilt)
	2	1	1	$2\rho\cos\theta$	Tilt X (horizontal tilt)
	3	2	-2	$\sqrt{6}\rho^2\sin2\theta$	Oblique astigmatism
	4	2	0	$\sqrt{3}(2\rho^2-1)$	Defocus
	5	2	2	$\sqrt{6}\rho^2\cos2\theta$	Vertical astigmatism
Higher-order Aberrations	6	3	-3	$\sqrt{8}\rho^3\sin3\theta$	Vertical trefoil
	7	3	-1	$\sqrt{8}(3\rho^3-2\rho)\sin\theta$	Vertical coma
	8	3	1	$\sqrt{8}(3\rho^3-2\rho)\cos\theta$	Horizontal coma
	9	3	3	$\sqrt{8}\rho^3\cos3\theta$	Oblique trefoil
	10	4	-4	$\sqrt{10}\rho^4\sin4\theta$	Oblique quatrefoil
	11	4	-2	$\sqrt{10}(4\rho^4-3\rho^2)\sin2\theta$	Oblique astigmatism 4th order
	12	4	0	$\sqrt{5}(6\rho^4-6\rho^2+1)$	Spherical aberration 4th order
	13	4	2	$\sqrt{10}(4\rho^4-3\rho^2)\cos2\theta$	Vertical astigmatism 4th order
	14	4	4	$\sqrt{10}\rho^4\cos4\theta$	Vertical quatrefoil
	15	5	-5	$\sqrt{12}\rho^5\sin5\theta$	Oblique pentafoil
	16	5	-3	$\sqrt{12}(5\rho^5-4\rho^3)\sin3\theta$	Oblique trefoil 5th order
	17	5	-1	$\sqrt{12}(10\rho^5-12\rho^3+3\rho)\sin\theta$	Vertical coma 5th order
	18	5	1	$\sqrt{12}(10\rho^5-12\rho^3+3\rho)\cos\theta$	Horizontal coma 5th order
	19	5	3	$\sqrt{12}(5\rho^5-4\rho^3)\cos3\theta$	Vertical trefoil 5th order
	20	5	5	$\sqrt{12}\rho^5\cos5\theta$	Vertical pentafoil
	21	6	-6	$\sqrt{14}\rho^6\sin6\theta$	Oblique hexafoil
	22	6	-4	$\sqrt{14}(6\rho^6-5\rho^4)\sin4\theta$	Oblique quatrefoil
	23	6	-2	$\sqrt{14}(15\rho^6-20\rho^4+6\rho^2)\sin2\theta$	Oblique astigmatism 6th order
	24	6	0	$\sqrt{7}(20\rho^6-30\rho^4+12\rho^2-1)$	Spherical aberration 6th order
	25	6	2	$\sqrt{14}(15\rho^6-20\rho^4+6\rho^2)\cos2\theta$	Vertical astigmatism 6th order
	26	6	4	$\sqrt{14}(6\rho^6-5\rho^4)\cos4\theta$	Vertical quatrefoil 6th order
	27	6	6	$\sqrt{14}\rho^6\cos6\theta$	Vertical hexafoil

For convenience, Zernike coefficients are sometimes ordered using a single index, j. Following the standard ordering scheme, conversion rules from a single index (j) to/from the dual index (n, m) [Schwarz, 2013] are:

$$j = \frac{n(n+1)}{2} + \frac{n+m}{2}$$

$$n = Round\left[\sqrt{\frac{-3+8j}{2}}\right], \quad m = 2j - n(n+1)$$

(1.5)

1.3.2. *Refraction from Zernike coefficients*

Second-order Zernikes represent quadratic forms that can be identified with sphero-cylindrical lenses. Accordingly, 2nd degree of the WA expansion coefficients (C_2^0, C_2^{-2}, and C_2^2) represent, in a first-order approximation, the sphero-cylindrical refractive error of the eye and an estimate
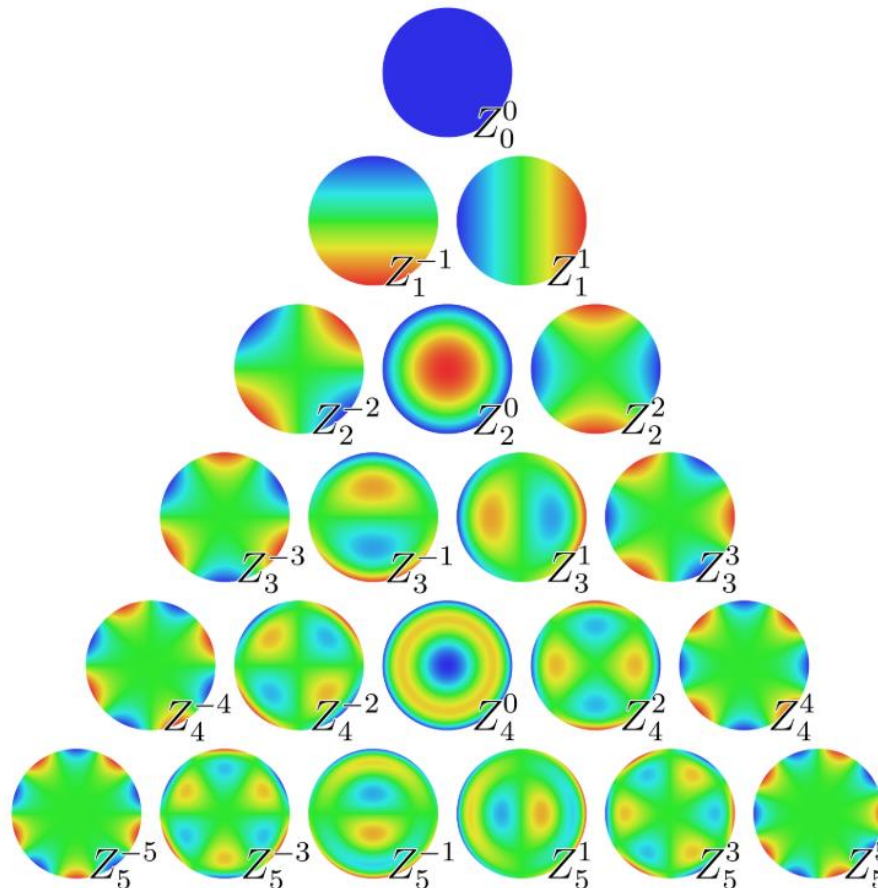
Figure 1.13. *Zernike pyramid up to 6th order. Zernike polynomials are sorted horizontally by azimuthal degree, m, and vertically by radial degree, n.*

of the subject's refraction can be obtained from them. The spherical equivalent (SE) is related with C_2^0:

$$SE = \frac{-4\sqrt{3}\, C_2^0}{r_p^2} \qquad (1.6)$$

Where r_p is the pupil radius [Salmon et al., 2003; Thibos et al., 1997, 2004]. Additionally, cylinder (CYL) can be estimated from C_2^{-2} and C_2^2, as:

$$CYL = \frac{-4\sqrt{6}\,\sqrt{C_2^{-2^2} + C_2^{2^2}}}{r_p^2} \qquad (1.7)$$

More elaborate expressions have been proposed to estimate SE and CYL including higher-order Zernike coefficients. However, they do not significantly improve the accuracy of the outcomes [Guirao & Williams, 2003]. Furthermore, In this thesis, we will always calculate SE from 2nd-order Zernikes.

1.3.3. *RMS Wavefront error*

The overall amount of aberrations of an optical system is frequently expressed in the form of a single number by means of the standard deviation of the optical path difference over the pupil, best known as the Root-Mean-Square or RMS, as it is the square root of the average across the pupil of the squared point-by-point wavefront lead or lag. Taking advantage of the Zernike polynomials orthonormality, the RMS can be readily obtained as the square root of the sum of squared coefficients [Marcos et al., 2017; Thibos et al., 2004]. The RMS Wavefront error, WF$_{RMS}$ is calculated as follows:

$$RMS = \sqrt{\sum_{n,m}(C_n^m)^2} \qquad (1.8)$$

When reporting ocular aberrations, different RMSs can be presented. Total RMS is obtained by considering all the coefficients n $\geq$ 2, i.e., excluding piston and tip/tilt, which do not degrade the image. High-order aberrations (HOA) are those with n $\geq$ 3. Sometimes, the RMS for a particular degree is provided (e.g., third-order RMS only involves n=3).

1.3.4. *WA and image formation: Point spread function*

The WA can be used to predict the image-forming properties of the optical system, in our case, the eye. The image of a point at infinity, or point spread function (PSF), can be calculated by Fourier transformation, directly derived from Kirchhoff diffraction formula [Goodman & Sutton, 1996]. The complex pupil function, $\mathcal{P}(\rho,\theta)$, combines the light-limiting properties of the pupil with the phase information provided by the WA:

$$\mathcal{P}(x,y) = p(x,y) \cdot exp\left(-i\frac{2\pi}{\lambda}\,WA(x,y)\right) \qquad (1.9)$$

where $p(x,y)$ is the pupil aperture function (1 inside, 0 outside), *(x,y)* are coordinates in the pupil plane, and λ is the wavelength. And the PSF can be calculated as:

$$PSF(u,v) = \left|\mathcal{FT}\big(P(x,y)\big)\right|^2 \qquad (1.10)$$

where (u, v) are coordinates in the image plane.

Figure 1.14 illustrates the PSFs associated with pure Zernike polynomials up to the 5th order. The PSF is a powerful tool for studying image formation by an optical system since the image of an extended object can be calculated by convolution. Furthermore, image quality metrics can be extracted from the PSF. Probably the most widely used metric is the Strehl ratio. It can

be defined as the ratio between the peak intensities in the PSF of a real, aberrated system and the PSF for its diffraction-limited counterpart (i.e., same pupil size but no aberrations [Atchison et al., 2000]:

$$Strehl\ ratio = \frac{Peak\ intensity\ of\ PSF_{aberrated}}{Peak\ intensity\ of\ PSF_{diffraction-limited}} \qquad (1.11)$$
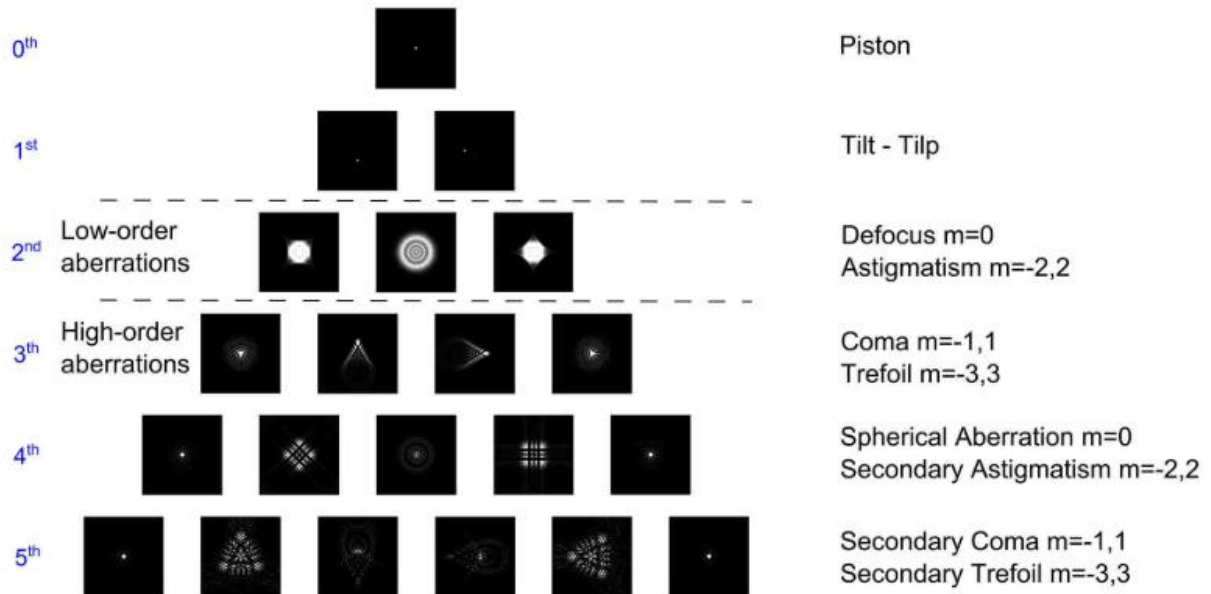
Figure 1.14. *The PSF of the Zernike polynomials up to 5th order (Image adapted from* [Chirre, 2017a] *)*

Figure 1.15 displays diffraction-limited and aberrated normalized PSFs to illustrate the concept of the Strehl ratio. Since aberrations expand the PSF, the maximum intensity of the resultant image is always lower than for the diffracted-limited and the Strehl ratio is always less than one (except for an aberration-free system, where it is exactly one). Being a single number characterizing a 2D function, the Strehl ratio is not perfect (two PSFs with the same peak intensity can produce different image degradations) but it is useful to roughly quantify the loss in quality and for optimization procedures. A system with a Strehl ratio above 0.8 is conventionally considered essentially diffraction-limited.

1.3.5. *Modulation transfer function*

In engineering, transfer function analysis is a convenient tool to model and study the output of a system. The equivalent treatment in image-forming optics can be used to analyze the effect of aberrations. Any object can be thought to be composed of a combination of periodic patterns
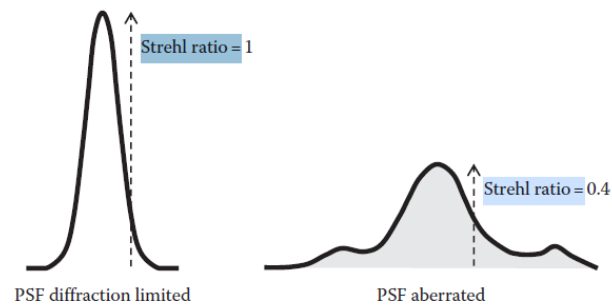
Figure 1.15. *diffraction-limited (left) and aberrated (right) normalized PSFs (figure adapted from* [Guirao, 2017]*)*

with different periodicity, and the relationship between object and image as a function of spatial frequency is the Optical Transfer Function (OTF), which in general is a complex-valued function. Its modulus, the Modulation Transfer Function (MTF), amounts to the ratio between image contrast and object contrast for each frequency. Mathematically, the OTF is the Fourier transform of the PSF. Therefore, the MTF can be calculated as:

$$MTF = |OTF| = |\mathcal{FT}(PSF)| \qquad (1.12)$$

where $\mathcal{FT}$ denotes Fourier transform.

The MTF typically decreases with spatial frequency. This means that image contrast for a fixed object contrast becomes worse or, put the other way around, to achieve a fixed image contrast the object contrast must be increased the higher the spatial frequency.

1.3.6. *High-order aberrations (HOA)*

In aberration theory, 2nd order Zernikes, identified with defocus and astigmatism, are termed low-order aberrations. In fact, they are not typically treated as aberrations but as sphero-cylindrical errors, which can be very large and have been routinely measured and corrected for more than a century.

Zernike terms of higher-than-3rd degree are known as a whole as high order aberrations, HOA. Their effect on visual quality is typically small, as their amplitude is usually low except in normal subjects and normal pupil sizes (*Figure 1.16*) [Atchison et al., 2000]. However, when the pupil size increases, e.g., due to low light levels, or in pathological conditions like keratoconus [Hofer et al., 2001; Thibos et al., 2002], or in many patients after laser surgery,

HOA magnitude increases and can severely increase the blur of the retinal image and reduce contrast sensitivity.
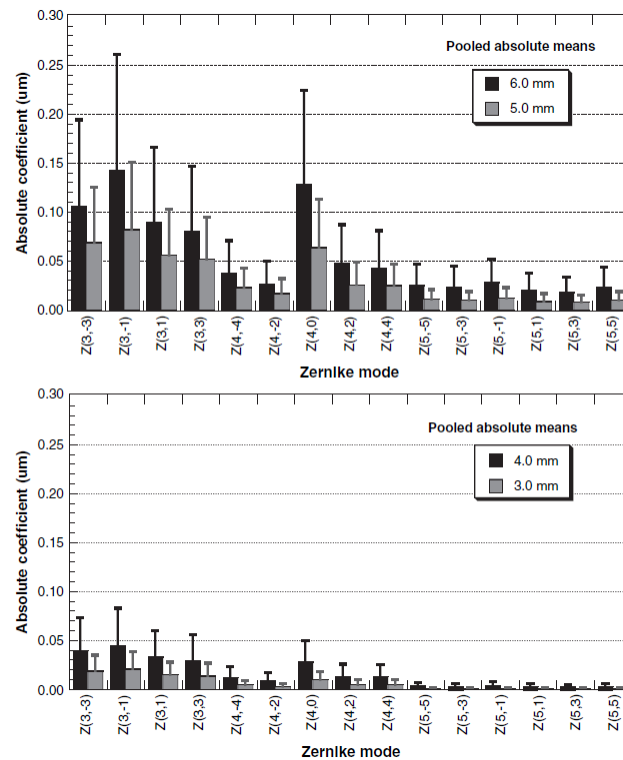

Figure 1.16. *Mean Zernike coefficients' amplitudes of HOAs for [µm] for 6, 5 (Up), 4, and 3 mm pupil size (bottom). The error bars represent standard deviations (Figure adapted from* [Salmon & van de Pol, 2006] *)*

1.3.7. *Hartmann-Shack sensor*

The principle of the HS sensor can be traced back to Christiaan Huygens (1629–1695) and Christopher Scheiner. In 1904, German astronomer Johannes Franz Hartmann invented the Hartmann screen test. Attempting to find the source of the low optical performance of a large telescope in his charge, Hartmann covered its aperture with a mask that consisted of an array of holes in the aperture of the telescope and inserted photographic plates on both sides of the focus plane [Hartmann, 1904; Schwiegerling, 2014]. By drawing lines connecting the spot diagrams registered on the plates, he found the location where the rays crossed the optical axis and realized that they did not converge on a single point (*Figure 1.17*). By using this test, Hartmann found the problem was in the primary lens of the telescope.

The Hartman method was an excellent test but had the disadvantage that in order to produce good spot images, the holes had to be very small, resulting in low light efficiency. Thus Shack
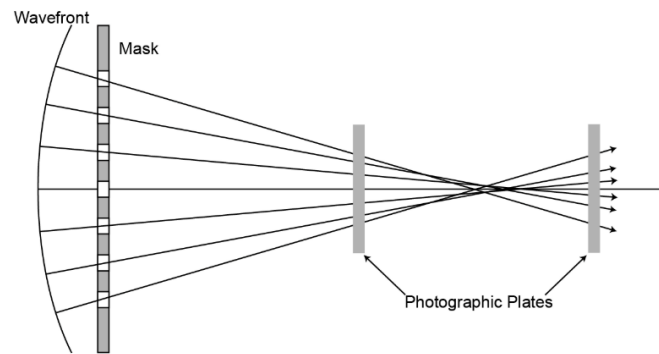
Figure 1.17. Hartmann screen test schematics (Image adapted from [Schwiegerling, 2014])

and Platt in 1971 made the holes larger to collect more light and used microlenses to focus the spots [Platt & Shack, 2001, 2003]. In the HS sensing method proposed by Shack and Platt, a microlens array is employed, with each lenslet producing a spot on the camera's sensor. A plane wavefront entering the HS sensor creates sharp spots at the focal point of each lenslet, which serve as measurement reference points. For an aberrated wavefront, spot positions are related to the incline across each microlens, i.e., to the local derivative of the wavefront. From this information, the WA can be integrated (*Figure 1.18*). The Hartmann-Shack method is a straightforward and robust technique, and it has become the standard wavefront sensing method in many fields, including vision science [Geary, 2015].
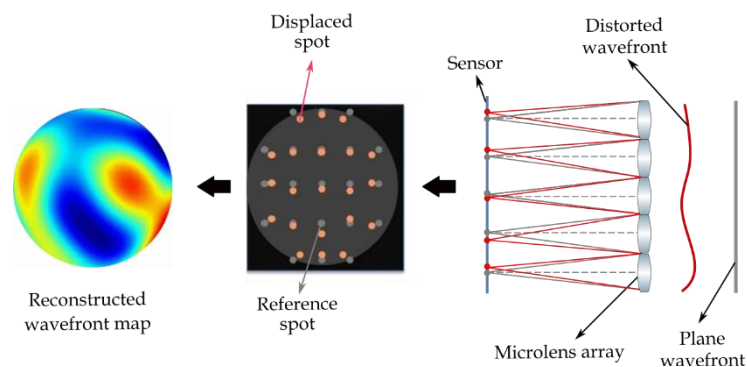
Figure 1.18. *The principle of the Hartmann-Shake sensor. The wavefront map is reconstructed as the difference between aberrated and plane wavefronts.*

1.4. *Ocular accommodation*

Having a clear vision when we gaze at objects at various distances is essential to functioning well in daily life. This process occurs in the eye, with complex mechanisms adjusting its optics to produce a blur-free image [Heath, 1956]. Accommodation is the ability of the human eye to modify its optical power and to focus from distant objects to near [Bharadwaj, 2017]. The

opposite process, focusing from near to far, is called disaccommodation. Accommodation is a "closed-loop" mechanism with negative feedback in which the visual information from the retina is processed in the visual cortex to stimulate the related visual organs to adjust the eye power [Von Helmholtz & Southall, 1924]. The altered sensory information is sent back to the brain for further image processing and, if necessary, to produce new neural feedback to optimize the image quality. This iterative process continues until a clear, blur-free retinal image is achieved.

1.4.1. *Theory and anatomy of accommodation*

To shift the gaze from far to near, the optical power of the eye is required to increase while the opposite move, from near to far, the optical power has to be reduced to achieve a clear image.
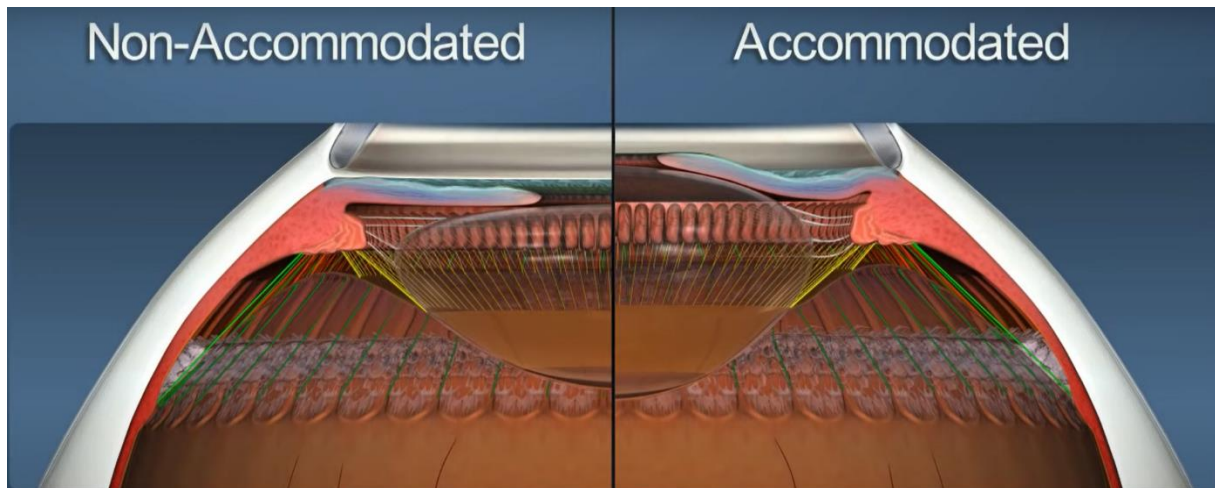
Figure 1.19. *Eye focusing far (left) and near (right). The crystalline lens radius of curvature is increased during the accommodation (Image adapted from [Goldberg, 2011])*

Figure 1.19 shows a computer-generated figure illustrating the changes in the crystalline lens and ocular morphology during accommodation and disaccommodation. Helmholtz's theory of accommodation [Martin et al., 2005; Ovenseri-Ogbomo & Oduntan, 2015; Von Helmholtz & Southall, 1924] is the generally accepted theory to explain the accommodation mechanism. Choroid, lens, ciliary muscles, and suspensory zonules are four ocular structures that are directly involved in the accommodation process (*Figure 1.20, (a)*). According to Helmholtz's theory, the forces applied to the lens change as a result of the ciliary muscle's contraction and relaxation, as well as its interaction with the choroid.

During the transition from a distant to a nearer object, the ciliary muscle contracts and forces the choroid to move anteriorly, therefore relaxing the zonules. This in turn increases the radius of curvature and thickness of the crystalline lens, hence increasing the eye's optical power. In contrast, when the fixation point shifts from near to far, the ciliary muscle relaxes, which pulls back the choroid posteriorly and stretches the suspensory zonules, hence the crystalline lens becomes thinner. The biomechanical schematics of the accommodation mechanism are shown in *Figure 1.20 (b)*, in which the suspensory zonules transfer the forces to the elastic crystalline lens in order
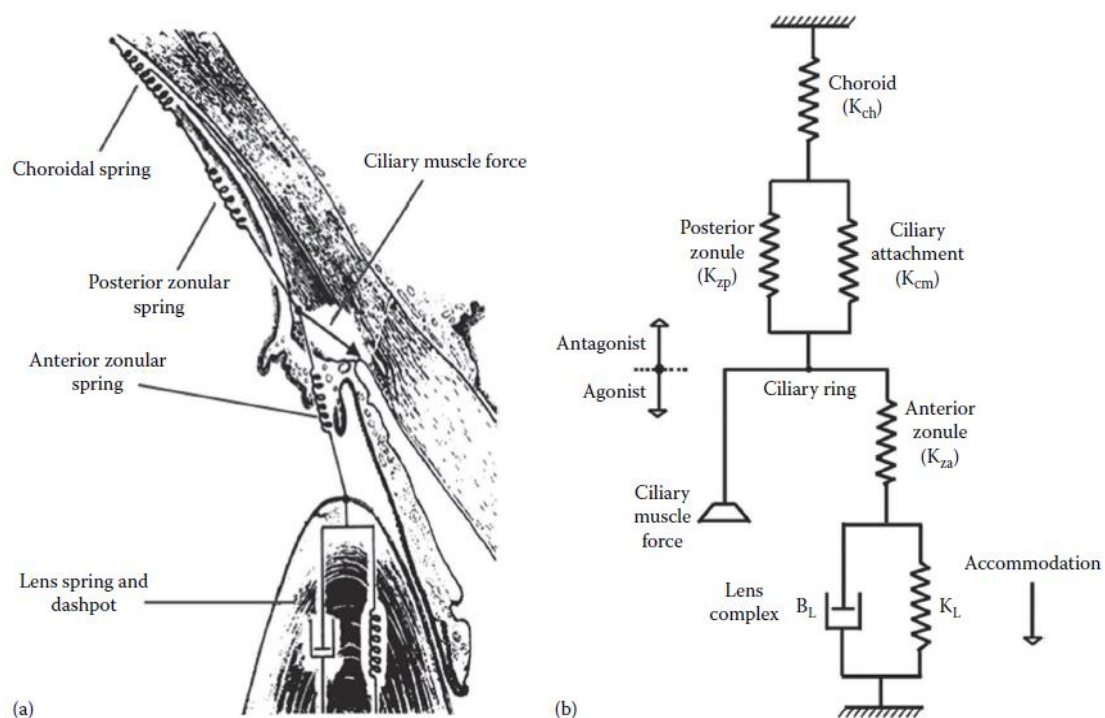
Figure 1.20. *Schematics of Helmholtz's theory of accommodation. (a) The model is drawn on the ocular components involved during accommodation (Figure adapted from [A. P. Beers & Van der Heijde, 1996])(b) Biomechanical model of the accommodation mechanism (Figure adapted from [A. P. A. Beers & Van Der Heijde, 1994])*

to alter its shape and curvature [A. P. A. Beers & Van Der Heijde, 1994; A. P. Beers & Van der Heijde, 1996]. It should be noted that the only active organ among the components that are involved in accommodation is the ciliary muscle, while the others are passive, relaying neural interventions and then stimulation from the ciliary muscle. Although there is a slight sympathetic element to the accommodation process, it is predominantly parasympathetic [Gilmartin, 1986].

1.4.2. *Accommodation dynamics and fluctuations*

Ocular accommodation is not constant and varies over time. There are accommodation microflucantions (AMFs) that were discovered eight decades ago [G. Collins, 1939]. The characteristics of AMFs were explained by Campbell et al. in the 1960s [Campbell et al., 1959; Campbell & Westheimer, 1960]. They have two frequency components: The high-frequency component (HFC) has frequencies in the range of $1 \text{ Hz} \leq f \leq 2.5 \text{ Hz}$, and a narrow peak in the power. The low-frequency component is below 0.6 Hz. [Charman & Heron, 2015]. AMFs vary between subjects and depend on the experimental conditions, such as spatial frequency [Day et al., 2009], stimulus type [Gambra et al., 2009], luminance [Day et al., 2009], and accommodation demand [L. R. Stark & Atchison, 1997].

The amplitude of AMFs is around ±0.5 D and their RMS tends to increase as the accommodation demand increases, at least up to the 5 D demands [Leahy et al., 2010; L. R. Stark & Atchison, 1997]. The mean standard deviation of the accommodation response for 1.5, 2.5, and 3.5 D demands has been reported to increase with refractive error and both LFC and HFC of AMFs showed the same trend [Harb et al., 2006]. For instance, in young subjects with their natural aberrations, Gambra et al. demonstrated a link between the AMFs and the accommodation demand for stimuli ranging from 0 to 6 D [Gambra et al., 2009]. The AMFs increase at lower luminance and low spatial frequencies [Day et al., 2009]. Their frequency components are thought to be related to the cardiopulmonary system [M. Collins et al., 1995]. Regarding the potential relationship between AMFs and accommodation, there are three competing hypotheses: AMFs could be an active part of the accommodation mechanism; they could have an independent origin but help the accommodation function; or they could indicate nothing more than a state of instability in the system with the minimal functional impact of the accommodation system. The potential role of AMFs as an accommodation cue is discussed in the next section.

1.4.3. *Blur-related accommodation cues*

Perception of blur in the image of the object of interest may trigger the accommodative process. The most immediate challenge for the eye at that point is to determine whether the sharp image is in front or behind the retina, that is, whether the accommodative system should decrease or increase optical power. Additionally, success to achieve and sustain a clear vision requires the right amount of power to change, within tolerance. To speed and bolster the process, the eye makes use of some cues that stimulate the accommodation mechanism to obtain a sharp retinal image [Bharadwaj, 2017]. These cues can come from the environment

outside or from the eye itself [Moulakaki et al., 2017]. In the remainder of this subsection, we will list the cues related to image blur.

1.4.3.1. *Defocus blur*

A blurry retinal image is considered the main cue for accommodation [Bharadwaj, 2017; Campbell & Westheimer, 1960; Fahrbach et al., 2013; Tucker & Charman, 1979]. Blur in the image can occur by pure defocus, various aberrations, or diffraction [Fry, 1963]. Blur caused by defocus degrades the retinal image contrast. This contrast loss is greater at higher spatial frequencies. However, the efficiency of this kind of blur as a cue for accommodation is debatable since retinal images affected by a certain amount of pure defocus are identical regardless of their sign. Therefore, if the only aberration is defocus, blur alone does not indicate the direction of accommodation, and lag or lead of accommodation can occur as the eye would accommodate randomly. However, in the actual human eye, the presence of ocular aberrations and other symmetry-breaking issues, such as the Stiles-Crawford effect can transform defocus from an even-error cue to an odd-error cue [Fincham, 1951].

1.4.3.2. *Monochromatic aberrations cues*

Monochromatic aberrations can act as odd-error cues for accommodation [Charman & Tucker, 1977; Fincham, 1951; Walsh & Charman, 1988]. There is evidence that even-order aberrations like second-order astigmatism and fourth-order spherical aberration can provide a sign of accommodation, but odd-order aberrations like third-order coma and trefoil cannot [Wilson et al., 2002]. [Artal & Fernández, 2005; Chen et al., 2006; Chin et al., 2009a; Gambra et al., 2009].

When the defocus blur is accompanied by even-order HOA, e.g. spherical aberration, the symmetry of blur with respect to defocus sign is broken, providing information about the axial direction [Wilson et al., 2002]. Actually, the presence of the blur from even-order HOAs transforms a pure defocus even-error cue into an odd-error cue [Bharadwaj, 2017]. Therefore, the visual system can distinguish between the various point spread functions for positive and negative defocus if it is combined with monocular aberrations (*Figure 1.21*).

1.4.3.3. *Chromatic aberration cue*

The role of longitudinal chromatic aberration (LCA) in the accommodative process is controversial. While some studies support the claim that LCA can be a cue for accommodation [Aggarwala, Kruger, et al., 1995; Aggarwala, Nowbotsing, et al., 1995; Rucker & Kruger, 2004; Seidemann & Schaeffel, 2002], others did not find the same behavior [Charman & Tucker, 1978; Kotulak et al., 1995]. Moreover, artificially removing LCA from the stimulus did not hinder accommodation [Metlapally et al., 2014]. This indicates the presence of other coexisting cues with LCA that contribute to the accommodation response. [Kruger et al., 1997].
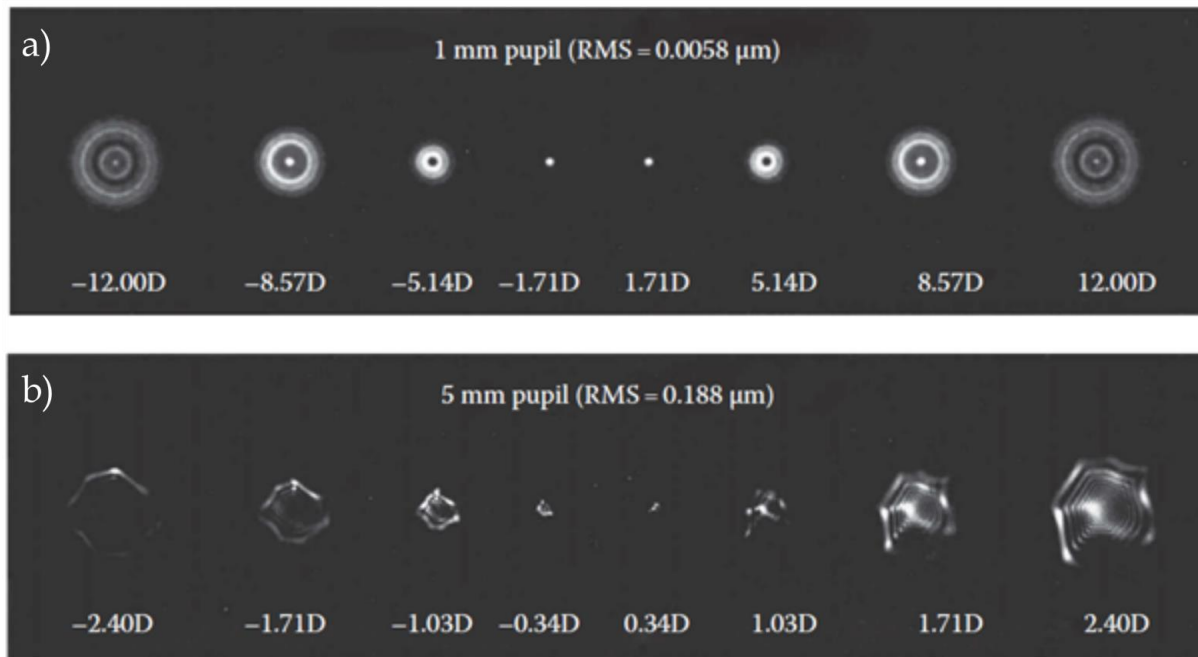
Figure 1.21. *Monochromatic point spread function simulations for positive and negative defocus values: (a) For a pupil size of 1 mm, where HOAs are negligible. (b) For 5 mm pupil diameter, when HOAs are sizable. (Image Adapted from [Wilson et al., 2002]).*

1.4.3.4.   Accommodation microfluctuations (AMFs) cue

Some studies suggest that AMFs may act as an accommodative cue [Charman & Heron, 2015]. Researchers argue that since positive and negative pure defocus produce identical blur in retinal images, the AMFs in one direction can improve the unfocused retinal image, and vice versa the AMFs in the other direction can degrade the image quality [Alpern, 1958]. Therefore, the AMFs can serve as an odd-error cue by optimizing the initial accommodation response or assisting to maintain the steady-state accommodation. Later it was noted by Campbell et al. that since the accommodation dynamics is a rather quick process, lasting less than 1 sec, the high-frequency components of the AMFs can only serve as an initiator cue [Campbell et al., 1959]. Further investigation showed that if odd-error accommodative cues are removed from the stimulus, the initial direction of accommodation can be random [L. Stark & Takahashi,

1965]. Therefore, the AMFs role as a cue for accommodation does not appear to be an active mechanism (particularly for the high-frequency components). All of this suggests that, if AMFs serve as a guide for accommodation, their function is confined to the maintenance of "steady-state" accommodation, with LFC possibly playing the most significant role [Charman & Heron, 2015].

1.4.4. *Maddox components of accommodation*

There are additional categories for accommodation cues. Three kinds can be distinguished: blur-driven, vergence-driven, and proximity-driven accommodation cues [Bharadwaj, 2017; Schor et al., 1992]. Vergence-driven cues are related to binocular disparity, i.e., convergence together with blur-related cues, are labeled retinoscopic cues [Kruger & Pola, 1987]. On the other hand, cues depending on proximity and apparent size of the object, are said to be spatiotopic [Kruger & Pola, 1986]. All of these cues generate negative feedback, but their range and precision vary [Schor et al., 1992]. Retinoscopic cues have a shorter range, of 2D ± 2D while spatiotopic cues have a wider range but rougher precision [Bharadwaj, 2017]. Hence, all of the cues are complementary, and the interaction between the retinoscopic and spatiotopic cues produces a proper accommodative response [Hung et al., 1996; Joubert & Bedell, 1990].

The combination of all three types of cues with tonic accommodation is referred to as the "four Maddox components of accommodation." Tonic accommodation is the baseline of accommodation, that is, the accommodative state in darkness or for a lack of stimulus. In normal emmetropic subjects it tends to be around 1D [McBrien & Millodot, 1987; Rosenfield et al., 1993, 1994].

1.5. *Binocular vision*

Binocular vision means being capable of viewing the surrounding objects through two eyes. However, not every animal with two eyes has binocular vision, as the term is reserved for species with a large overlap between monocular visual fields. In binocular vision, both retinal images should fuse to provide a single impression of the environs. According to Panum's fusional area, two lines, one in each retinal image, can be fused if their separation is in the range of 15 to 25 arc minutes [Mitchell, 1966]. At higher spatial frequencies and in peripheral vision, the fusion range is reduced. The horizontal fusion area is greater than the vertical [Ogle, 1952]. This fusion is accompanied by convergence and by sensory and motor drive controllers, which are described in detail in the accommodation and convergence cross-link section.

1.5.1. *Binocular versus monocular vision*

Binocular vision has advantages over monocular vision in many aspects [Fielder & Moseley, 1996]. Having a spare eye in case of ametropia, disorder, or accident is an obvious advantage, but the benefit of the combined use of both eyes to produce binocular vision is considerably larger. Binocular vision increases the overall field of view (FOV). Monocular FOV is roughly 105º temporal and 60º nasal (*Figure 1.22*), while the entire horizontal binocular FOV is approximately 210 degrees with 120 degrees of binocular overlap [Atchison et al., 2000]. Binocular visual acuity and contrast sensitivity are typically better than in monocular vision [Campbell & Green, 1965a; Home, 1978]. In addition, binocular accommodation is faster and the accommodation response is larger in magnitude [Chirre et al., 2015]. Finally, even though there are several monocular depth cues, e.g., apparent size and occlusion, the retinal disparity in binocular vision plays a key role in depth perception [Reichelt et al., 2010], enabling 3D vision.

1.5.2. *Convergence*

During binocular accommodation, the eyes are also moved to gaze at the target. Convergence is the nasal rotation of the eyeballs to fixate on a near visual stimulus. The reverse, i.e., temporal rotation of the eyes when fixating from a nearby to a distant object, is known as divergence. Accommodation and convergence are closely linked together as the change in one of them affect the other one. The reason is that both accommodation and vergence share the same neural controllers in the brain [Atchison et al., 2000; Mutti et al., 2017]. For instance, if one eye is occluded and a negative lens is positioned in front of the other eye, the occluded eye will also turn inward (as accommodation is triggered in the unoccluded eye) [Chirre et al., 2015]. The cross-link between accommodation and convergence is explained in detail in the next section.

1.5.3. *Accommodation and vergence cross-link*

In binocular vision, both types of retinoscopic cues, i.e., blur and disparity, trigger both accommodation and vergence to sustain the clear 3D vision. A visual stimulus for either vergence or accommodation can change the other one [Atchison et al., 2000]. To explore the blur and disparity effects in accommodation mechanisms Schor proposed a cross-coupling model between vergence and accommodation (*Figure 1.23*) [Schor, 1992].
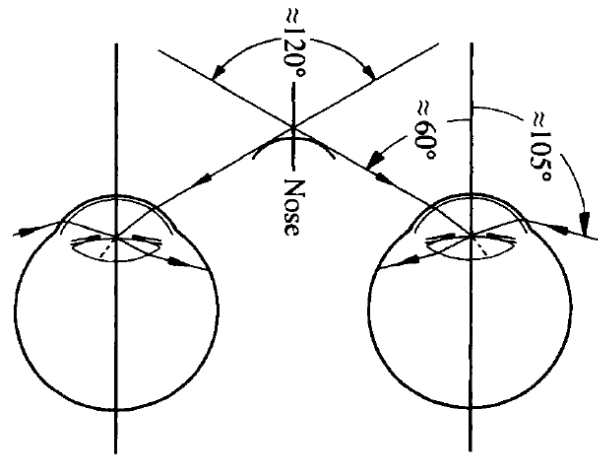
Figure 1.22. *The horizontal FOV for binocular and monocular vision (Image adapted from [Atchison et al., 2000]).*

The accommodation process should be discussed in static and dynamic modes. In the static mode, the accommodation blur cue is the primary control factor, while in dynamic accommodation, the disparity cue is the dominant factor in triggering the vergence-linked accommodation response [Bharadwaj, 2017]. The two linked motor responses are referred to as accommodation-convergence (AC) and convergence-accommodation (CA). The blur-driven accommodation stimulates the AC, and disparity triggers the CA. Both AC and CA are negative feedback loops, and they act until the retinal blur reaches the acceptable threshold for depth of focus (DOF) or the disparity threshold (i.e., Panum's fusional area).

The AC and CA interactions involve phasic and tonic controllers to convert the sensory information to motor drive (i.e., reaction in extraocular muscles in convergence and ciliary muscles in accommodation). Phasic and tonic controllers have different natures. The phasic ones have a short time constant but high gain and are more effective in dynamic accommodation. On the other hand, tonic controllers have a larger time constant and smaller gain, better suited in steady-state accommodation. Therefore, the retinoscopic cues first trigger a phasic response and then, after achieving the threshold in the steady-state accommodation, the tonic controllers are activated.

1.5.4. *Stereopsis and depth perception*

The primary advantage of binocular vision is providing three-dimensional (3D) depth perception, which is referred to as stereopsis.[Tsutsui et al., 2005]. The stereopsis is the depth cue employed in 3D displays and 3D cinema. In stereoscopic 3D displays, the right and left

eyes receive different images via various technologies such as polarization, active shutters, or lenticular lenses [Lueder, 2012].
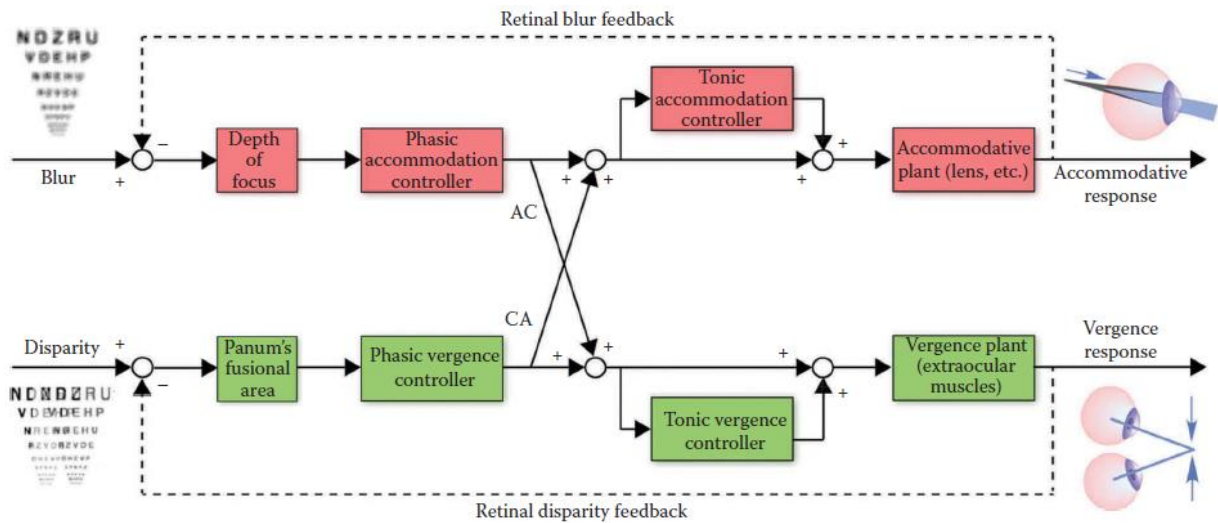
Figure 1.23. *Accommodation and vergence interaction model proposed by Schor [Schor, 1992]. Phasic controllers are fast with high gain, while tonic controllers are slower with lower gain (Image adapted from [Bharadwaj, 2017]).*

However, this technology can cause visual discomfort for the user by causing a conflict between accommodation and vergence (*Figure 1.24*) [Hoffman et al., 2008; Shibata et al., 2011]. It is because the disparities between the left and right images vary during viewing the 3D content, resulting in proper convergence, but the plane of focus is fixed on the display's screen [Woods, 2012]. However, state-of-the-art holographic 3D displays contain all natural depth cues, i.e., multiple focus planes, [Onural, 2016] and there has been continuous research to improve their image quality, refresh rates, and hologram computation speed [Ghoushchi et al., 2017; Z. He et al., 2019; Yaraş et al., 2010].

1.6. *Pupillary response*

Pupil size is influenced by several physical and psychological factors, including illumination, accommodation, object structure, attention, excitement, drugs, and sleep. The range of pupil sizes spans roughly from 2 to 8 mm. Pupil constriction is known as miosis, while pupil dilation is called mydriasis.

As illustrated in *Figure 1.25,* the size of the pupil is regulated by the sphincter (or circular) and radial muscles of the iris. In conditions of bright light, the sphincter muscle contracts and
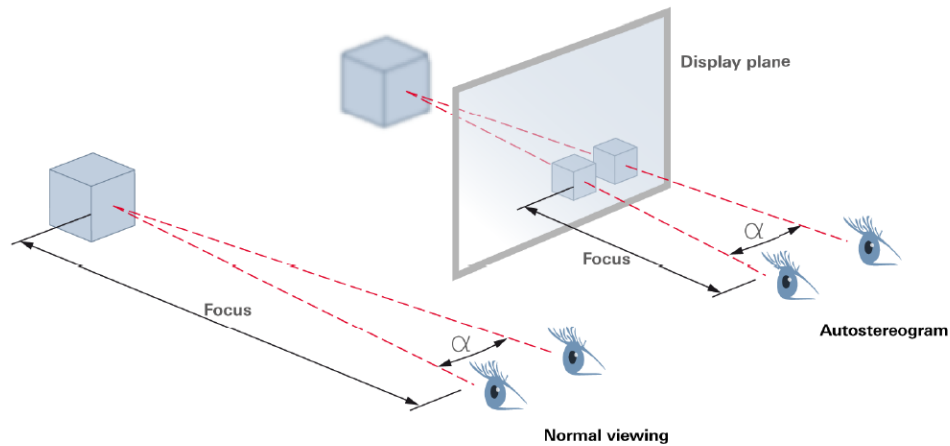
Figure 1.24. *Natural viewing conditions (left) and a 3D stereoscopic display view (right). The normal vision and a holographic display provide all depth cues. On stereoscopic displays even though the vergence changes correctly, the focus plane remains fixed. (Image adapted from* [Reichelt et al., 2010]*).*

decreases the size of the pupil, whereas, in dim light, the radial muscles of the iris dilate the pupil to allow more light into the eye. During fixation on a nearby stimulus, convergence, accommodation, and miosis are initiated almost simultaneously, which is known as the near response complex or triad [Ghoushchi et al., 2021]. The amplitude and speed of the pupillary response to high luminance are larger than for accommodation.
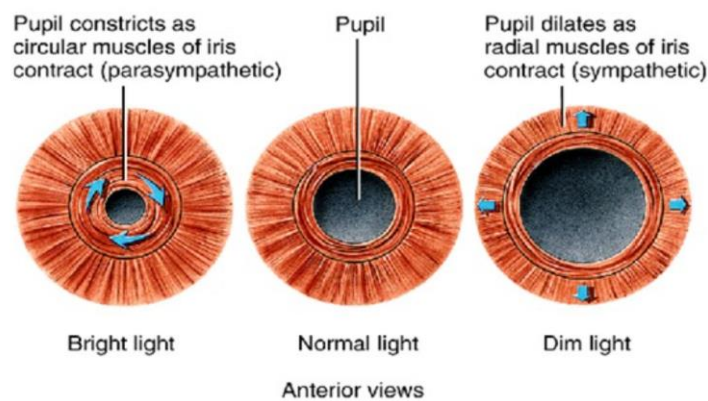
Figure 1.25. *Representation of pupil miosis and mydriasis with changing light levels (Image adapted from [Curtis Sparks, n.d.])*

1.7.   *Emmetropia and refractive errors*

1.7.1. *Emmetropia*

Emmetropia is derived from the ancient Greek word "emmetros" meaning "well-proportioned" + "ōps" which means "eye" [Beekes, 2009]. In an emmetropic eye, light from infinity provides a clear, high-contrast image on the retina. Although a smaller refractive error

can be detected, an eye is considered emmetropic if -0.5 D <SE ≤ 0.5 D [Morgan et al., 2010]. If the refractive error is outside this range, the eye is said to be ametropic.

1.7.2. *Emmetropization process*

The newborn infants have hyperopia but gradually become emmetropes; this process is known as emmetropization [Flitcroft, 2014]. This myopic shift in the refractive error happens due to changes in lens and corneal curvature, and axial length of the eye [Mutti et al., 2005]. In addition to the gradual reduction in hyperopia, there is also a decrease in astigmatism in the first year of born [J. Gwiazda et al., 2000]. *Figure 1.26* shows refractive error frequency in infants at different ages [Mutti et al., 2005; Ingram & Barr, 1979; Flitcroft, 2014]. Refractive errors follow a normal distribution in all cases but the mean value shifts with age. There are two theories, active and passive, regarding emmetropization. The passive emmetropization theory claims that refractive error is more related to heredity and the genetics of the parents. [Mutti et al., 2005].

According to passive emmetropization, the reduction in refractive error in infants is due to the children's natural growth process. Moreover, myopia research indicates that parental myopia increases the chance of having a myopic child. If both of the parents are myopic, the probability of having a myopic child is 30% to 40%, and this chance is 10% to 15% if only one of the parents is myopic [Mutti & Zadnik, 1995].

On the other hand, the active theory of emmetropization claims that emmetropization is continuously affected by the retinal image quality and there is closed-loop visual feedback. It argues that the blurry, defocused retinal images further stimulate eye growth. Some researchers suggest that, while myopia correction methods only correct the central retina, peripheral hyperopic defocus can lead to myopia progression in children. This has been the motivation for recent myopia

studies employing multifocal contact lenses in an effort to delay myopia onset, decrease its advancement rate, or stop myopia progression [Jonas et al., 2021].The active emmetropization theory is also supported by animal studies. Schaeffel et al. performed an experiment on chickens, inducing myopic and hyperopic defocus by applying positive and negative lenses. They found that in chickens wearing negative lenses, the hyperopic defocus stimulated axial
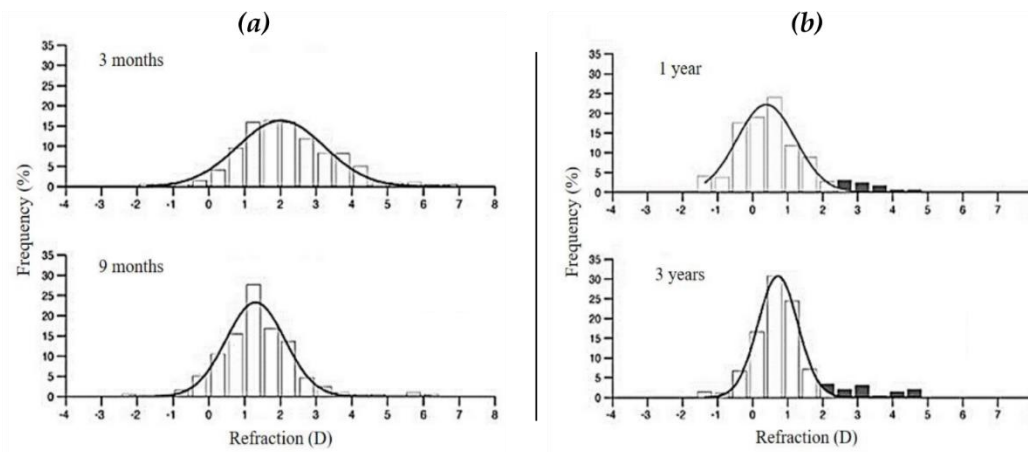
Figure 1.26. *Refractive frequency [%] in various age groups of infants. (a) Results for 3-months and 9-months babies (Adapted from [Mutti et al., 2005]) (b) Results for 1-year and 3-years infants (Adapted from [Ingram & Barr, 1979]). Gray bars represent outliers (Adapted from [Flitcroft, 2014])*

eye growth, which supports the active emmetropization hypothesis. [Schaeffel et al., 1988]. It can be assumed that both passive (heredity) and active factors (visual feedback) stimulate myopic shift and axial elongation in the emmetropization mechanism and can lead to myopia if the process is upset [Babinsky & Candy, 2013; Siegwart & Norton, 2011].

1.7.3. *Myopia*

The term myopia is derived from the Greek term "myein", meaning "shut the eyes", and "ōps", meaning "eye" [Beekes, 2009]. Myopia, also known as nearsightedness, is defined as a refractive error in which light rays coming from distant objects are focused in front of the retina when ocular accommodation is relaxed, resulting in blurry vision [Atchison et al., 2000]. The primary sign of myopia in children seems to be axial elongation [D. A. Goss & Wickham, 1995; Morgan et al., 2021]. This affects the distant point of the eye, which moves it to a nearer distance [Atchison et al., 2000].

Based on the most recent classification of the International Myopia Institute (IMI), Individuals with SE ≤ -0.5 D are myopes whereas those with SE ≤ -6 D are defined as high myopes [Flitcroft et al., 2019]. From a clinical point of view, myopia can be classified as developmental myopia (also simple or school myopia) [Ramamurthy et al., 2015], pathological or degenerative myopia (also progressive or high myopia) [Jong, 2021], congenital myopia [Tedja et al., 2019], and acquired myopia [Benjamin, 2006]. In general, myopia causes more discomfort at night and uncorrected myopia can negatively impact individuals' education and reduce their quality of life [Congdon et al., 2019; Sankaridurg et al., 2021].

1.7.3.1. Myopia risk factors

There are several theories regarding the cause and prevalence of myopia [Pan et al., 2012]. There is a strong hereditary factor: children with myopic parents are at a considerable risk of having early myopia onset. [Liang et al., 2004]. However, a recent study in southern Spain suggests that refractive error is mostly affected by a shared environment rather than hereditary factors. [Pusti et al., 2020]

Another risk factor is near work and a considerable amount of literature has been published on its possible effect on myopia [Ghoushchi et al., 2021; H. M. Huang et al., 2015; Ip et al., 2008; Z. Lin et al., 2016; Mutti et al., 1996; Saw et al., 2001; Tan et al., 2000]. Highly educated people are more likely to have a higher degree of myopia [D. A. Goss, 2000]. Furthermore, the recent increase in myopia could be attributed to the fact that the younger generation spends more time doing homework and reading books [L. L. K. Lin et al., 2004], watching TV, or using electronic devices such as mobile phones and computers [Czepita et al., 2010].

On the other hand, some researchers suggest that indoor activities have a significant impact during the time of vision development in children. Data from several studies suggest that having enough outdoor activities can prevent myopia in children [Pusti et al., 2020; Ramamurthy et al., 2015; Saw, 2003]. Another issue that affects myopia is the amount of light in the environment [Norton & Siegwart, 2013]. Persistent low luminance conditions can expedite myopia onset and progression [Wang et al., 2018].

1.7.4. *Hyperopia*

The term hyperopia derives from the Greek word "huper","beyond" and "ōps", meaning "eye" [Stevenson, 2010]. In hyperopia, which is also called far-sightedness or hypermetropia, the rays from faraway objects focus behind the retina when the accommodation is relaxed, causing the perceived images to be blurry. In this scenario, the distant point is virtual but young mild hyperopes routinely compensate for this situation by accommodating, so no symptoms are apparent. However, continued accommodation, especially near work, may cause eye strain (asthenopia), amblyopia (lazy eye), strabismus (misalignment of the eyes), and accommodation malfunctions during prolonged close work [Moore et al., 1997]. Furthermore, the degree of convergence is insufficient for the required accommodation response. As the accommodation amplitude decreases with age, hyperopic subjects may become aware of presbyopia earlier than emmetropes and myopes. In general terms, hyperopia is due to a mismatch between the eye

size and its optical power [Atchison et al., 2000]. There are two possibilities: Either the eye's axial length is too short or the eye's optical power is too low (i.e., the cornea and/or lens are flatter than in emmetropic eyes) [Benjamin, 2006; Wu et al., 2013]. Each 1 mm of reduced axial length leads to 6 D, and each 1 mm flatter radius of curvature in the cornea causes 3 D of hyperopia [Strang et al., 1998]. Depending on its magnitude, hyperopia is classified as low (+0.5 < SE ≤ +2.00 D), moderate (+2.00 < SE ≤ +5.00 D), or high hyperopia (SE > +5.00 D) [Moore et al., 1997].

1.7.5. *Astigmatism*

The word astigmatism is derived from the Greek words "a" (without) and "stigma" (point). [Stevenson, 2010]. Astigmatism is a refractive error due to a lack of axial symmetry in the optical surfaces of the eye. As a consequence, the optical power varies angularly, leading to multiple focus points on the retina (*Figure 1.27*) [Atchison et al., 2000; Liu & Thibos, 2017]. From a clinical point of view, the condition in which the highest and the lowest negative cylindrical axes are perpendicular is called "regular" astigmatism. Regular astigmatism is in turn divided into with-the-rule (WTR) (highest negative cylindrical axis close to horizontal), against-the-rule, (highest negative cylindrical axis close to vertical), and oblique (negative cylinder axis between 120º and 150°or 30º and 60°) [Read et al., 2014]. WTR is more prevalent in children and ATR in adults [Leung et al., 2012]. Oblique astigmatism is less common but fairly stable with the age [Fledelius & Stubgaard, 1986].
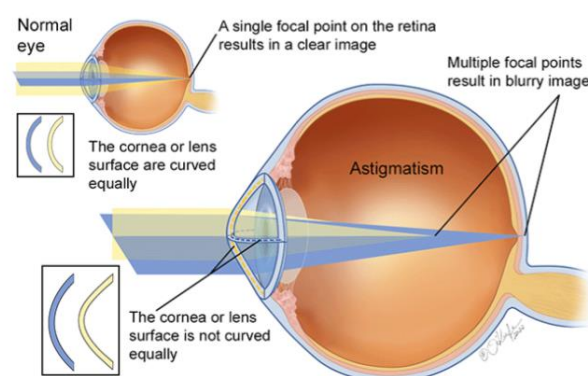
Figure 1.27. Astigmatism aberration on the human eye. (Image credit: Laurie O'Keefe, adapted from [Laurie O'Keefe, n.d.]).

Figure 1.28 illustrates image quality for various types of astigmatism and defocus blur [Read et al., 2014]. Astigmatism makes the vision blurry at all distances and is normally accompanied by myopia or hyperopia [Atchison et al., 2006]. Astigmatism is typically less than 0.5D in

normal subjects and magnitudes greater than 3D are uncommon. Astigmatism affects more at night and, if uncorrected, it can substantially impact the quality of vision.
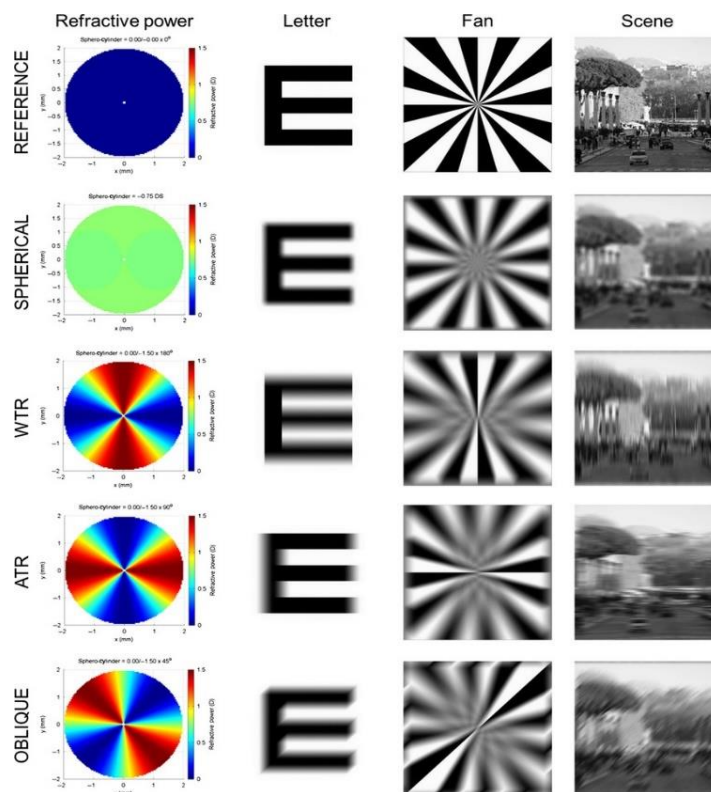
Figure 1.28. *Image formation for defocus and various types of astigmatism (Image adapted from [Read et al., 2014]).*

1.8. *Myopia prevalence and its importance*

Myopia is increasing dramatically in recent decades among the young generation, making it a major public health concern [Ang et al., 2020; Dolgin, 2015; B. Holden et al., 2014; Jong & Ian Flitcroft, 2019]. According to Holden et al., about 2.5 billion individuals currently suffer from some degree of myopia worldwide, and if the trend persists (*Figure 1.29)*, approximately half of the world's population will be myopic in 2050 [B. A. Holden et al., 2016].

The epidemic of myopia is exacerbated by the increasing urbanization rate in developing and underdeveloped countries, long hours spent indoors, the rise in higher education, and increased screen time [Dolgin, 2015]. Myopia has increased its prevalence all around the world. For example, from the early 1970s to the early 2000s, the number of myopes in the 12-54 age group increased from 25% to 41% in the USA [Vitale et al., 2009]. The situation is even worse in several parts of East Asia. For instance, in 2010, 96.5% of 19-year-olds in Seoul were myopic [Jung et al., 2012]. Myopia can be corrected by spectacles, contact lenses, or laser surgery, but

the axial elongation of the eyeball is irreversible [G. Morgan et al., 2012]. Many people's quality of life is impacted by myopia, and they may struggle with routine daily activities such as reading, working, driving, social events, and sports. Also, in some developing nations, many people may lack access to proper medical care and remain uncorrected.

The dramatic increase in high myopia is also a serious concern, as the number of high myopic people, now about 300 million, is expected to increase to roughly 1 billion in 2050 (*Figure 1.29*). High myopia can lead to pathological myopia, which is one of the primary causes of visual impairment and blindness [Jonas et al., 2021; Xu et al., 2006]. Pathological myopia refers to severe degrees of high myopia in which the ocular posterior segment changes and may cause myopic macular degeneration (MMD) and myopic maculopathy (*Figure 1.30*) [Jong, 2021]. Moreover, the risk of retinal detachment increases with the rate of refractive errors, and even though it can happen in mild or nonmyopic individuals, high myopic people have the highest risk [Moisseiev & Yiu, 2017]. In highly myopic individuals with excessive axial length, glaucoma-like optical neuropathy can happen, which leads to blindness [Flitcroft et al., 2019]. Less frequently myopia may also cause glaucoma, or cataract [Haarman et al., 2020].
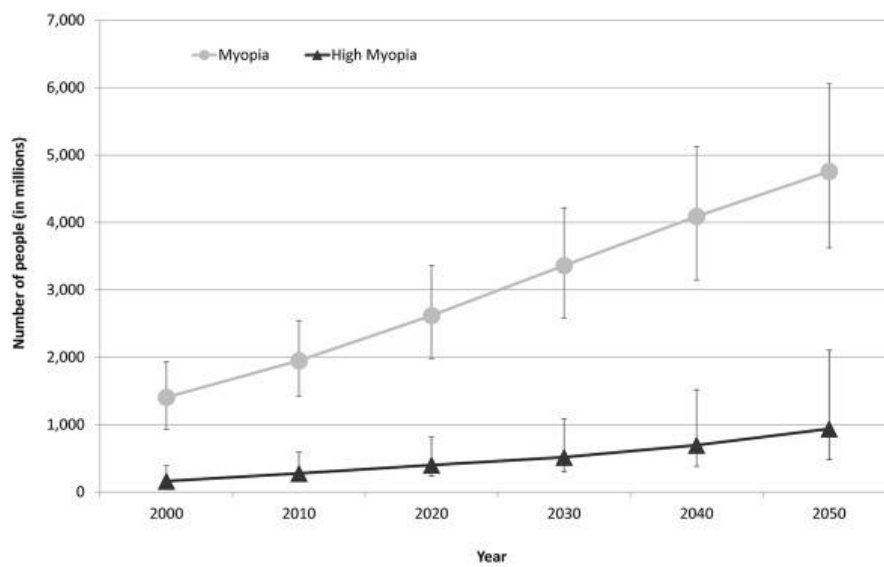
Figure 1.29. Myopia and high myopia prevalence from 2000 to 2050 (Figure adapted from [B. A. Holden et al., 2016]).

Furthermore, myopia is a significant economic burden on society, with an estimated annual cost of €234 billion ($250 billion) in the United States and €307 billion ($328 billion) in Asia [Chua & Foster, 2020; Sankaridurg et al., 2021]. These factors indicate the substantial need to investigate myopia's risk factors and conduct some interventions to control the myopia epidemic.
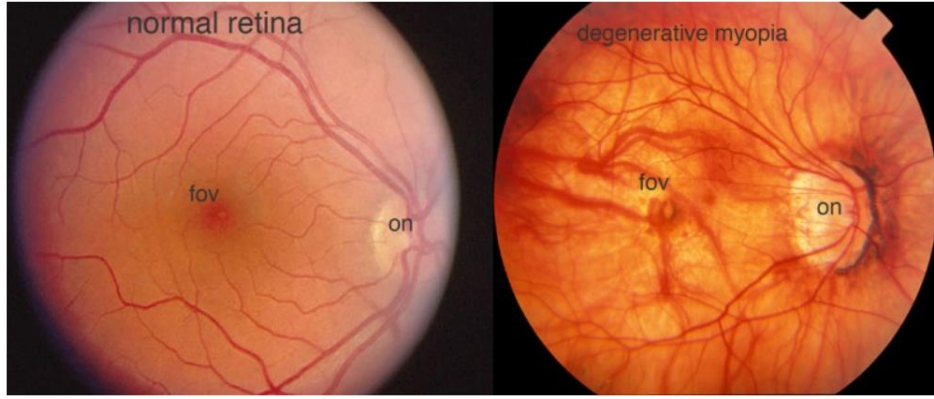
Figure 1.30. *Fondus retinal images of a healthy eye (left) and a degenerative myopic eye (right). The latter is thinner and stretched. Furthermore, there is optic nerve damage (on) and pigmentation on the fovea (fov) (Image credit: James Gilman and the Moran Eye Center ophthalmic photography department. The figure is adapted from* [Carr & Stell, n.d.]*).*

1.9. Contrast sensitivity

"Contrast sensitivity defines the threshold between the visible and invisible" [Pelli & Bex, 2013]. It is a critical factor in everyday tasks such as reading, face recognition, and driving. In this section, the contrast sensitivity function, its relationship with VA, and its measurement methods are discussed.

1.9.1. Definitions

The contrast threshold, usually expressed in percent, refers to the minimum difference in luminance between bright and dark areas that is required to distinguish between an object and its background. Various definitions of contrast, including Michelson, Weber, and RMS, have been proposed:

$$C_{Weber} = \frac{L_{max} - L_{min}}{L_{background}}, \qquad C_{Michelson} = \frac{L_{max} - L_{min}}{L_{max} + L_{min}}, \qquad C_{RMS} = \frac{L_{\sigma}}{L_{\mu}} \qquad (1.13)$$

where L_{max}, L_{min}, and L_{μ} are, respectively, the maximum, minimum, and mean luminance of the object, L_{σ} its standard deviation, and $L_{background}$ the luminance of the background. Selection of each formula is dependent on the stimulus and experimental conditions. For letter stimuli, Weber contrast is typically used, Michelson contrast is more appropriate for gratings, and RMS contrast is chosen for efficiency calculations and natural targets [Pelli & Bex, 2013]. Bouguer (1698–1758) was the first to measure contrast sensitivity with a screen, two candles, one close to the screen and the other 10 times farther, and a bar in between them. The subject was asked to identify the shadow of the bar on the screen. The Weber contrast was approximately d^2 / D^2,

D and d being the distance to the far and near candles, and a 1.6 % threshold was obtained. In 1860, Fechner, in his revolutionary book "Elemente der Psychophysik," reported a 1% threshold for numerous stimuli, regardless of their size and luminance. In 2012, Robson and Pelli replicated Bouguer's experiment and found a very similar value [Pelli & Bex, 2013].

1.9.2. *Contrast sensitivity function (CSF)*

Contrast sensitivity is the inverse of the contrast threshold. The contrast sensitivity curve for sinusoidal gratings as a function of spatial frequency is known as the contrast sensitivity function (CSF) [Watson, 2018]. A variety of stimuli types are used in basic studies of contrast sensitivity, but sinusoidal patterns are typically preferred. The benefit of the sinusoidal pattern is that, according to Fourier optics, the luminance distribution of a scene may be regarded as a linear combination of several sinusoidal luminance gratings [Barten, 1999]. Schade performed the first measurement of contrast sensitivity at various spatial frequencies in 1956 [Schade, 1956]. Later CSF studies show that neurological and ocular factors can both influence the CSF. There is a neurological effect because different visual channels are influenced by specific spatial frequency bands [Campbell & Robson, 1968]. *Figure 1.31 (a)* shows the typical behavior of a CSF. With increasing frequency, the CSF climbs to a peak at 3 to 6 cycles per degree and then gradually falls. This tail is dominated by the loss in retinal image quality caused by diffraction, aberrations, or scattering, and therefore it resembles the MTF [Artal & Navarro, 1994]. *Figure 1.31 (b)* shows the CSF function to sink and shift toward lower spatial frequencies as the aging eye losses the ability to convey fine details to the retinal image.

1.9.3. *Contrast sensitivity as a clinical test*

Even though contrast sensitivity and visual acuity are connected, they assess separate visual function parameters, and a measurement of contrast sensitivity may expose a change in visual function that is undetected by a conventional VA test [Arditi, 2005]. The VA test concentrates on the maximum spatial frequency an individual can see in high contrast, while the contrast sensitivity measurement quantifies the lowest contrast that can be detected at each spatial frequency. Therefore, a subject may have normal VA but decreased contrast sensitivity causing them a loss in visual quality. A mixture between these two tests, the contrast acuity test, consists of measuring visual acuity with stimuli of different contrast levels.

Low contrast sensitivity can reveal a hidden clinical condition [Owsley, 2003]. Poor contrast sensitivity may be due to ocular disorders such as myopia, cataracts, glaucoma, and age-related

macular degeneration (AMD) [Pelli & Bex, 2013]. Many ocular diseases decrease the CSF at all spatial frequencies, while others only affect certain ranges. For instance, mild myopia and amblyopia do not seriously affect contrast sensitivity at low spatial frequencies but reduce sensitivity at high frequencies [Charman, 1979; Freedman & Thibos, 1975]. Glare (e.g., due to cataract) and AMD, on the other hand, have less of an influence on contrast sensitivity at higher spatial frequencies but they impact the CSF at lower frequencies. [Abrahamsson & Sjöstrand, 1986; Sunness et al., 1997]. Thus, contrast sensitivity measurement can be a more sensitive test in some cases and provide significant information that may be hidden from the VA test [Owsley, 2003].

(a) *(b)*
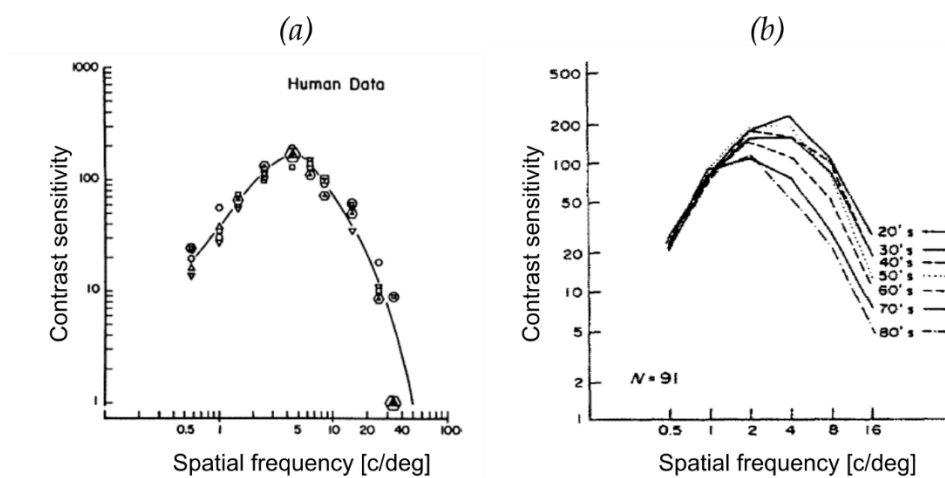
Figure 1.31. *(a) Individual (symbols) and mean (line) CSF for 5 young to middle age adults (Figure adapted from [De Valois et al., 1974]). (b) Mean CSF for various age groups (Figure adapted from [Owsley et al., 1983]).*

1.9.4. *Measuring contrast sensitivity*

Contrast sensitivity can be measured using printed charts, e.g., Pelli-Robson charts, or by computer-controlled displays. In clinical examinations, the faster printed charts approach is utilized, whereas the computer method is a common practice in psychophysical research experiments. The computer measuring method is flexible and can be customized; however, the display must first be gamma corrected [Owsley, 2003]. A typical stimulus in contrast sensitivity studies is the Gabor patch, consisting of a sinusoidal grating with Gaussian-blurred boundaries to avoid sharp edges with the background.

Contrast sensitivity can be evaluated either objectively or subjectively. Subjective techniques such as the adjustment method where the subjects are instructed to search for the lowest contrast that allows them to see a grating of a specific spatial frequency are simpler and faster

but less accurate and precise as they depend too heavily on the subject's decision-making consistency. Objective techniques rely on forced-choice tasks to avoid this problem. They can be considered accurate but precision depends on the number of repetitions so these methods tend to be more time-consuming. Different forced-choice schemes can be used, including discrimination, yes/no tasks, and identification [Pelli & Bex, 2013]. The procedure typically consists of several trials with a series of fixed contrast levels for each spatial frequency explored. The success rate of the subject as a function of contrast is then fit to a psychometric function to determine the contrast threshold as a function of frequency. This type of arrangement requires a large number of trials and is time-consuming. As a consequence, several strategies have been developed to optimize psychophysical data acquisition, such as the adaptive staircase technique, APE, QUEST, PEST, ZEST, or φ [Leek, 2001], although they will not be used in this thesis.

1.10. Objectives of this thesis

Until it is lost with age, the human eye can change its optical power to focus at different distances, a process known as accommodation. In most young subjects, it is a fast and fairly accurate mechanism that allows them a clear vision at all distances. It has been suggested that myopia onset and/or progression may be related to alterations in the accommodative process that could upset the emmetropization process.

On the other hand, even when steadily looking at an object at a fixed distance, the optical power of the eye fluctuates more or less randomly. It is unclear if these fluctuations are an undesired inability of the eye to keep a constant focus or may serve a purpose in the accommodative process. In any case, from an optical point of view, fast fluctuations of defocus would be expected to produce some kind of blurring in the retinal images, which could degrade visual quality. In this context, the objectives of this thesis are the following:

I. To improve a preexisting binocular open-view Hartmann-Shack system and to increase its data acquisition speed. To incorporate a tunable lens to induce defocus fluctuations in order to study its effect on visual function.

II. To study accommodation dynamics in emmetropic and myopic subjects. To perform a correlation analysis between refractive error and different parameters related to focus, convergence, and pupil size, trying to determine if there are potential risk factors of myopia related to accommodation.

III.   To study the effect on contrast sensitivity of fast periodic oscillations of defocus with different amplitudes, to determine the vulnerability or resilience of the visual system when confronted with fast changes in focus. To develop a simulation protocol to account for the loss in image quality that said oscillations of defocus are expected to produce in the retinal image.

Chapter *2*

"As for me, I want to have fun while I'm working. Now not everyone thinks physics is fun, but I do. I think experimental physics is especially fun, because not only do you get to solve puzzles about the universe or on Earth, there are really cool toys in the lab."

Donna Strickland

Chapter 2.   Instrumentation and methods

This chapter describes the optical setup, instruments, and calibration methods employed in this thesis. The open-view system and its different arms are outlined. The system was constructed on an optical bench at the University of Murcia's Laboratory of Optics (LOUM). The steps for calibrating the wavefront sensor and its optomechanical construction are explained. Following that, the software package that was developed in the LOUM for the HS for real-time measurements, as well as to control the stimuli and the tunable lens is covered. Furthermore, the principles of operation of the electrically focus tunable lenses, as well as the calibration procedure in both static and dynamic modes are addressed. The LCD's gamma correction for the contrast sensitivity experiment is also described. Finally, the simulation of contrast loss caused by induced periodic blur fluctuation is discussed.

2.1.   Binocular open-view HS optical setup

The binocular open-view Hartmann-Shack system consists of three arms: illumination, measurement (including a monitoring sub-path), and calibration (*Figure 2.1*). The eye is illuminated from the outside and the beam reflected back from the retina travels through the measurement path and is detected by the HS sensor that is positioned conjugated to the pupil plane. In *Figure 2.1*, top and lateral views of the optical system are provided. The dual illumination paths, the measurement path, and the pupil monitoring path are shown in magenta, red and blue colors, respectively. The calibration arm is depicted with dashed lines and will be discussed later. The calibration arm is mounted on the same table for convenience, but it is detached from the instrument. The concept and basic arrangement of the open-view sensor used in this study were previously reported [Chirre et al., 2014]. For this thesis, it has been improved both optically and computationally [Ghoushchi et al., 2021].

2.1.1. Illumination arm

An infrared (IR) laser source with peak emission at 1055 nm (Broadband ASE source 1μm band, Multiwave Photonics, Portugal) was used for illumination. The application of IR laser sources for ocular wavefront sensing with HS sensors has been successfully shown [Fernández & Artal, 2008], but using this source causes longitudinal chromatic aberration, which was compensated in the software. Since the IR laser source is invisible, the subject is unaware of its presence while fixating on near and far targets. This gives our setup an advantage over
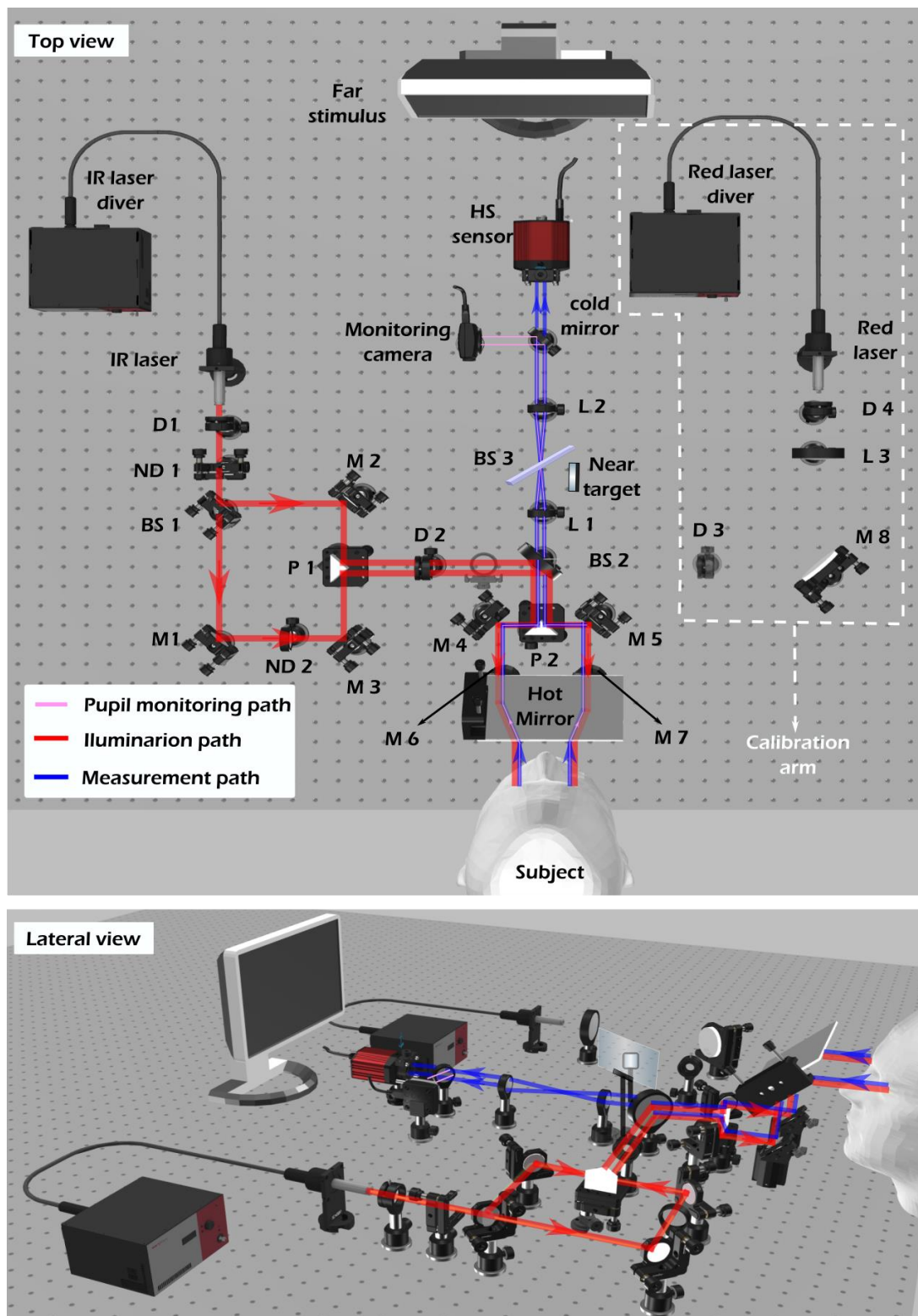
Figure 2.1. *Top and lateral views of the open-view apparatus. The illumination, pupil monitoring, and measurement paths are displayed in the figure. D, ND, BS, P, and L stand for diaphragm, neutral density filter, beam splitter, prism, and lens, respectively (The 3D schematics were drawn using 3doptix [3doptix, n.d.])*

that used 850 - 900 µm wavelength which is partially visible to human vision [Hampson et al., 2008; M. Kobayashi et al., 2008], although it makes the setup construction and alignment process more complex.

The laser beam is expanded using a fiber collimator and its size and intensity are controlled by diaphragm D1 and a rotating Natural Density (ND) filter ND1, respectively. The laser light passes a pellicle beam spiller BS1 (%45 reflection/ %55 transmissions) and is split into two same-size beams. One beam after being reflected by beam splitter BS1 and mirror M2 hits one side of reflective IR-coated prism P1. The other beam is transmitted by BS1, reflected by mirrors M1 and M3, and hits the other side of prism P1. Since the pellicle beam splitter is 45/55, we used neutral density filter ND2 to equalize the intensity of the beams. Prism P1 redirects them parallel to each other through double diaphragm D2, to produce two narrow pencils with a convenient distance between them to fit into a single two-inch pellicle beam splitter, BS2 (%8 reflectance / %92 transmission). This high transmission beam splitter was selected to make the measurement arm light efficient by maximizing the intensity returning to the HS sensor. The beams reflected from DS2 are redirected toward reflective prim P2 and mirrors M4 and M5 mounted in stages in order to increase the distance between them to account for the interpupillary distance while keeping them parallel to each other. Finally, a twin periscope arrangement composed of M7 and M6, and a large hot mirror convey the illumination beams to an upper level towards the subject's pupil plane. The reflectance of the hot mirror (Edmund Optics, NT43-453, USA, dimension 101.6×127.0 mm) is above 95 % for 750 – 1150 nm light (*Figure 2.2*) and it is tilted 45° horizontally to provide the subject with a large open field of view. The intensity of the illumination beams is at least one order of magnitude below the safety limits [Laser Institute of America, 2007].
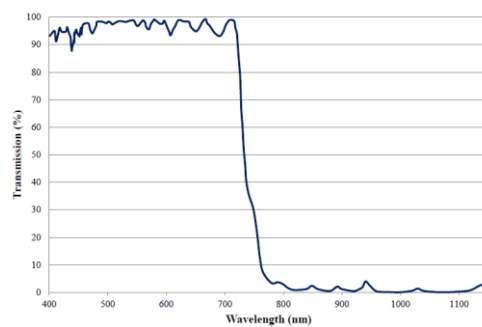
Figure 2.2. *Transmission spectrum of the hot mirror (Figure adapted from [Edmund Optics, n.d.])*

2.1.2. *Measurement arm*

The IR light reflected from each eye's retina is redirected back to the lower level by the hot mirror, compacted by the mirror arrangement to remove most of the interpupillary distance, transmitted by beam splitter BS2, and de-magnified by a 0.3-magnification telescope. The two packed, contracted beams fit inside the aperture of the H-S sensor conjugated to the subject's pupil plane. The telescope consists of lenses L1 and L2, with focal distances of f_1=300 mm and f_2= 100 mm, respectively. This arrangement produces two circular distributions of spots close to each other but not overlapping and allows simultaneous measurement of both eyes' aberrations, avoiding hardware duplication. In this thesis we used a 192-mm-pitch microlens array (APO-Q-P192-F3.17, OKO Tech, The Netherlands) with 3.17-mm focal length, which is shorter than in previous versions of the open-view HS sensor [Chirre, 2017b], thus increasing the dynamic range for myopic subjects. The system for accommodation dynamics measurements included a CCD camera that operates at 25 Hz (Hamamatsu C7500-51, Hamamatsu K.K., Japan) and a chinrest mounted on a 3D stage. For the experiment on contrast sensitivity under defocus oscillations, the system was upgraded with a 60 Hz CMOS camera (DCC3240N, Thorlabs, Inc., USA) and the chinrest was replaced with a bite bar.

The distant target was an SXGA LCD monitor (Dell UltraSharp 1704FPT 17" Flat Panel) located 2.8 m (0.36 D) away. Spatial resolution was 210 c/deg and 91 c/deg for near and far targets, respectively. The near target for the accommodation experiments was an SVGA+ 0.6" OLED micro-display (eMagin, USA) located 36 cm (2.8 D) from the subject. Both stimuli had the same field of view (1.3°) and were calibrated to have roughly the same luminance (14.3 and 15.4 Cd/m2, respectively). The stimuli were combined using a 50/50 beam splitter, BS3 in *Figure 2.1,* vertically tilted to put them both in line with the subject's gaze direction.

2.1.3. *Pupil monitoring path*

The apparatus includes a pupil monitoring path to ensure that the subject's pupils are adequately positioned. *Figure 2.3* shows its schematics. Two IR LEDs (λ=850 nm) are used for illuminating the anterior part of the eyes. The 850-nm light reflected from the irises follows the same path of the 1050-nm light for wavefront sensing but after the de-magnifying telescope is reflected on a long pass dichroic edge filter (Thorlabs, DMLP950, USA), with a cutoff frequency of 950 nm (*Figure 2.4*), towards a second CCD camera (Hamamatsu C7500-51, Hamamatsu K. K., Japan).
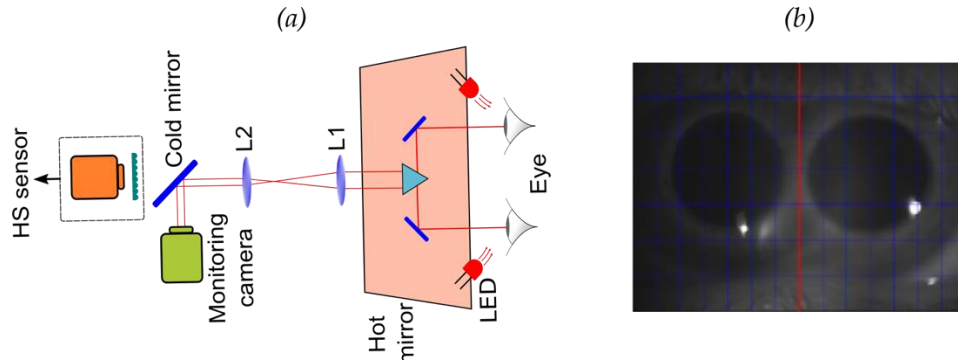
Figure 2.3. *(a) Pupil monitoring path (b) Example of pupil monitoring image*

This camera is focused at a plane in object space that is conjugate to the HS sensor. therefore when the subjects' pupils are seen in focus, proper conjugation with the HS sensor's measurement plane is assured.
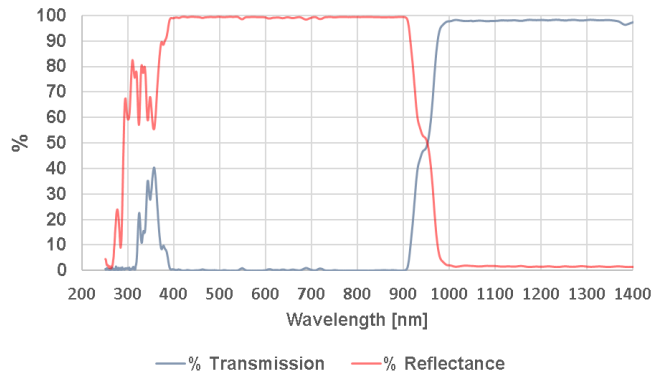
Figure 2.4. *Transmission and reflectance spectra for DMLP950 long pass filter (Figure adapted from [Thorlabs, n.d.-b])*

2.1.4. *Measurement arm alignment*

For aligning the measurement arm a diaphragm was positioned in one of the channels in the pupil plane that was illuminated with a collimated beam. Lenses L1 and L2 were adjusted to make an afocal system with the diaphragm in the focal point of L1 (*Figure 2.5*). Both lenses L1 and L2 were mounted on 2D stages, and their tilts were corrected by following their back reflections on the diaphragm. Later the HS sensor unit was added to the measurement arm. The sensor was placed in a plane conjugate to the pupil plane, with its micro-lenses array in the focal plane of L2, which was ensured by imaging the micro-lenses through lens L2 with another camera that was focused to infinity. Finally, the dichroic cold mirror, which is mounted on a flip mount, was added, and the pupil monitoring camera was focused on the diaphragm in the pupil plane.
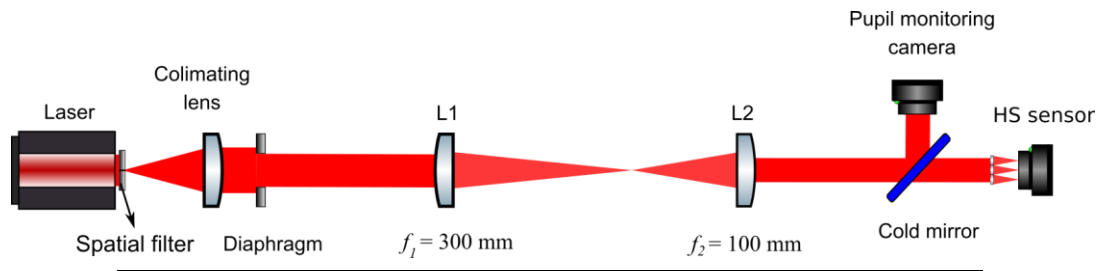
Figure 2.5. *Measurement arm alignment.*

2.1.5. *Calibration arm*

The calibration arm uses a fiber-coupled 660-nm laser source with an FC/PC fiber head (S1FC660, Thorlabs, Inc., USA). The single-mode fiber output has a diameter of 3.6 to 5.3 µm, so it can act as a pseudo-point source. A diaphragm (D4) and a collimating lens (L3) produce a collimated beam of controlled diameter. Disconnected from the system in normal operation, it can be engaged to replace the IR dual beam by means of mirror M8 and a flip mirror and is used to reset the twin periscope arrangement before starting experiments on a new subject, to a ground state of horizontal, parallel beams, 60 mm away from each other, which is the mean IPD. For each particular subject, mirrors M4 to M7 are adjusted to both avoid corneal reflection and adjust for the individual interpupillary distance to keep the images of both pupils inside the HS sensor (*Figure 2.6 (a)*).
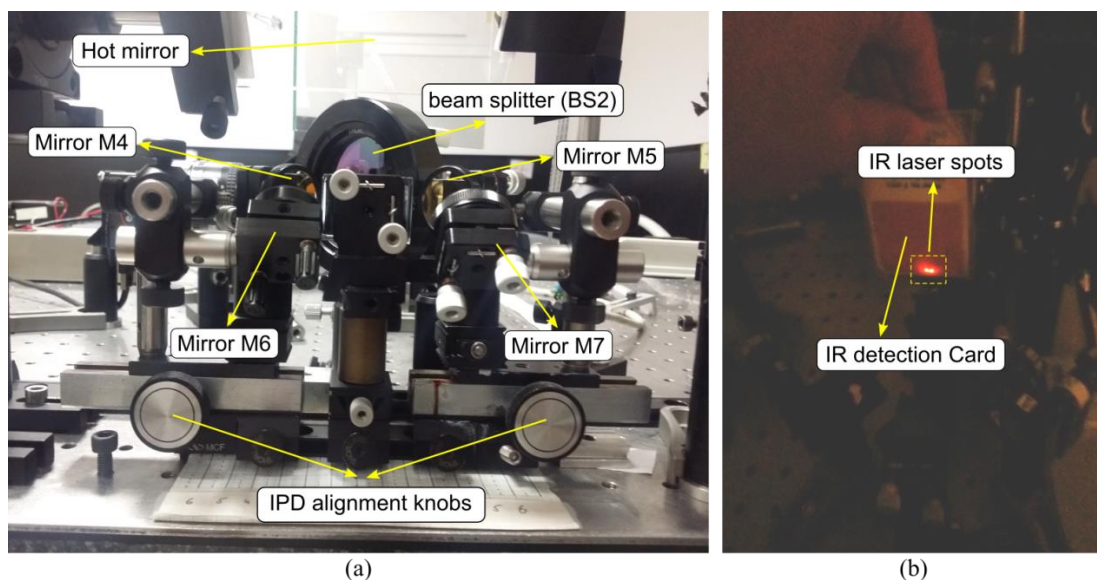
Figure 2.6. *The twin periscope (a) The IPD can be adjusted by using two stages that change the distance between the mirrors M6 and M7. (b) An IR detection card was used to detect the IR laser spots.*

The final arrangement is particular to each subject and it is sensible to restore the system to its initial position for the next one. However, this resetting is easier in visible light and the

calibration arm was installed in the same optical table for this purpose. After use, the flip mirror is folded and double-check is taken with the IR beams (*Figure 2.6 (b)*).
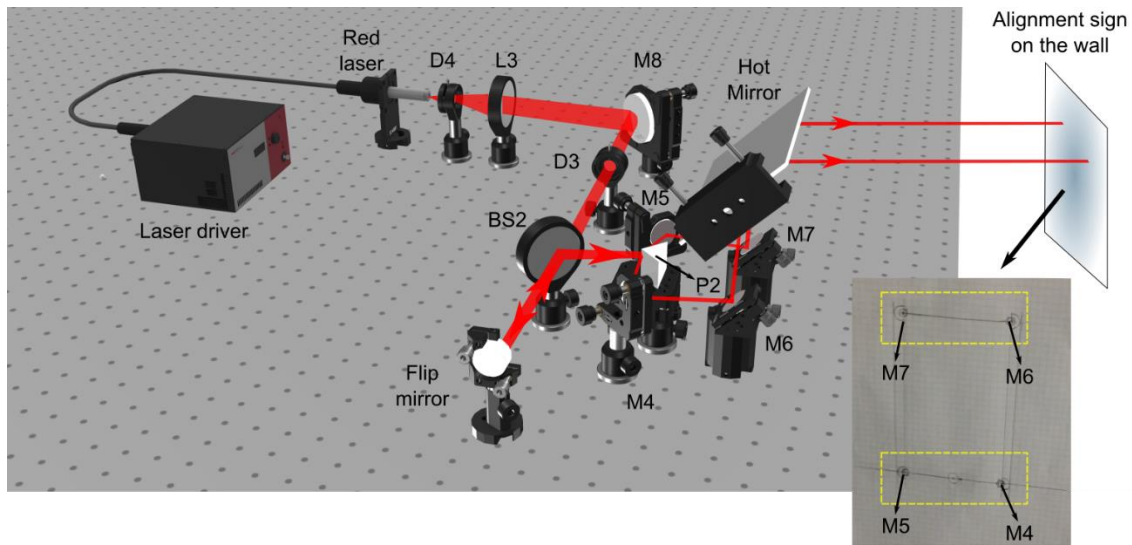
Figure 2.7. *Calibration arm engaged for twin periscope resetting. Inset: marks in the wall for alignment*

Additionally, the calibration arm was also used to calibrate the HS sensor, although this was done off-line, as will be described in the next section.

2.2. Hartmann-Shack sensor

The Hartmann-Shack sensor consists of a camera and a microlenses array. The trade-off between the dynamic range and sensitivity of the HS sensor is related to the microlens pitch size and its focal distance. It is important to calibrate the distance between the microlenses array and the CCD sensor and to ensure they are parallel to each other. The optomechanical design of the HS sensor was enhanced by attaching it as a single unit. With this approach, the sensor is portable and can be easily detached from the system, e.g., for calibration.

2.2.1. *Camera*

For the first experiment in this thesis (accommodation dynamics), a 25 Hz camera was employed (Hamamatsu C7500-51, Hamamatsu K. K., Japan). It contains a half-inch CCD sensor with a resolution of 752×582 and a pixel size of 8.3×8.6 μm (H × V). This camera's quantum efficiency drops towards IR but was still high enough to record good HS images with our selected 1050 nm wavelength (*Figure 2.8*). The camera has a BNC connection which was converted to USB with an adaptor.
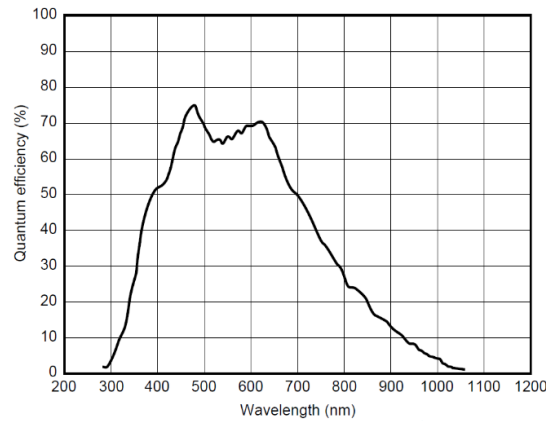
Figure 2.8. *Hamamatsu C7500-51 quantum efficiency as a function of wavelength (Figure adapted from C7500-51 datasheet).*

For the second experiment (contrast sensitivity through defocus oscillations), the HS sensor was updated to a faster CMOS camera (DCC3240N, Thorlabs, Inc., USA) to improve image acquisition speed to 60 Hz frame rate. It is a 1.3-Megapixel camera (1280×1024) with square 5.30-µm pixels. Its 1/1.8-inch sensor provides a reasonable quantum efficiently in the NIR range (*Figure 2.9)*. Connection is via USB3 and frame rate and exposure time can be controlled digitally.
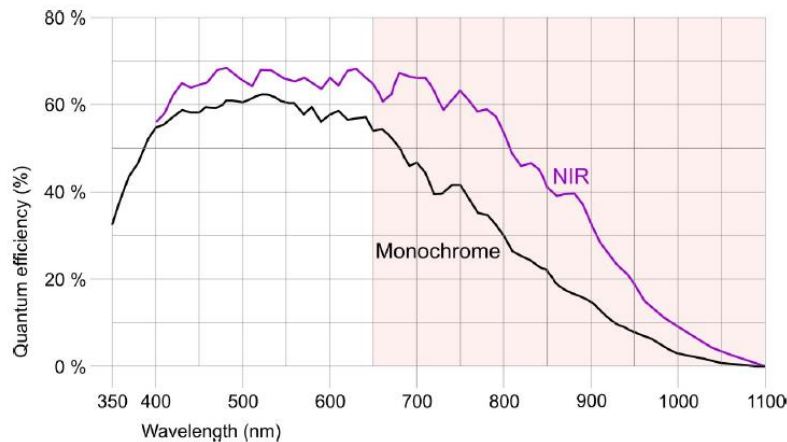
Figure 2.9. *Thorlabs DCC3240N quantum efficiency (purple line) as a function of wavelength (Figure adapted from* [Thorlabs, n.d.-a]*).*

2.2.2. *Microlenses arrays*

The same microlenses array (APO-Q-P192-F3.17, OKO Tech, The Netherlands) was used for both experiments, with a 3.17-mm nominal focal length and 192-µm lens pitch (*Figure 2.10*). Each lenslet corresponds to 23 C7500-51 pixels and 36 DCC3240N pixels, and considering the magnification of the system, is conjugated to a 572-µm square section of the subject's pupil. Using a shorter focal length than previous versions of the apparatus increases the dynamic range of the sensor, particularly for defocus.
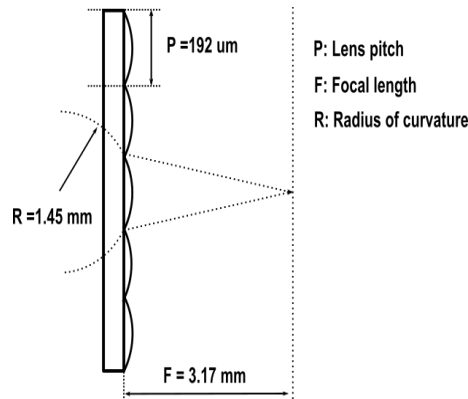
Figure 2.10. *Microlenses array schematics.*

2.2.3. *HS calibration*

Two versions of HS were used in this thesis, employing the same microlens array but two different cameras. However, the calibration process is identical for both of them and only the Thorlabs-camera-based case will be described.

Any tilt or rotation or other kinds of misalignment between the image detector and microlens array may lead to the dislocation of the HS sensor spots and can affect the sensor accuracy [Pfund et al., 1998]. Although some defects can be compensated by using a reference image, proper positioning of the microlens and image detector is still important [Neal et al., 2002]. To minimize the misalignment issues due to mechanical housing, a holder for the microlens array was CAD-designed and printed with a high-precision 3D printer (Form 2, Formlabs Inc., USA). The camera was mounted on a precision stage so that the distance between CCD and the microlenses could be fine-tuned. The whole arrangement was mounted on a breadboard as a single unit (*Figure 2.11*).

To convert spot displacement into wavefront local derivative, simple triangulation can be applied using traveling distance or "effective" focal length. Although this distance can be conceptually identified with the nominal lenslet focal length, experimentally it is typically shorter because the plane producing sharper spots tends to be closer [Ruffieux et al., 2006] and is calibrated after the assemblage of the HS. The calibration procedure consists of measuring a series of known defocus values and obtaining, from fitting the sensor output, the ratio between nominal and effective focal distances [Chirre, 2017b; Prieto et al., 2000]. Although the open-view uses an invisible 1050-nm laser as illumination, calibration was performed in red using the calibration arm, as it is simpler to manage a visible beam and no discrepancies are expected

due to the wavelength change, since the physical distance to the image sensor and not the microlenses focal length.

Figure 2.11. *The arrangement of the HS sensor mounted on a precision stage. The microlens array in its 3D-printed holder is shown on the top right.*

To start the calibration the first step was obtaining a reference image (*Figure 2.12 (b)*) by shining a plane wavefront on the HS. A Plano-convex lens was used to achieve collimated illumination (*Figure 2.12 (a)*). The spot positions for that aberration-free case were taken as origin to compute spot displacement for aberrated wavefronts.

The effective focal length of the microlens, or the actual distance between the CCD and microlens array, is calculated by multiplying this correcting factor by the nominal focal length.
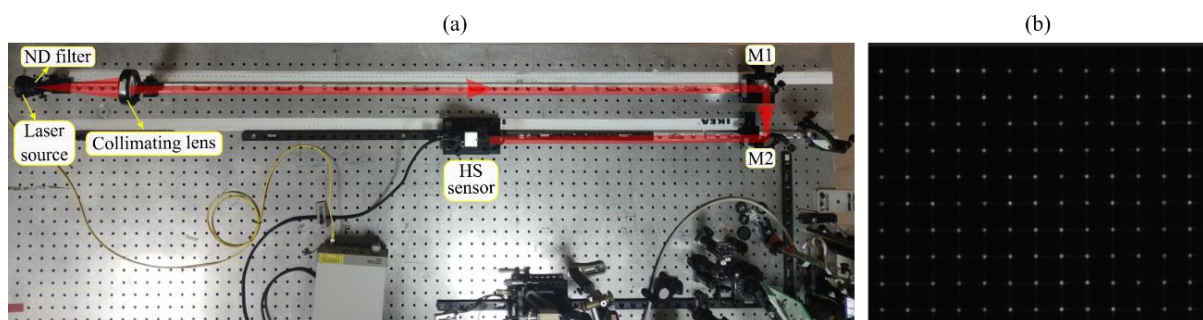
Figure 2.12. *(a) The calibration arm was built in parallel with the optical setup. (b) The reference image was obtained with collimated illumination.*

Next, the collimating lens was removed and the HS in its stage was placed at a series of distances, from 10 cm to 3 m, from the laser source, as illustrated in *Figure 2.13*. This presented the sensor with a series of spherical wavefronts with known curvature (the inverse of the distance). Processing the resulting spot images using the nominal focal distance yielded SE values slightly smaller than the expected ones.
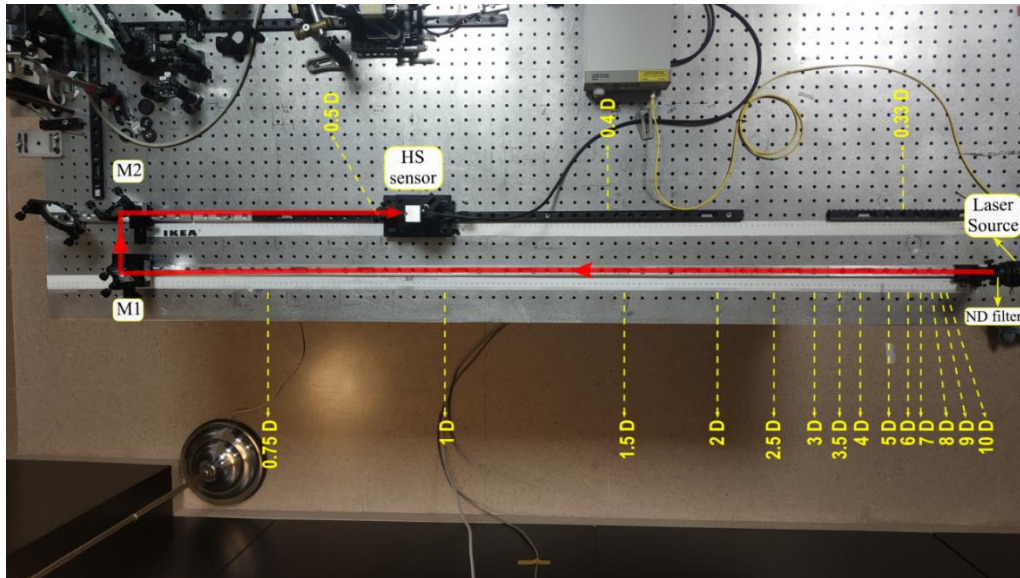
Figure 2.13. *HS sensor was moved in a rail system to various distances, from 10 cm to 3 m (10 D to 0.33 D defocus values). Since the single-mode fiber illumination represents a pseudo-point source the wavefront curvature in each distance is related to the defocus value of that location.*

The slope of the regression between them (*Figure 2.14(a)*) coincides with the ratio between nominal and effective focal length and can be used to determine the latter. Reprocessing the HS images with this value for the distance between microlenses and image detector produced SE values very close to expectations (regression slope virtually 1, see *Figure 2.14 (b)*). The effective focal length obtained was 3.15 mm.
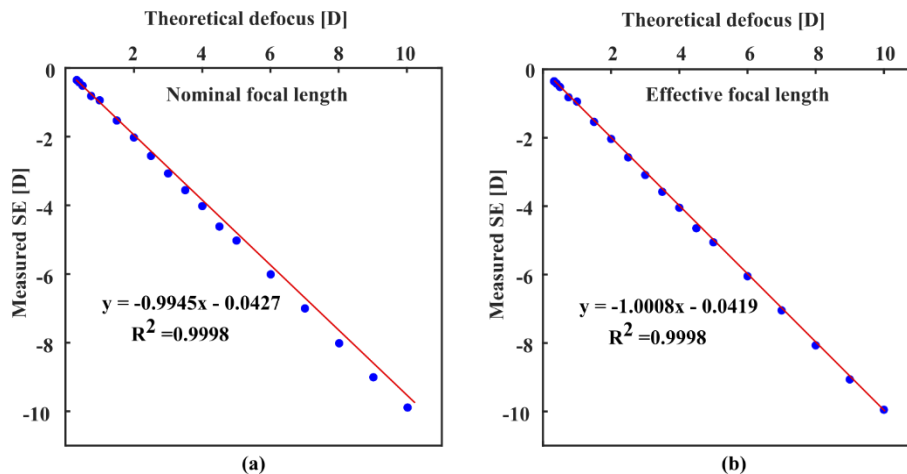
Figure 2.14. *Measured spherical equivalent vs. theoretical defocus in the center of the HS sensor for a pupil diameter of 2 mm for (a) nominal and (b) effective focal distance. The red line shows the y= -x line for reference and the blue dots are experimental data points.*

To test parallelism between the microlenses and the CCD sensor, the series of HS images for different distances were reprocessed over virtual pupils at the four corners (*Figure 2.15*).

Figure 2.16, shows the relationship between theoretical defocus and measured SE over 2-mm virtual pupils, corresponding to 6 mm in the subjects' pupil plane, using the effective focal length calculated for the center of the image. For each plot linear regression was applied and the slope values diverged from 1 by 1.6 %, or less, which was taken as an indication that the parallelism was good.
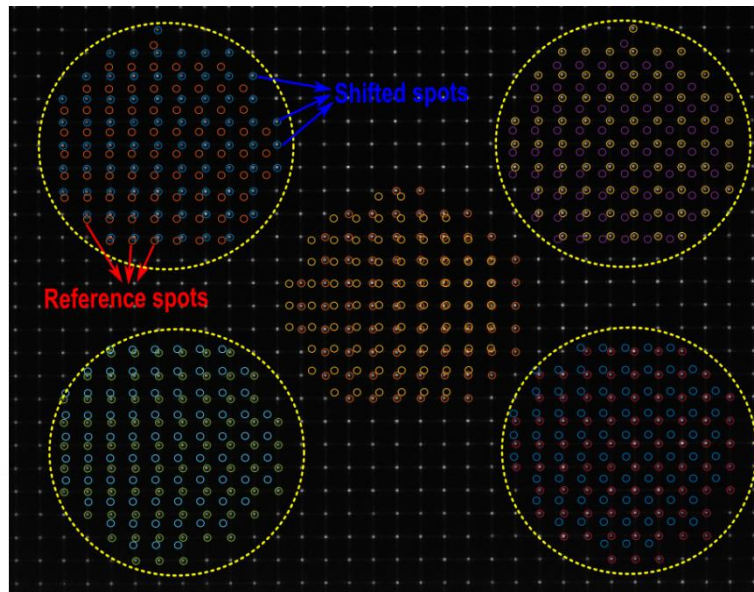
Figure 2.15. *Virtual pupils for testing parallelism (2 mm diameter). The hollow circles are reference spots and the filled circles are slightly shifted spots due to defocus.*

2.2.4. *HS sensor sensitivity calibration*

To test sensitivity, measurements were taken for distances between the source and HS ranging from 170 to 250 cm in 10 cm steps. This corresponded to changes in defocus in the range of hundredths of diopter, from 0.058D to 0.040 D (see *Figure 2.17*). In these measurements, the HS unit positioning error, (± 1 mm) was negligible in comparison with the displacement steps. Since pupil size determines the number of processed spots in each pupil, it can affect the sensor's accuracy [Neal et al., 2002]. To test this issue different virtual pupil sizes were considered, with radiuses ranging from 0.5 to 2 mm.

It is important to note that since there is a 0.33X magnification, a 0.5 mm pupil radius in the HS plane corresponds to a 1.5 mm pupil radius in the eye's plane. Applying smaller pupils becomes problematic as the data points become too scarce. The data for both measured and theoretical defocus Zernike, C_2^0, correspondent to distances of the HS sensor from the laser
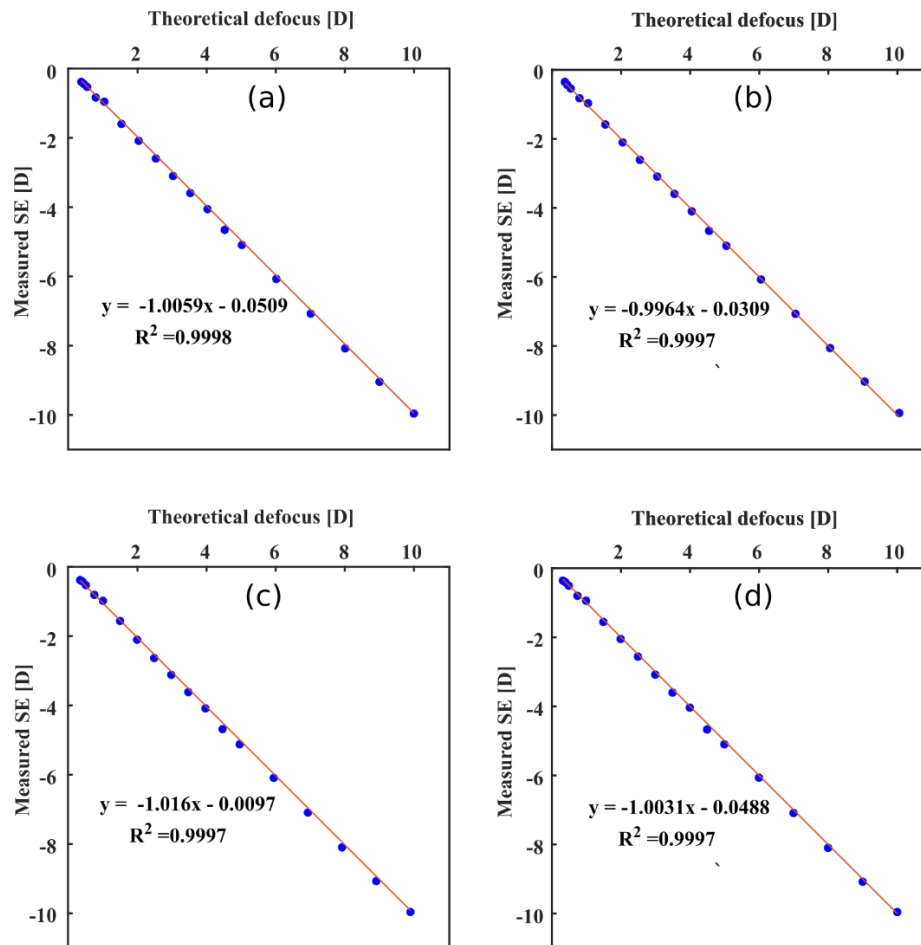
Figure 2.16. *Measured spherical equivalent vs. theoretical defocus at the four corners of the HS images: (a) Top left, (b) top right, (c) bottom left, and (d) bottom right. The red line shows the ideal case ($y = -x$), and the blue dots represent experimental data points.*

source were calculated for various virtual pupil sizes and presented in *Table 2.1*.

Even for very small defocus changes, the sensor shows good sensitivity and accuracy.
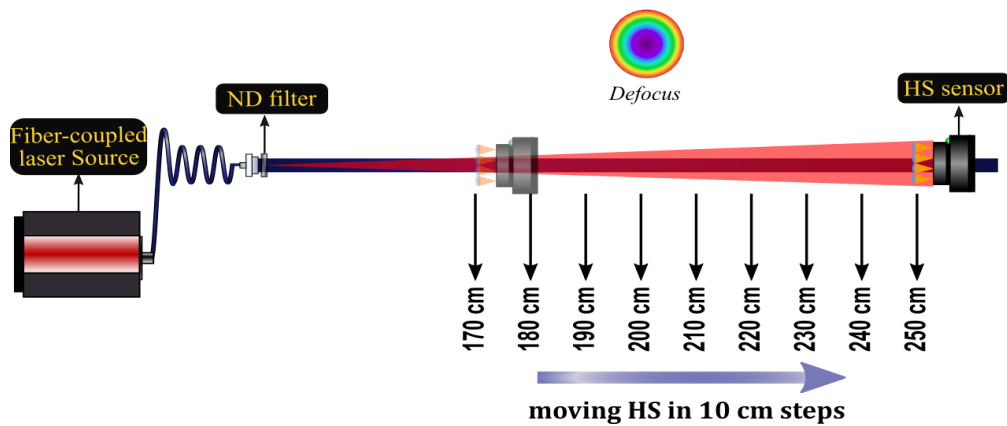
Figure 2.17. *Procedure for sensitivity calibration*

Table 2.1. *Theoretical and experimental defocus Zernike coefficients C_2^0 in µm, for various distances between HS sensor and laser source, from 170 to 250 cm, and different virtual pupil radiuses, from 0.5 to 2 mm.*

Disdtance [cm]	Theoretical C_2^0 [µm]					Experimental C_2^0 [µm]				
	r = 0.5 mm	r = 0.75 mm	r = 1 mm	r = 1.5 mm	r = 2 mm	r = 0.5 mm	r = 0.75 mm	r = 1 mm	r = 1.5 mm	r = 2 mm
170	0.02329	0.05071	0.08725	0.19500	0.33831	0.02331	0.05089	0.08729	0.19515	0.33845
180	0.02077	0.04599	0.08149	0.18393	0.32015	0.02028	0.04576	0.08084	0.18316	0.32051
190	0.02129	0.04654	0.07886	0.17517	0.30488	0.02075	0.04686	0.07939	0.17548	0.30502
200	0.02113	0.04323	0.07356	0.16587	0.28908	0.02081	0.04352	0.07379	0.16623	0.28960
210	0.01733	0.04025	0.07009	0.15953	0.27667	0.01716	0.04007	0.06974	0.15909	0.27650
220	0.01983	0.03946	0.06747	0.15264	0.26778	0.01963	0.03979	0.06760	0.15261	0.26782
230	0.01870	0.03796	0.06406	0.14580	0.25546	0.01800	0.03832	0.06418	0.14580	0.25561
240	0.01691	0.03517	0.06154	0.14153	0.24712	0.01686	0.03523	0.06141	0.14125	0.24697
250	0.01631	0.03477	0.05872	0.13444	0.23580	0.01631	0.03493	0.05868	0.13423	0.23578

In *Figure 2.18. (a)* the relationship between measured and theoretical defocus Zernike coefficients, for various vergences and processing virtual pupil radiuses is shown with colored circular markers. Moreover, the sensitivity of the sensor can be better appreciated in *Figure 2.18. (b)*, where the changes in C_2^0, both measured and theoretical, using the values at 250 cm as reference. All the data points lay on the 1:1 line.

2.3.   Detection algorithm and GPU implementation

2.3.1. Pupil tracking

There is an embedded pupil tracker in our HS system for accurate pupil detection that was previously reported [Mompeán et al., 2019]. The first task in the pupil tracking algorithm is selecting the pupil border. *Figure 2.19* shows an example image of the binocular HS sensor. The pupil detection steps are shown in *Figure 2.20*. First, the binocular HS image is divided into two sub-images, by simply taking half of the original image as the border for the left and the right eye images. The left image is represented in *Figure 2.20 (a)*. Since most of the brightness is in the spots and the aim is to detect the pupil border, a Gaussian filter is applied to smooth the image (see *Figure 2.20. (b)*) [Deng & Cahill, 1994]. The Gaussian filter provides the smooth circular area that is required for characterizing the pupil border.

In the next step, the thresholding algorithm is employed to choose the pixels inside the pupil [Sahoo et al., 1988]. The brightness of the left and right pupils may be different due to retinal reflectance and backscattering, as well as differences in pupil sizes. Therefore, each pupil is
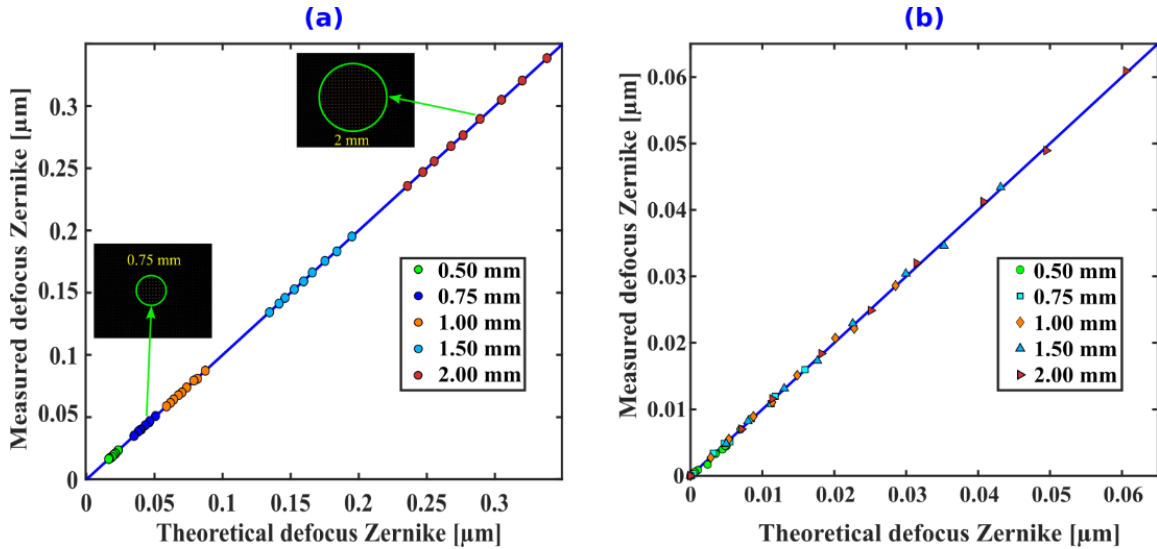
Figure 2.18. *Measured vs theoretical C_2^0. (a) Absolute values; (b) relative to 250 cm. Green, blue, orange, light blue, and brown markers correspond to 0.5, 0.75, 1, 1.5, and 2 mm pupil radii, respectively. Blue lines represent the 1:1 relationship.*

considered an independent image and processed separately, which results in a separate threshold value for each pupil. To select a proper threshold level for each frame, the Otsu method is applied [Otsu, 1979]. In this method, pixels are classified as background or foreground based on a threshold value. The threshold is calculated by iterating several threshold values to find the value that maximizes the intensity difference between the foreground and background.
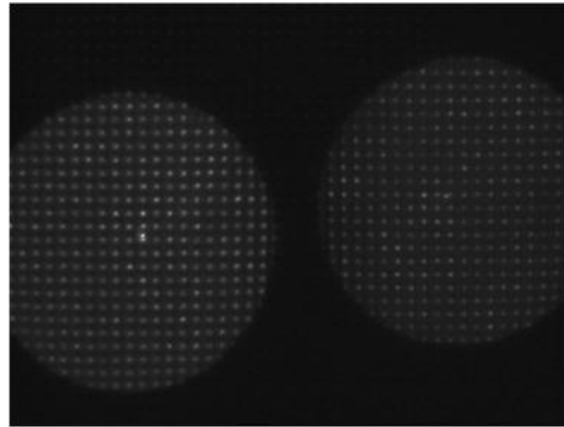
Figure 2.19. *Hartmann-Shack image of the left and right pupils (Figure adapted from [Mompeán et al., 2019]).*

On the other hand, the image after thresholding usually contains holes inside the pupil (see *Figure 2.20. (c)*), which must be eliminated to prevent false internal borders from interfering with the ellipse fitting in the last step of the algorithm. In order to remove these holes and

smooth the edge of the pupil, a morphological close operation is employed (*Figure 2.20. (d)*). This kind
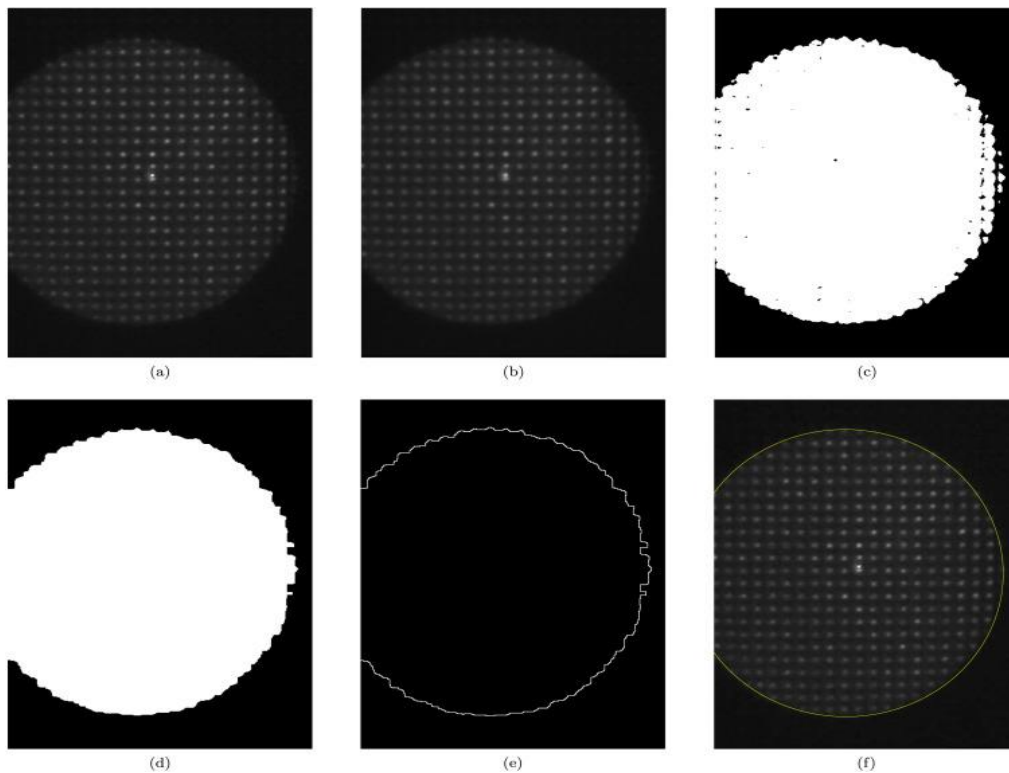
Figure 2.20. *Steps of pupil detection: (a) Original left sub-image. (b) Gaussian filtering. (c) Thresholding. (d) Morphological close operation. (e) Border pixels detected. (f) RANSAC algorithm (Figure adapted from [Mompeán et al., 2019]).*

of operation is typically used in image processing to remove small, isolated noise pixels or to connect broken parts of an object. The close operation is achieved by using a structuring element, which defines the shape and size of the neighborhood to be processed, and a dilation followed by an erosion operation. *Figure 2.20. (e)* shows the boundary identified by applying a straightforward method: a higher-threshold pixel is recognized as a bordering pixel if any of the eight surrounding pixels have lower threshold values. The last step is fitting an ellipse for the boundary pixels by Random Sample Consensus (RANSAC), which decides on the best-fitting ellipse (*Figure 2.20. (f)*). The RANSAC algorithm is an iterative method that detects outliers in data sets and provides a fitting or mathematical model for the data that does not include those outliers [Fischler & Bolles, 1981]. The RANSAC algorithm is a highly efficient approach when some of the boundary points are incorrect as it attempts to avoid those points in the fitting process. In addition, the RANSAC method is still able to produce good results when a section of the pupil is missing (falling out of the imaging area) or false (e.g., obscured by the eyelids producing border points that do not correspond to the pupil rim).

2.3.2. *Centroid search algorithm*

The critical part of image processing with the HS sensor is calculating the centroid spot locations in order to compute the correct wavefront aberrations. The algorithm that was used for centroid detection for the HS sensor was the pyramidal algorithm [Prieto et al., 2000]. The original algorithm was time consuming and, therefore, used for monocular offline aberration calculation. Recently, it has been improved and parallelized for binocular realtime aberration calculation and adopted in the current open-view system, with higher number of lenslets and shorter focal length [Mompeán et al., 2019]. The evolved algorithm is called Parallel Pyramidal Centroid Search (PaPyCS).

The algorithm divides the detected pupil into small square regions, each one representing a microlens. The theoretical size of these cells is known from the lenslet dimensions. The pyramidal algorithm iteratively searches for the center of mass in diminishing sub-apertures, re-entered for each iteration to the center of mass produced in the previous one. In each step, the minimum intensity in the window is subtracted from all pixels, allowing faster convergence of the algorithm. Window size is reduced by one pixel after each iteration until a sub-window of 3×3 pixels is reached. In eyes with large amounts of defocus (e.g., high myopes), spot cross-over is common in peripheral lenslets, especially for large pupils, limiting the dynamic range of the sensor. To overcome this issue the PaPyCS algorithm precalculates defocus in a small centered pupil and redistributes the positions of the sub-apertures using the probable inter-spot distance estimated from this information (see *Figure 2.21*). This dynamic grid increases the range of refractive errors that can be managed.

Additionally, the following discarding criteria are applied to reject suspect centroid data, e.g. due to blinks and corneal reflexes:

1) If a cell in the grid is empty or saturated, it is rejected.

2) If a cell is located too far or too close to the adjacent cells, it is rejected.

3) Any isolated centroid is rejected since it is difficult to compare it to the adjacent spots.

2.3.3. *GPU-based HS image processing*

Although standard ocular wavefront sensing for clinical use is typically static, several applications require real time measurements [Artal & Fernández, 2005; Chirre et al., 2015; Ghoushchi et al., 2021; Hofer et al., 2001]. In our case, we aim to study accommodation dynamics and other fast changes in aberrations. HS image processing using advanced methods

for spot tracking, such as the pyramidal algorithm, is a computationally demanding problem, especially when using fast, high-resolution cameras and dense microlens arrays. However, the calculations involved can be efficiently parallelized, making them suitable for graphical processing unit (GPU) processing [Mompeán et al., 2019].
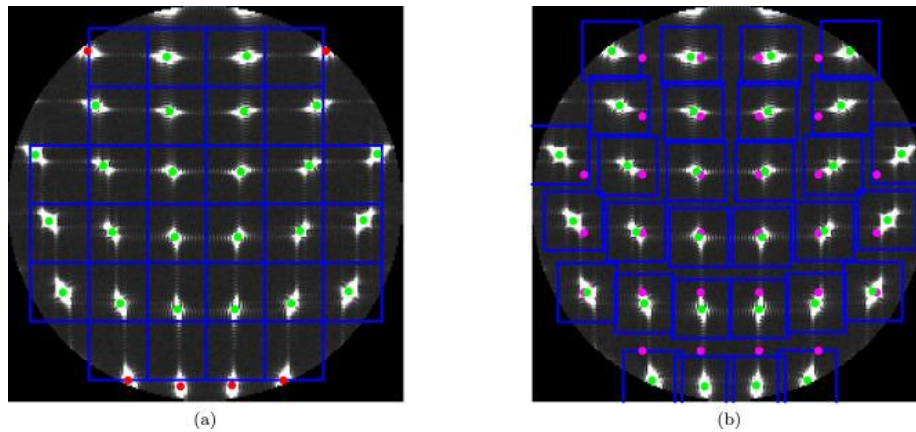
Figure 2.21. *Static (a) and dynamic (b) grids for centroid search (blue cells) Green dots: spots inside the window. Red dots: unreliable spots due to cross-over. Magenta dots in (b): center of the static grid. (Figure adapted from [Mompeán et al., 2019]).*

Nowadays, high-speed, high-resolution image processing is possible with the GPU. Nevertheless, the application of the GPU in high-speed image processing is not common in optics yet, and the algorithms are not optimized for GPUs. Although some researchers are starting to look at specialized implementations to speed up their programs [Reichenbach et al., 2014]).

The Parallel Pyramidal Centroid Search algorithm [Mompeán et al., 2019], is a parallel and robust method to process the images regardless of noise and other artifacts. Furthermore, various steps in HS image sensing are highly parallelized, including pupil tracking, detecting the centroids or center of mass in HS images, computing the local gradient of the wavefront, Zernike polynomial fitting, and reconstruction of the wavefront map. The mentioned steps were parallelized using CUDA [CUDA, n.d.]. A comparison of the GPU implementation for processing HS images with Reichenbach's and simple center of mass algorithms showed superiority in terms of processing time and accuracy for PaPyCS [Mompeán et al., 2019]. The GPU-powered system can process up to 380 high-resolution images of 1280×1280 per second. The graphics card used was a NVIDIA 980 GTX with 2048 cores, and CUDA was version 8.0. The complete description of the GPU approach is out of the scope of this thesis but can be found in [Mompeán et al., 2019].

2.4. Controlling software

For the open-view HS sensor, a customized program including an embedded eye tracking unit was implemented in C++ [Mompeán et al., 2019]. *Figure 2.22* shows a screenshot of the graphic user interface (GUI) of the HS program. The GPU computation provides binocular, fast calculations of aberrations and objective refraction at 60 Hz, limited by the frame rate of the   camera.
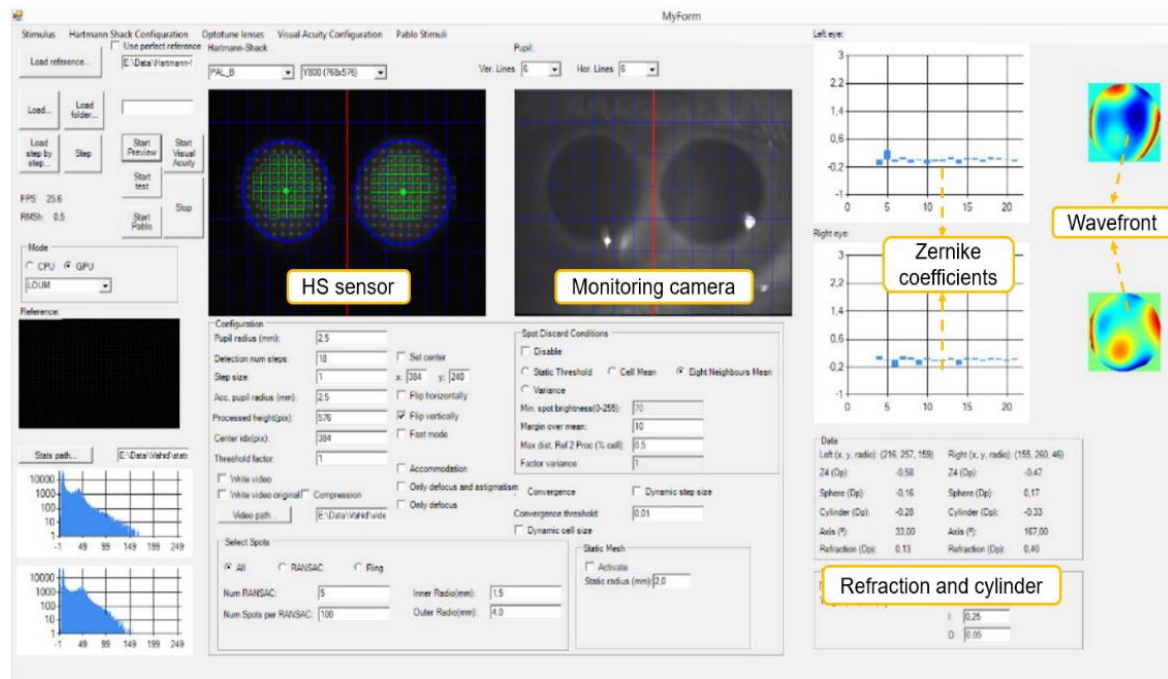
Figure 2.22. *Screenshot of the GUI of the binocular open-view HS sensor.*

The operator can observe the aberrations in real time. The GUI includes pupil tracking (blue pupils in *Figure 2.22*), initial windows for the pyramidal algorithm (green cells in *Figure 2.22*), and the wavefront map. Both pupil monitoring camera and HS sensor camera images are included in the GUI.The histograms allow the operator to monitor the intensity distribution in the HS images, and this is important to regulate the illumination beam in order to avoid saturation. The HS software produces a file with a series of results for each image in the frame sequence. Subsequent analysis was performed in MATLAB.

2.5. Focus tunable lens

In the last experiment of the thesis, we investigated the effect of fast, periodic changes in defocus on visual performance. These changes were introduced with an electrically focus tunable lens. Focus tunable lenses (liquid or optofluidic lenses) are active optical components whose focus can be rapidly altered in a specific range by changing electric voltage or current.

Focus tunable lenses have been around for a long time with a wide variety of applications in machinery, robotics [Chen et al., 2021] virtual reality (VR), augmented reality (AR) [Stevens et al., 2017], drone technology, and microscopy [Ghoushchi, 2015; Jabbour et al., 2014]. Recently, there have been applications in visual science in wearable presbyopia glasses [Mompeán et al., 2020a] and visual simulators for the simulation of various multifocal contact lenses that have been used in myopia control [Akondi et al., 2018]. The advantages of using these lenses include fast response time, various working distances, a one-time calibration, and reducing the setup size by avoiding using conventional zoom lenses.

2.5.1. *Operating principle*

The working principle of the tunable lens is shown in *Figure 2.23*. There is a liquid embedded in a polymer membrane. The electromagnetic actuator, through various electrical currents, applies force on the container, pumping or draining liquid from the lens. Therefore, the shape of the polymer changes and its focus can be actuated continuously. This is similar to the eye accommodation mechanism, in which the ciliary muscle actuates the crystalline lens focus by altering the lens shape.

We used an electrically focus tunable lens (EL-16-40-TC-VIS-20D, Optotune Switzerland AG). The lens has a 16 mm clear aperture, 7 ms response time, 40 ms settle time, and a -10 to +10 D optical power range. *Table 2.2* shows the tunable lens specifications.
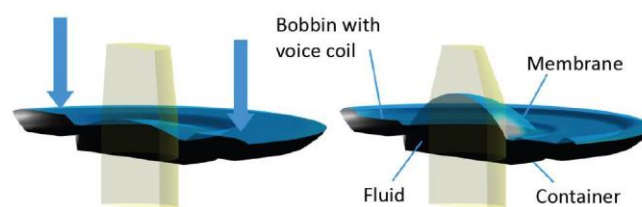
Figure 2.23. Working principle of an electrically tunable. The container shape can be changed by applying different electrical currents. Therefore, the lens focus can be controlled actively (Image adapted from [Optotune, 2022]).

There are some limitations to using this lens. Defocus changes can lead to temperature changes which can result in residual defocus drifts. There is a temperature sensor embedded in the lens housing to tackle this issue. The temperature sensitivity (S), in diopter/°C, can be defined as the defocus change per degree Celsius. The temperature sensitivity correlation with optical power is shown in *Figure 2.24*. Note that the temperature effect can be minimized by using a heat sink. Moreover, the wavefront of the tunable lens should be spherical; however, due to

Table 2.2. *Focus tunable lens (EL-16-40-TC-VIS-20D) characteristics (Table adapted from [Optotune, 2022]).*

Main specifications

Clear aperture	16	mm
Optical power: tuning range @ 30°C with Optotune's Lens Driver 4	-10 to +10	dpt
Wavefront error (@525 nm, 0 mA) Optical axis vertical / horizontal	~ 0.5 / ~ 2.5 (due to gravity coma)	λ RMS
Lens type	plano-concave to plano-convex	
Refractive index & Abbe number	nD=1.300, V=100	
Cover glass coating	420 to 1500 [1]	nm
Optical retardance @590nm	6.1	nm
Response time (typical at 30°C, 0 to +/- 250mA step)	7	ms
Settling time (typical at 30°C, 0 to +/- 250mA step)	40	ms
Lifecycles (10%-90% sinusoidal)[2]	>1'000'000'000	
Operating temperature[3]	-20 to 65	°C
Storage temperature	-40 to 85	°C
Weight	40	G
Temperature sensor & memory	STTS2004 (STMicroelectronics)	

Electrical specifications

Nominal control current with Lens Driver 4	-250 to 250	mA
Absolute max. control current	-500 to 500	mA
Power consumption	0 to 0.7 (nominal), 0 to 1 (absolute max.)	W
Motor coil resistance @ 30°C	12	Ω
Absolute maximum voltage (coil)	5	V
Absolute maximum voltage (temp. sensor)	4.3	V

gravity, there was a coma term of (2.5 λ wavefront error measured at 532 λ) in the horizontal axis. And finally, another issue with the lens is hysteresis [Torres-Sepúlveda et al., 2020] which means the output defocus of the lens depends on its starting point. *Figure 2.25* illustrates this effect by displaying the optical power response of several current steps from 0 mA to desired current value and vice versa.
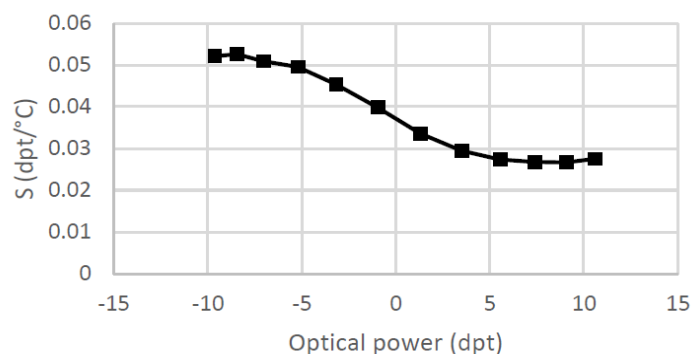
Figure 2.24. *Temperature sensitivity, S, for various defocus values (Figure adapted from [Optotune, 2022]).*
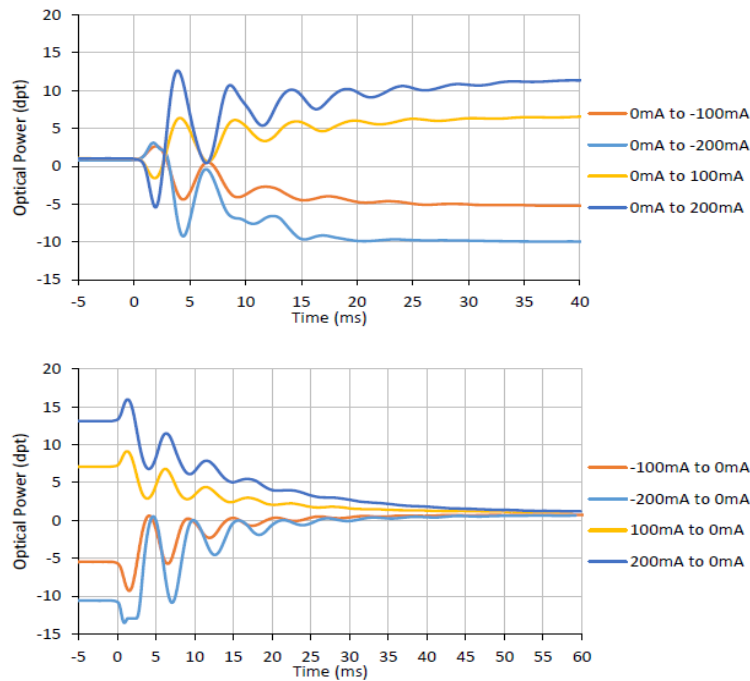
Figure 2.25. *Top and bottom plots display the optical power response of the tunable lens (EL-16-40-TC-VIS-20D) for several current steps from 0 mA to desired current value and vice versa (Figure adapted from [Optotune, 2022]).*

2.5.2. *Static calibration*

Since the tunable lens power is non-linear with voltage, a calibration was made. We attached the lens to the optical setup and calibrated it in static mode (setting the values one by one) using the HS sensor and an artificial eye (AE). We monitored the temperature to ensure focus stability and avoid overheating. We used the current range from -67 to 121 mA and measured the correspondent defocus values between -5.5 and 5.5 D. The values of current were randomized, applying each value for 100 ms, and the defocus values were measured with the HS sensor by employing the AE shown in ***Figure 2.26***.
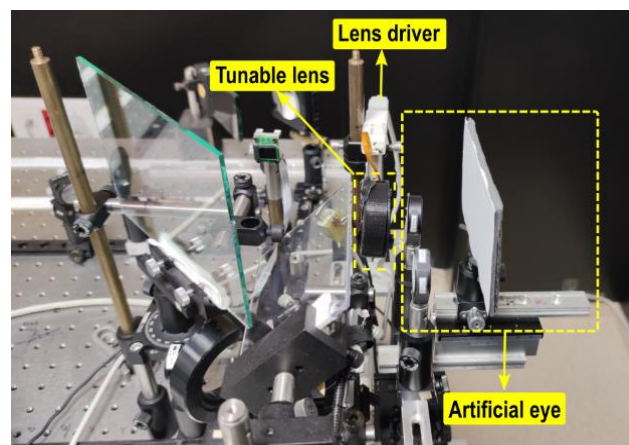
Figure 2.26. *Lens calibration setup.*
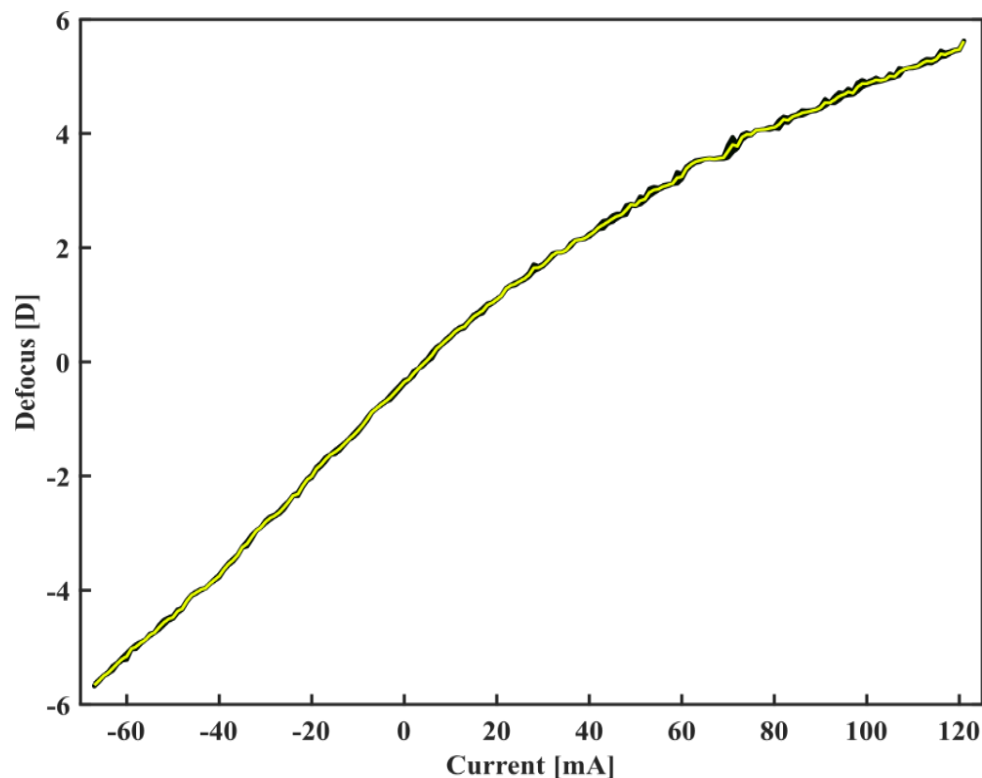
Figure 2.27. *Measured defocus with HS sensor as a function of the applied current in mA. The yellow line depicts the mean value of three measurements, and the black area shows the standard deviation.*

We repeated the measurements three times**. *Figure 2.27*** shows the mean values of the three measurements in Diopters and their standard deviations. It can be seen that the hysteresis is not an issue in this case, since the standard deviation for randomized voltages is low and the measurements showed good repeatability. We performed a backtest by applying the defocus value corresponding to each current and measured the defocus value with the AE. As illustrated in ***Figure 2.28*** the data shows linearity and the lens works properly in the range of -5.5 to 5.5 D.

2.5.3. *Dynamic calibration*

We were interested in inducing the defocus oscillations and investigating their effect on contrast sensitivity and the driver of the lens provided such an operation mode. However, for high-frequency oscillations, neither the nominal amplitude nor the offset defocus are fully achieved. Furthermore, the actual outcomes are dependent on the driving frequency. As a consequence, a trivariate calibration was performed. The lens was employed in dynamic mode to oscillate around the nominal offset with various amplitude values. The defocus values were simultaneously measured in real time at 60 Hz with an AE (see *Figure 2.26*). that was added to the system, and each measurement lasted at least 10 s Temporal frequencies of 5, 15, and 25

Hz were applied. Lens offset values ranged from -0.5 to 0.5 D, with peak-to-valley amplitudes from 1 to 5 D.
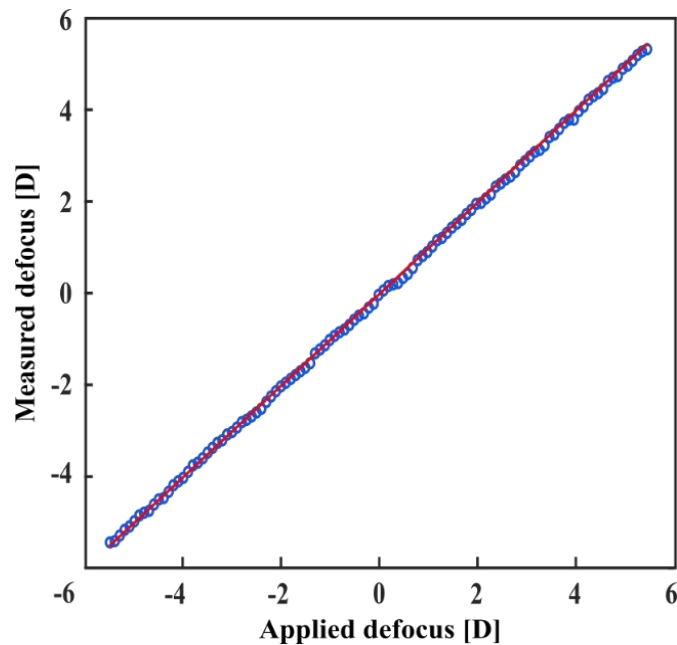
Figure 2.28. *Defocus measured with the HS sensor vs defocus applied by the tunable lens (after calibration).*

For each combination of nominal parameters, the amplitude and temporal frequency of the oscillation actually produced were determined by Fourier analysis and the offset by average. *Figure 2.29* compares the experimental curve for 5 Hz frequency, 0 D offset, and 2 D peak-to-valley (nominal) to the sinusoidal function with the experimental values of these parameters obtained from the spectral peak (*Figure 2.30*). In *Figure 2.31*, experimental peak-to-valley and offset values are plotted against nominal values. While the experimental offset matched the programmed values (in a ±0.5D range around 0D), the amplitude of the oscillation was lower than required, proportional to the nominal value by a factor dependent on frequency.
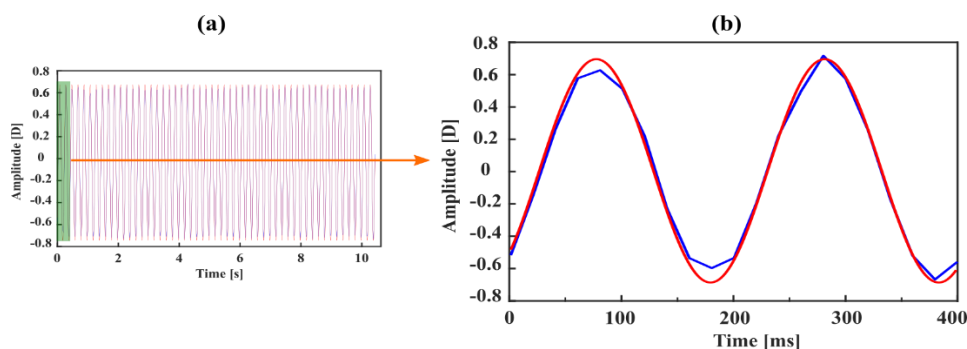
Figure 2.29. *Experimental (blue) and reconstructed (red) defocus oscillations for nominal 5 Hz, 0 D offset, and 2 D peak-to-valley. Panel (b): detail of the initial 400 ms in panel (a).*
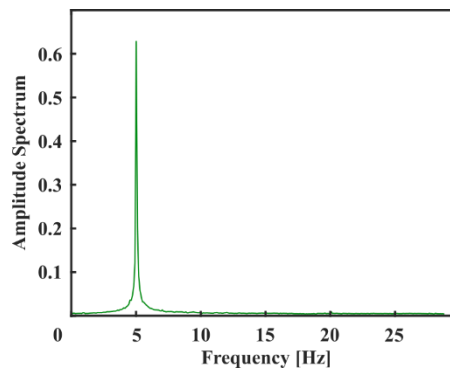
Figure 2.30. Fourier analysis of the experimental oscillations of defocus

For each frequency, a bidimensional fitting was performed (***Figure 2.32***) to obtain the relationship between nominal and experimental values. The formulae obtained were inverted and added to the HS software in order to achieve the targeted defocus oscillations.
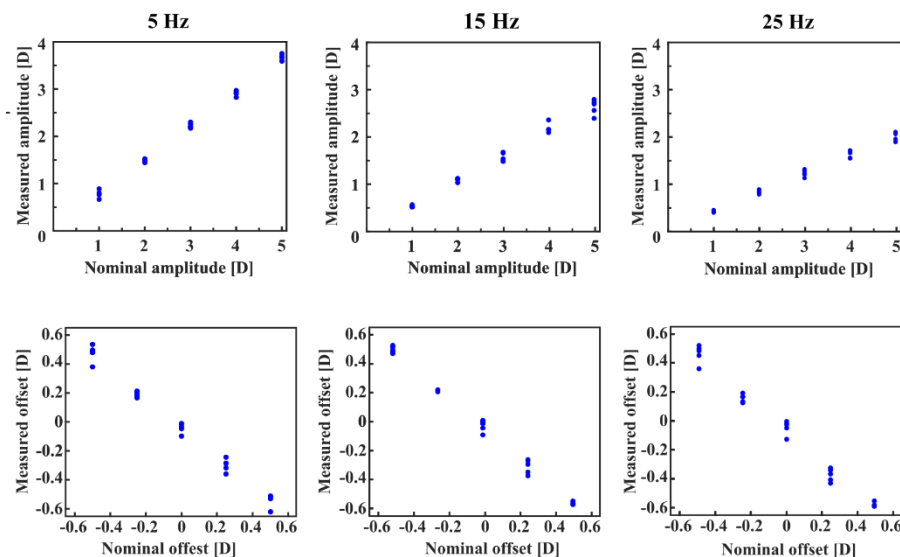
Figure 2.31. *Measured vs nominal peak-to-valley (top) and offset values (bottom) for various temporal frequencies. Multiple data points correspond to different values of the other variable (offset when representing peak-to-valley and vice versa)*

2.6. Gamma Correction

In order to ensure accurate contrast values, the display was gamma-corrected before performing the experiment. The luminance was measured as a function of grayscale level with a luminance meter (Konica Minolta, LS-100, Japan) in a dark room and a gamma curve was fitted. The equation obtained was inverted to create a look-up-table of gray levels to produce a linear

luminance progression. *Figure 2.33* depicts experimental results, with each data point being the mean of three measured luminance values. The standard step was 5 levels but a finer 1-

level scan was performed from 170 to 210, since these values around half maximum luminance were
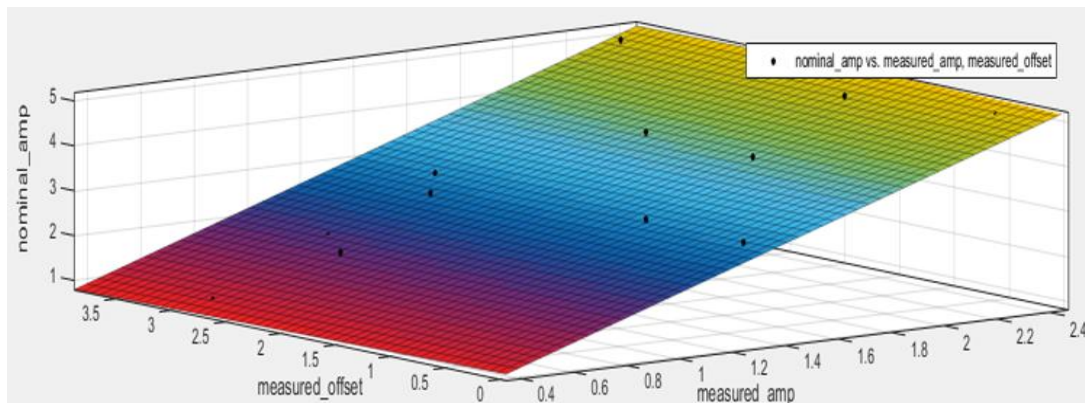
Figure 2.32. An example of bidimensional fitting for 25. The independent parameters (x,y) are measured amplitude and measured offset and the nominal amplitude is the dependent parameter(z).

more likely to be required for the typical contrast values expected in the experiment. The lowest and highest luminance levels were 0.256 and 135.97 cd/m^2, respectively, with a contrast range extending from 0.005 to 0.995.
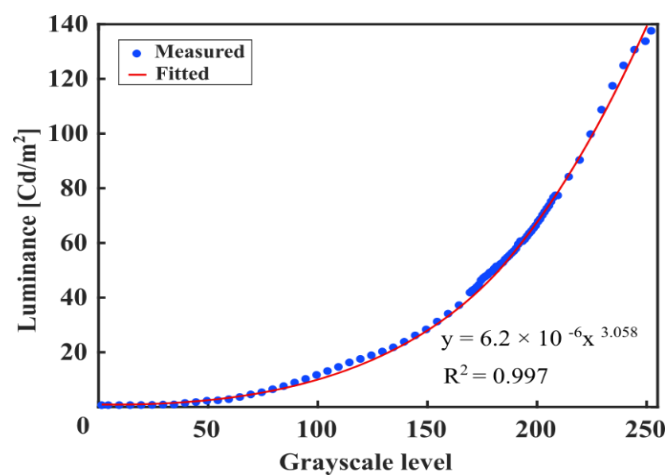
Figure 2.33. Luminance as a function of grayscale level. Each marker is the mean of three measurements.

Chapter *3*

"You are under no obligation to remain the same person you were a year ago, a month ago, or even a day ago. You are here to create yourself, continuously."

Richard Feynman

Chapter 3.   Accommodation dynamics measurements

A large number of studies on accommodation have been conducted in static mode or under monocular conditions. However, there are a few studies that investigate accommodation dynamics under binocular, natural viewing conditions.[Chin et al., 2008; Chirre et al., 2015; M. Kobayashi et al., 2008; Mira-Agudelo et al., 2009]. When the eye changes fixation from a distant to a near object, accommodation, vergence, and pupillary response are triggered together. Therefore in accommodation dynamics analysis, obtaining near triad dynamics simultaneously under realistic viewing circumstances would be more informative [Chirre et al., 2015]. This chapter presents dynamic measurements of accommodation, convergence, HOAs, and pupil miosis in young emmetropes and myopes. In addition, correlation analyses of several far-to-near response parameters with refractive error and accommodation speed are provided. These analyses aim to evaluate whether there is a difference in accommodation mechanism between myopes and emmetropes and to explore if an abnormal accommodation function is linked to myopia development.

3.1.   Accommodation dynamics and myopia

Despite a considerable amount of research on accommodation, the relationship between myopia and accommodation still remains unclear [Charman & Radhakrishnan, 2009; Cheng et al., 2019; Culhane & Winn, 2000; J. E. Gwiazda et al., 2004; Hughes et al., 2020; Jung et al., 2012; Kaphle et al., 2022b; Logan et al., 2021; Maddock et al., 1981; Radhakrishnan et al., 2007; Roberts et al., 2015; Rosenfield et al., 2002; Rosenfield & Gilmartin, 1999; Sankaridurg et al., 2021; Schmid & Strang, 2015a, 2015b; Tarrant et al., 2008; Vitale et al., 2008]. An insufficient amount of accommodation, known as the accommodative lag, results in hyperopic defocus on the retina, which, if prolonged, might induce axial elongation and promote myopia development during emmetropization in children [Z. Lin et al., 2020; Sanz Diez, Yang, et al., 2019; Wolffsohn et al., 2019]. Numerous studies suggest that myopes have a higher lag of accommodation than emmetropes [Ghoushchi et al., 2021; Kaphle et al., 2022a; Labhishetty & Bobier, 2017; Maddock et al., 1981]; however, this association has not been found by others [Hughes et al., 2020; Mutti et al., 2006; Weizhong et al., 2008]. In addition, myopes appear to require higher spatial frequencies to trigger accommodation [Sanz Diez, Ohlendorf, et al., 2019]. The topic is still open for debate and further research is needed to assess whether the accommodative lag is associated with myopia, either as a consequence or as a cause for its

onset and progression. Other accommodation mechanism parameters that may affect myopia are pupil size, convergence, and accommodation fluctuations [Charman, 2005; Charman & Radhakrishnan, 2009; Hazel et al., 2003].

3.2.   *Subjects*

As illustrated in *Table 3.1,* this study included eighteen young subjects, ten females and eight males, with an average age of 25.0 ± 4.7 years (mean $\pm$ standard deviation). The average refractive error was -2.3 D with a range from -7.5 D to 0 D. Cylinder values were below 2 D in all cases. The subjects' objective and subjective refractive errors were measured with VAO, an adaptive optics visual simulator (VAO, Voptica SL, Murcia, Spain) [Hervella et al., 2019] (*Figure 3.1*). The subjects' vision was corrected to have 20/20 VA or better in both eyes during the measurement with their spectacles if required (two participants wore their contact lenses).

Table 3.1*. Subjects' information*

Subject	Sex	Age [years]	SE [D]		
			OD	OS	Mean
1	f	23	-0.88	-0.38	-0.62
2	f	22	-1.00	0.12	-0.44
3	m	24	-0.75	-0.68	-0.71
4	f	21	0.00	0.00	0.00
5	m	21	0.00	0.00	0.00
6	f	23	-0.75	-0.75	-0.75
7	f	21	-7.62	-7.32	-7.47
8	m	21	-5.00	-5.00	-5.00
9	f	27	-2.50	-2.50	-2.50
10	f	26	-3.35	-3.75	-3.55
11	m	32	-2.00	-2.50	-2.25
12	f	26	-5.75	-4.75	-5.25
13	m	33	-2.00	-1.75	-1.88
14	m	34	-2.25	-2.00	-2.12
15	m	34	-2.88	-2.88	-2.88
16	m	28	-0.25	-0.25	-0.25
17	f	21	-2.00	-2.50	-2.25
18	f	21	-3.38	-3.00	-3.19

Since accommodation dynamics were measured in binocular conditions, anisometropia, i.e., having different refractive errors in each eye, which may affect accommodation, was an exclusion criterion. Other exclusion criteria included ocular pathologies, prior surgery, difficulty to fixate, and abnormal binocular vision. The subjects were briefed about the objectives, methods, and possible risks of the experiment prior to taking any measurements, and signed informed consent before the experiment. This research followed the ethical principles of the University of Murcia and adheres to the Declaration of Helsinki.

Figure 3.1. *Measuring the objective and subjective refraction with VAO.*

3.3.   *Experimental setup and procedure*

The open-field HS system was discussed in detail in the methods section. *Figure 3.2* shows the apparatus used during accommodation measurements. The vertical and lateral stages were adjusted to keep the pupils inside the pupil monitoring camera. The pupil images were then focused to ensure that the pupil plane was conjugate to the HS sensor. In addition, the subject position was fine-tuned to avoid or reduce corneal reflections from entering the HS, while keeping both pupils inside the HS area. This was possible because the HS sensor contains an embedded pupil tracker, so the subject does not need to be aligned to a fixed position. When the proper HS sensor image was achieved, the LEDs were switched off and measurements proceeded.
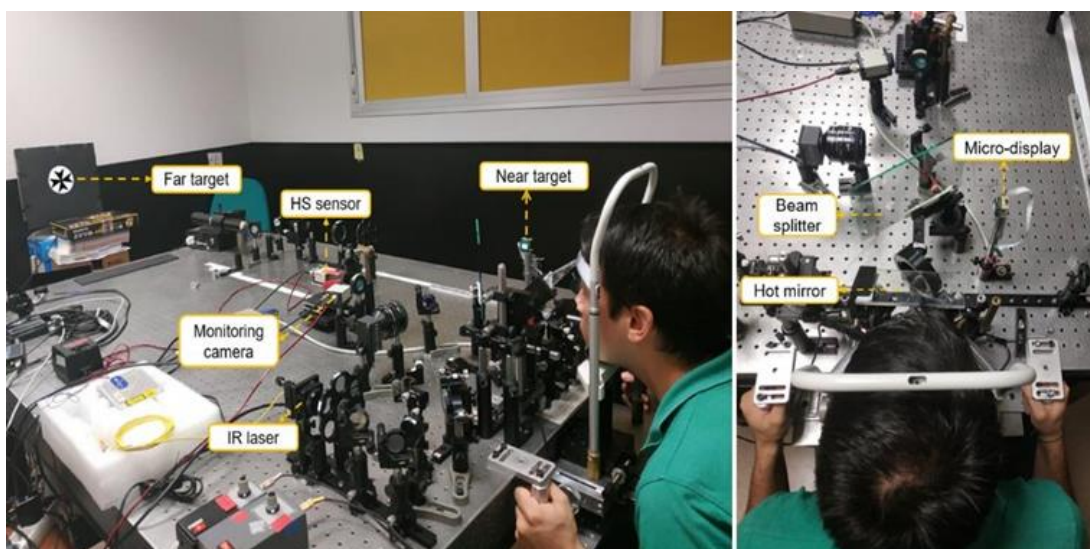
Figure 3.2. *The lateral (left) and top views (right) of the open-field HS system.*
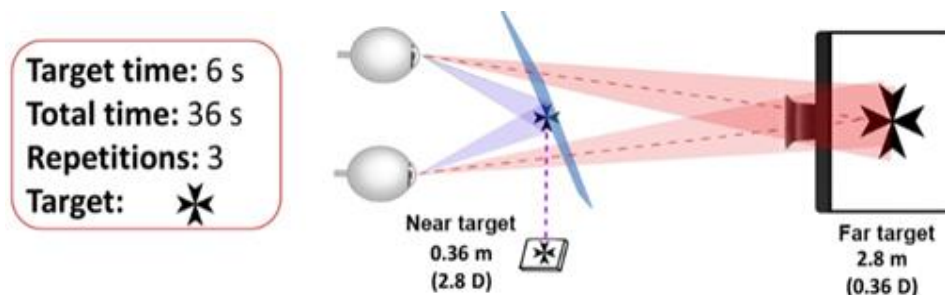
Figure 3.3. *Stimuli arrangement for the accommodation-disaccommodation experiment.*

Subjects were presented with alternating far and near targets and their task was to accommodate and disaccommodate spontaneously (*Figure 3.3*) The far and near stimuli were high-contrast black Maltese crosses on a white background, with the same angular size of 1.3° of the visual field. The Maltese cross is a standard visual stimulus that serves as an effective cue for central fixation since it extends in different orientations and includes a wide variety of spatial frequencies [Kruger et al., 2004; Mathews & Kruger, 1994]. The stimuli were displayed on an LCD at 2.8 m and a microdisplay at 36 cm. Through the HS software package, the operator can control the far and near displays, the experiment duration and repetition, the visual target, and the field of view (*Figure 3.4*).
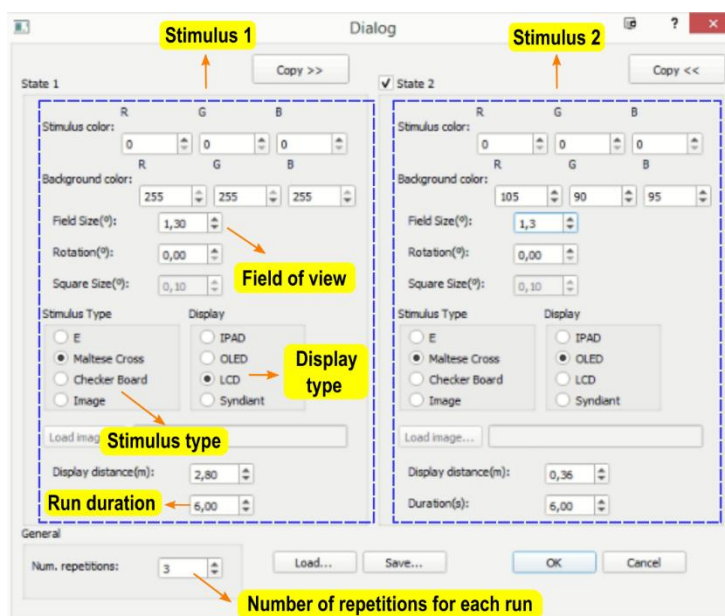
Figure 3.4. *The GUI options for stimuli presentation.*

Each run consisted of six presentations of far and near targets, i.e., far-near-far-near-far-near, resulting in three far-near accommodation tasks. Each presentation lasted 6 seconds, and the

whole run was 36 seconds long. Each run was repeated three times resulting in nine accommodation and nine disaccommodation events for each subject. The subjects were asked to blink halfway through each presentation to prevent blinking too close to the stimuli switch. The refractive error was represented in spherical equivalent. The high-order aberrations were measured over a 2.5-mm-radius pupil. As an example, *Figure 3.5* depicts the results of a single run for the right eye of an emmetropic subject. During the disaccommodation and accommodation events, the mentioned parameters were synchronized and changed almost simultaneously.
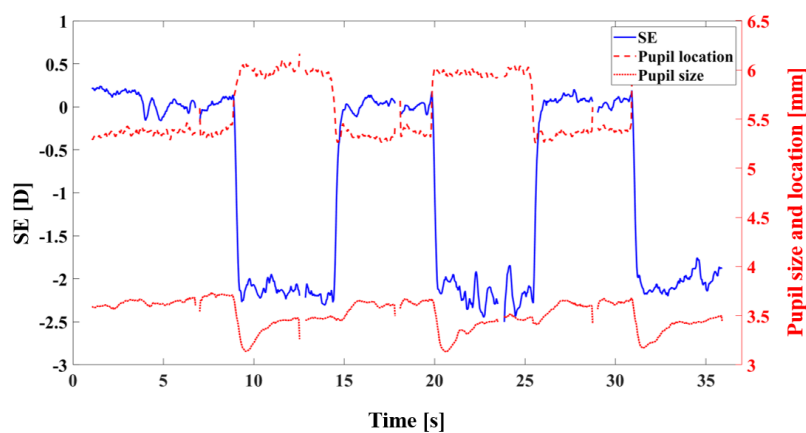
Figure 3.5 Example of results in a run (subject 1, OD). SE in diopters (blue line) is associated with the left axis; interpupillary distance (dashed red line), and pupil size (solid red line), both in mm respond to the right axis.

3.4. Data analysis

Blinks were removed from the raw data using a customized MATLAB code [MATLAB version R2018b, The MathWorks, Inc., United States]. The blink-removal algorithm consists of rejecting measurements when the difference between instantaneous values (i.e., obtained from individual frames in the HS video output) and local median values (in a ±15 frame range, i.e., ±0.5 s) exceed a prefixed threshold for either pupil size or SE.

Typical methods for estimating the speed of accommodation include fitting a Boltzmann sigmoid function [Charman, 2005; Chin et al., 2010], fitting an exponential function [A. P. A. Beers & Van Der Heijde, 1994; Jiang & White, 1999], and employing Fourier analysis [Suryakumar et al., 2007a, 2007b]. Instead, we used a previously reported threshold-based method [Chirre et al., 2015]. As illustrated in *Figure 3.6*, the method estimates the steady-state values for each variable by averaging for at least 2 sec out of each 6-sec presentation. The

beginning and finishing points for calculating the accommodation speed were selected by taking 80% of the accommodation response. In order to calculate the speed of pupil size change and convergence, similar threshold-based approaches were employed.
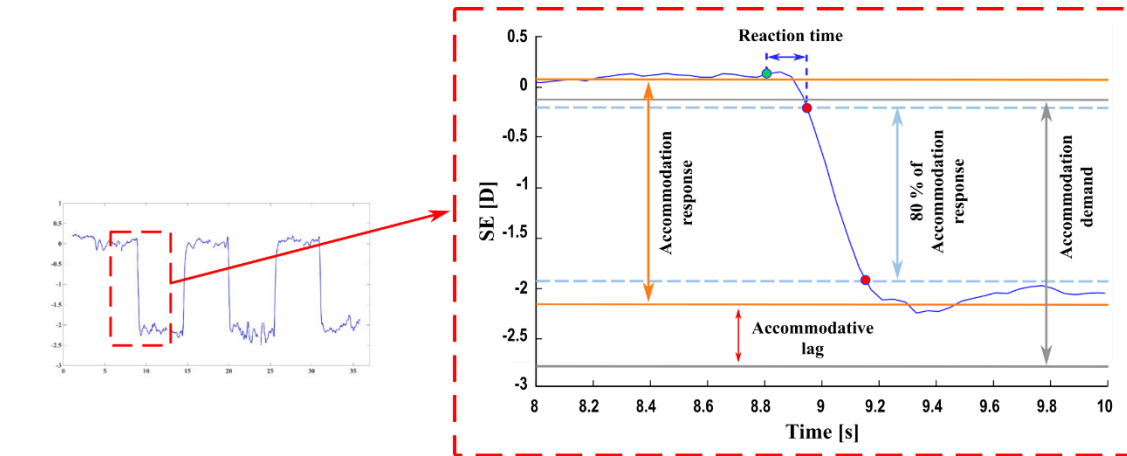
Figure 3.6. *Implementation of the threshold method. Solid blue curve: studied parameter (in this case, SE) during one accommodation event. Gray lines: far and near accommodation demands. Orange lines: steady accommodation states calculated as the average across at least 2 seconds. Dashed blue lines: limits of the central 80% response. Green dot: change-of-target time. Red dots: 80%-response crossing points.*

Since the changes in HOA-RMS and spherical aberration were comparable to steady-state variability throughout the measurements, they did not permit the same sort of processing. Instead, we calculated the difference between the mean values of these parameters for near and far steady states (far minus near). As shown in *Figure 3.6*, the response is the difference between steady-state SEs for far and near stimuli. The lag of accommodation is the difference between accommodation demand and accommodation response. The reaction time is the delay between target switch time (green circle), and the 10%-of-accommodation-response time (Top left red circle).

It is worth noting that the convergence was quantified using the change in inter-pupillary distance. Hence the units for this variable are in millimeters. The convergence angles can be approximately estimated by assuming a standard distance between the pupil plane and the center of rotation of the eye, so that pupil displacements can be converted to rotation angles. However, this variable transformation was not carried out because, for the small angles involved, it is very close to linear, and therefore irrelevant, for the correlation analysis to be performed.

3.5. Results

We found a strong correlation between each subject's left and right eyes for the measured parameters (*Figure 3.7*). The bottom-right plot shows a strong association between the right (x-axis) and left (y-axis) eye's spherical equivalent among the subjects (R = 0.98, p = 2.5·10^{-12}). In addition, we analyzed various parameters between left and right eyes, such as HOA-RMS and spherical aberration changes, accommodation speed, lag of accommodation, and its duration, finding strong correlations between eyes in all cases.
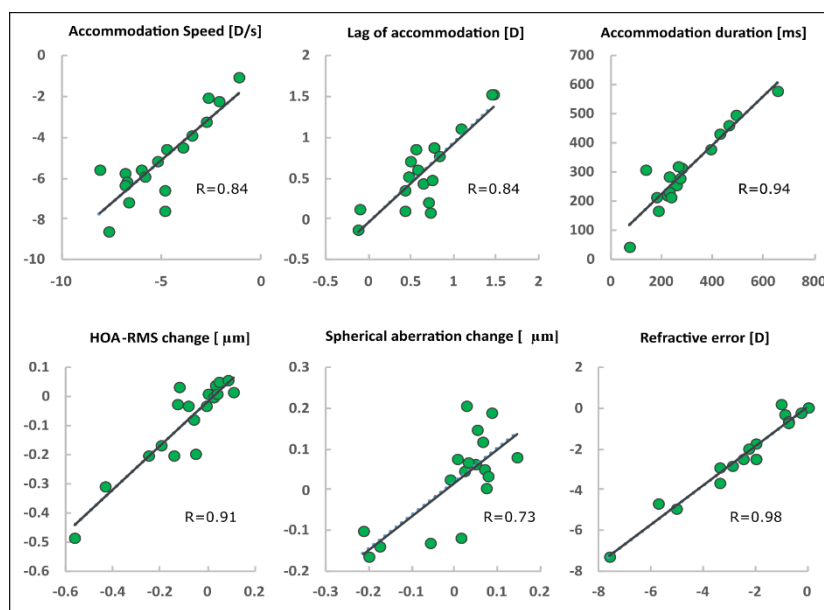
Figure 3.7. *Right eye (x-axis) vs. left eye (y-axis) near response parameters for every subject.*

Since the measurement was conducted in binocular conditions, the measured parameters are available for both eyes. However, it is not good practice to treat them as independent data points due to the internal correlation between them. In such circumstances, computing the mean between eyes or randomly picking one eye has been proposed as a possible method to produce a single data point per subject for statistical analysis [Armstrong, 2013; Armstrong et al., 2002; Murdoch et al., 1998]. Although the strength of the relationship is not the same for every measured parameter, we selected the former procedure, i.e., averaging between eyes.

Figure 3.8 depicts the far-near response parameters as a function of spherical equivalent for each participant, to investigate myopia's impact on convergence, accommodation, and pupil size dynamics. In the mentioned plots x-axis represents the subjects' refractive error and the y-axis the relevant far-to-near response parameters.
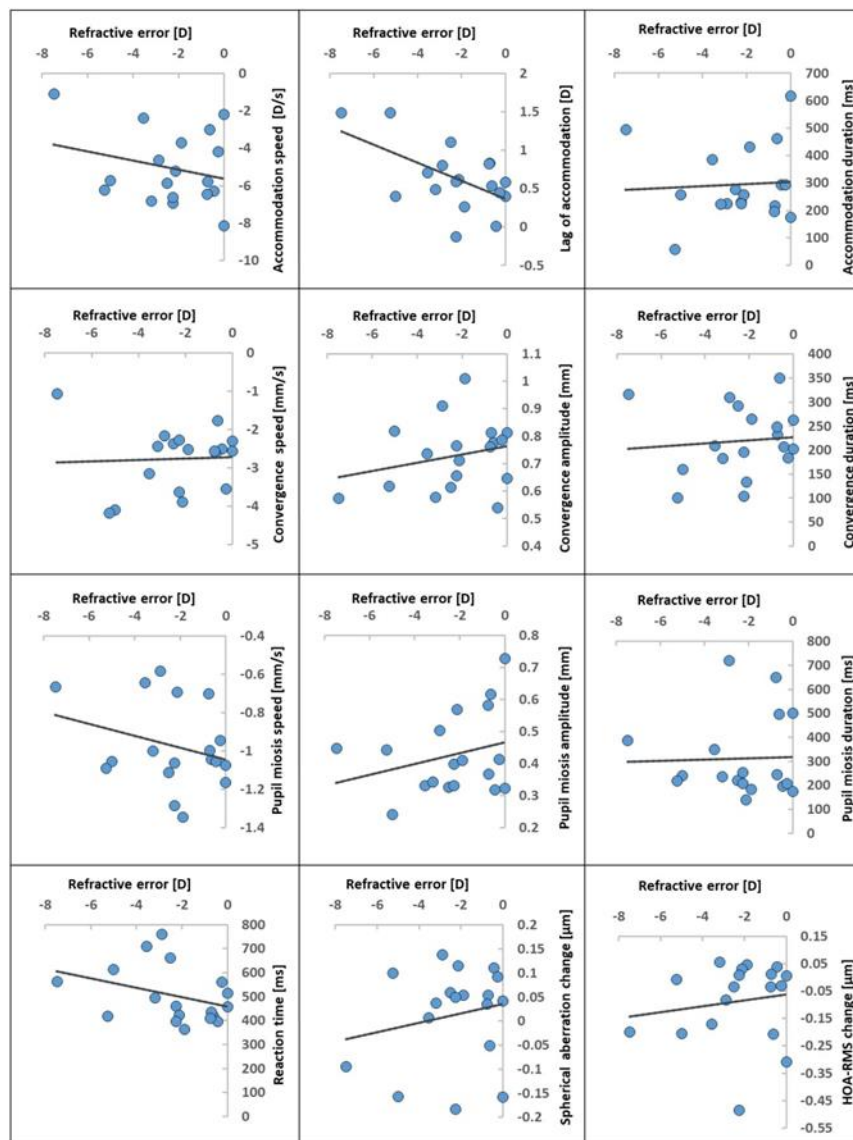
Figure 3.8. *Parameters of far-to-near response dynamics as a function of refractive error.*

A correlation study was conducted to evaluate any potential association between refractive error and far-to-near dynamics. The left panel in *Table 3.2* shows the correlation of refractive error with various parameters evaluated in this study. These parameters include accommodation speed, lag of accommodation, accommodation duration, convergence speed, convergence amplitude, convergence duration, pupil miosis speed, pupil miosis amplitude, pupil miosis duration, reaction time, spherical aberration change, HOA-RMS change, and age. The correlation coefficient (R), the determination coefficient (R^2), and the relevant p-value are presented for each analysis. We detected trends with p-values lower than 0.05 (highlighted in *Table 3.2*) for the accommodative lag (p = 0.014) and pupil miosis speed (p = 0.041). The remaining correlation coefficients, including correlation coefficients of refractive error with response time and convergence amplitude, exhibited p-values above 0.05.

To investigate the potential factors that may impact the accommodation process, the accommodation speed was plotted as a function of the far-to-near response parameters (see *Figure 3.9*). Bear in mind that since the accommodative state was represented as SE (negative for myopes and accommodating eyes), the accommodation speed values were negative. The right panel in *Table 3.2* displays the results of a correlation analysis between accommodation speed and all the other computed variables, and three correlation values with p below 0.05 were obtained: for convergence speed ($R=0.48$, $p=0.044$), pupil miosis amplitude ($R=0.47$, $p=0.049$), and convergence duration ($R=0.57$, $p=0.014$).

3.6. Discussion

An altered accommodation mechanism may be a contributor to myopia development, thus we studied the link between a variety of far-to-near response parameters and refractive error.
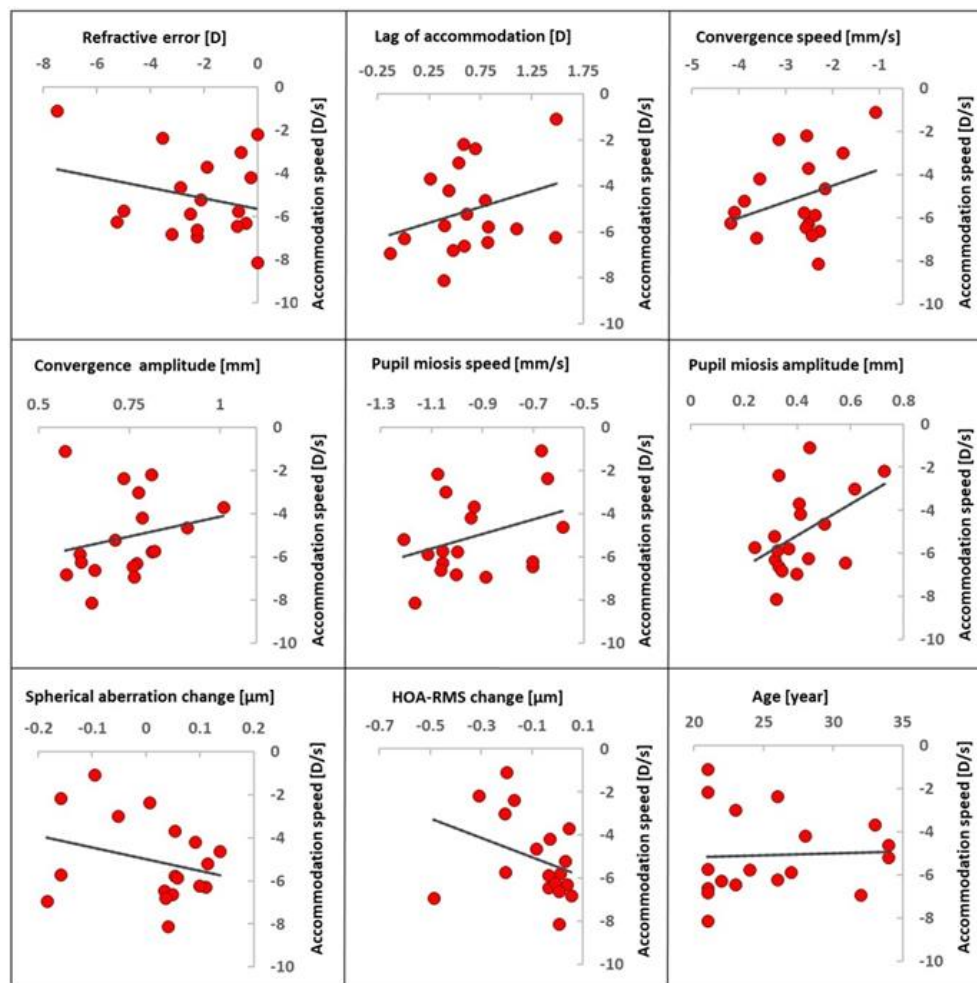
Figure 3.9. *Relationship between far-to-near response parameters and accommodation speed.*

Table 3.2. Correlation analyses of accommodation speed (right) and refractive error (left) with various far-to-near response factors and variables. Correlation values with p < 0.05 are highlighted in green.

SE correlations with:	R^2	R	p-value	Accommodation speed correlations with:	R^2	R	p-value
Accommodation speed	0.0677	-0.2601	0.2971	Spherical Equivalent (SE)	0.0677	-0.2601	0.2971
Lag of accommodation	0.3219	-0.5674	0.0141	Lag of accommodation	0.0935	0.3058	0.2172
Accommodation duration	0.0035	0.0592	0.8155	Convergence Speed	0.2310	0.4806	0.0435
Convergence speed	0.0045	-0.0671	0.7912	Convergence amplitude	0.0479	0.2189	0.3828
Convergence amplitude	0.1393	0.3732	0.1271	Convergence duration	0.3250	0.5701	0.0135
Convergence duration	0.0002	0.0158	0.9504	Pupil miosis speed	0.1155	0.3398	0.1677
Pupil miosis speed	0.2367	-0.4865	0.0406	Pupil miosis amplitude	0.2206	0.4697	0.0492
Pupil miosis amplitude	0.0722	0.2686	0.2811	Pupil miosis duration	0.1548	0.3934	0.1063
Pupil miosis duration	0.0017	-0.0415	0.8702	Reaction time	0.1040	0.3225	0.1918
Reaction time	0.1209	-0.3477	0.1574	Spherical aberration change	0.0800	-0.2828	0.2555
Spherical aberration change	0.0404	0.2010	0.4238	HOA-RMS change	0.1145	-0.3384	0.1696
HOA-RMS change	0.0231	0.1521	0.5469	Age	0.0018	0.0423	0.8676

It should be noted that instead of classifying the subjects into two groups according to their refractive error (myopes and emmetropes), we conducted our correlation analyses using the subjects' refractive error. This method offers more clarity, particularly in the boundary of myopia definition. Statistically speaking, a correlation analysis merely shows the co-evolution of two variables. If a cause-effect relationship has been hypothesized by some means, a high R can be taken as supportive evidence. But the same value can be obtained if the cause-effect relationship is the other way around or if there is no such a relationship but both variables are controlled by a third factor. Therefore the studied correlation values show the impact of refractive error on different components of the far-to-near response, while the opposite may be true.

In this study, a Hartmann-Shak sensor was applied to measure accommodation dynamics since it is more accurate than eccentric infrared photorefractors and autorefractors [Lundström et al., 2005]. Another advantage of this study is that it explores the binocular accommodation response utilizing real stimuli under realistic viewing conditions. To the best of our knowledge, no study analyzes the possible links between all of the far-to-near factors in accommodation response and myopia, nor their possible effect on accommodation speed under realistic binocular vision circumstances.

3.6.1. *Accommodation and myopia*

According to our analysis, myopes have a higher lag of accommodation (R = 0.57, p = 0.01). The lag of accommodation varied between 0 and 1.48 D among subjects, and its mean

value ± standard deviation was 0.64 D ± 0.42 D. Just in one case, there was a mild lead of accommodation of 0.12 D. If we classify the subjects in three groups based on refractive errors less than 2 D, between 2 and 3 D, and more than 3 D, then the mean lags values are 0.49 D ± 0.27 D, 0.59 D ± 0.45 D, and 0.91 D ± 0.53 D, respectively. Various researchers reported mixed results regarding the lag of accommodation in myopes. According to the International Myopia Institute (IMI) report [Wolffsohn et al., 2019], the accommodative lag could be caused by the measuring method failing to account for negative spherical aberration; however, this was not the case in our results. According to some studies myopes and emmetropes have a similar lag of accommodation [Wagner et al., 2019] or even the other way around [Rosenfield et al., 2002]. On the other hand, there are many reports of higher lag of accommodation in myopes, in agreement with our results [Charman, 2005; Ghoushchi et al., 2021; J. E. Gwiazda et al., 2004; Hughes et al., 2020; Maiello et al., 2018; Nakatsuka, 2003; Schaeffel et al., 1993].

Additionally, several accommodation dynamics factors, including accommodation speed and accommodation duration, were calculated by the threshold method. We found that accommodation speed was unrelated to refraction. Considering that the myopes showed a larger accommodative lag, it was reasonable to expect that they accommodated more slowly. Nonetheless, there was little evidence to support this hypothesis, possibly because our study sample was small. We did not find further evidence in the literature of this potential correlation. Schaeffel et al. found no link between refractive error and accommodation speed [Schaeffel et al., 1993] when they measured subjects with various refractive errors employing a photorefractor, with a restricted sample rate of 5.3 Hz. In addition, a recent study [Wagner et al., 2019] that measured myopes and emmetropes with a higher refresh-rate photorefractor did not find any relationship between accommodation speed and refractive error, either. The relationship between accommodation speed and other measurable variables will be discussed in detail.

3.6.2. *Pupil miosis and myopia*

According to Schaeffel et al. the amplitude of the pupillary response was lower in myopes compared to emmetropes, [Schaeffel et al., 1993]. Since the p-value for this association was 0.28, our analysis does not support this relationship. However, the association between miosis speed and refractive error ($R = 0.49$, $R^2 = 0.24$) showed a p-value of 0.04, suggesting that myopic individuals may have slower miosis. Schaeffel et al. [Schaeffel et al., 1993] did not investigate miosis speed, and to the best of our knowledge, this association has not been

reported before in the literature. Finally, we found that the miosis duration had no link with refractive error.

3.6.3. *Convergence and myopia*

A recent study on vergence-driven accommodation in stereoscopic content [Maiello et al., 2018] found that myopes have slower vergence responses. In contrast, our correlation analysis found no associations between refractive error and convergence parameters (speed, duration, and amplitude).

3.6.4. *Spherical aberration and HOAs vs. myopia*

In a study, Collins et al. [M. J. Collins et al., 1995] suggested that highly myopic subjects have larger ocular aberrations. On the other hand, several researchers have reported no evidence that myopic eyes are more aberrated than emmetropic ones [Charman, 2005; Cheng et al., 2003; Hartwig & Atchison, 2012; J. C. He et al., 2002]. We could not identify a correlation between myopia and spherical aberration change ($R = 0.20$, $p = 0.42$) or HOA-RMS change ($R = 0.15$, $p = 0.55$).

3.6.5. *Accommodation speed correlations*

Since the 1960s [Campbell & Westheimer, 1960], scientists have been investigating the relationship between accommodation dynamics, age, and refractive error. It has been found that the accommodation response, in both monkeys [Vilupuru & Glasser, 2002] and humans [Ciuffreda & Kruger, 1988], increases linearly with accommodation demand. Many studies investigated the dynamics of accommodation for a variety of accommodation demands employing devices with varying refresh rates, therefore reporting various accommodation speeds. For instance, Hung et al. [Hung & Ciuffreda, 1988] and Campbell et al. [Campbell & Westheimer, 1960] reported an accommodation speed of 10 D/s for the accommodation demand of 2 Diopters. Howland et al. [Howland et al., 1987] found an accommodation velocity of 4.6 D/s in babes, measuring at a modest frame rate of 2 Hz. In contrast, Yamada & Ukai [Yamada & Ukai, 1997] measured accommodation and disaccommodation and reported a maximum speed of 25 D/s for disaccommodation. Nevertheless, several studies have reported that disaccommodation and accommodation dependencies on demand are different, with disaccommodation being faster [Schaeffel et al., 1993; Yamada & Ukai, 1997].

Our results for 2.5 D far-to-near accommodation demand showed that the average accommodation speed was —5 ± 1.9 D/s, ranging from –1.1 D/s to –8.4 D/s. It has to be pointed out that we calculated the average accommodation speed instead of the maximum speed as reported in many earlier studies. We aimed to avoid noise and spikes in speed calculation. However, since the accommodation mechanism is not uniform, the threshold method yields reduced speed values. As seen in *Table 3.2,* right panel, in the accommodation speed correlation analysis, three parameters that have p-values below 0.05 are highlighted in green, including convergence duration, convergence speed, and pupil miosis amplitude.

The link between convergence and accommodation has been extensively investigated and is considered to be complicated by having multi-channel feedback. Hence, it may be unsurprising to find a low p-value for the correlation between convergence speed and accommodation speed (R= 0.48, p = 0.04). However, it is worth noting that, to the best of our knowledge, this correlation has not been reported before. Moreover, the correlation between convergence duration and accommodation speed is stronger (R = 0.57, p = 0.01), which might show that the dynamics of the mentioned mechanisms are different [Chirre et al., 2015]. In contrast, our data does not show a link between accommodation speed and convergence amplitude.

Pupil miosis is a well-known and intensively studied feature of the accommodative process. Our data do not support an association between miosis speed and accommodation speed. Nonetheless, the correlation between accommodation speed and miosis amplitude yielded a p-value below 0.05, indicating a potential link between these two parameters (R = 0.47 and p = 0.049). Thus, quicker accommodation may be associated with a larger miosis amplitude.

It is unclear how high-order aberrations can influence accommodation. It has been proposed by [Wilson et al., 2002] that the HOAs could serve as a cue for accommodation. According to Chin et al., [Chin et al., 2009b], high-order aberrations affect the disaccommdation process but not the accommodation. In contrast, Gambra et al. [Gambra et al., 2009] found that correcting aberrations can enhance rather than degrade accommodation. Fernández and Artal [Artal & Fernández, 2005] concluded that correcting high-order aberrations increases accommodation response time and thus decreases its peak velocity. Our correlation analysis shows no link between HOA-RMS initial state or change from far to near and accommodation speed. We also found no correlation between the initial value of spherical aberration or its far-to-near change

and the accommodation speed. Furthermore, our correlation study showed that the speed of accommodation appears to be unaffected by age in young subjects.

3.6.6. *Multiple comparisons and statistical significance*

By implementing several statistical tests on the same dataset, the possibility of making at least one type I error, i.e., incorrectly attributing statistical significance to a false result, rises as the number of tests grows. To address this issue, several approaches for adjusting the statistical significance labeling process have been developed to limit the possibility of false conclusions [Armstrong, 2014]. Bonferroni's correction is one of the most straightforward, extensively used, and conservative techniques for addressing multiple testing issues. It is calculated by dividing the overall significance level (usually $\alpha = 0.05$ in Vision Sciences and other research areas) by N, the total number of tests. The Bonferroni correction can be applied on the significance level (dividing by N, as we did) or on the p-values (multiplying them by N). The results of the inequalities to determine statistical significance are, obviously, the same.

In our scenario, employing Bonferroni correction would imply using a per-comparison significance level of $0.05/24 = 0.0021$, and no correlation coefficient in *Table 3.2* has a p-value lower than that. As a result, while the necessity of using Bonferroni's or other multiple-testing corrections is not ubiquitous and is even debatable [Armstrong, 2014], we reported all the numerical p-values and refrained from using the term "statistically significant.".

On the other hand, all approaches that seek to decrease the chance of a type I error, in turn, increase the chance of type II errors (i.e., failing to identify a real correlation). By definition, the significance level, α, is the probability of a type I error if the null hypothesis is correct [McKillup, 2005]. In our analysis, if there is no correlation then each comparison is an independent event with a probability of α of resulting in type I error, i.e., mistakenly finding a relationship. If all null hypotheses are valid while conducting multiple tests, the chance of having K type I errors when completing N tests follows the binomial distribution. Thus, if there is no correlation in our study, each comparison represents an independent procedure with α probability of producing a type I error. When performing 24 comparisons, the chance of incorrectly "discovering" five false correlations is 0.00501. As a result, it is unlikely for all five correlations highlighted in *Table 3.2* to be simultaneously false, and wholly rejecting them based on a multiple testing correction greatly increases the risk of type II errors.

Chapter *4*

"I do not know what I may appear to the world, but to myself I seem to have been only like a boy playing on the seashore, and diverting myself in now and then finding a smoother pebble or a prettier shell than ordinary, whilst the great ocean of truth lay all undiscovered before me"

Isaac Newton

Chapter 4.   Contrast sensitivity through periodic defocus fluctuations

The retinal image quality of the human eye is not static and changes with time [Charman & Heron, 2015; Walsh & Charman, 1988]. This instability is mainly due to defocus, although HOA fluctuations are also present [Hofer et al., 2001; Mira-Agudelo et al., 2009]. The fluctuations due to accommodation are in the range of ±0.5 D for temporal frequencies up to 2–5 Hz but gradually decrease at higher temporal frequencies. Despite the later, Fourier analysis has shown that the power spectra of defocus during accommodation have non-zero components even for oscillations above 10 Hz [Hofer et al., 2001].

There is almost no research on how the eye processes images subjected to dynamically changing defocus. Moreover, it is not clear how the visual system interprets the series of instantaneously defocused PSFs and how fast the eye integrates these images. In other words, if the eye is assumed to be a detector, what is its exposure time for processing defocus? This chapter studies the effect of induced fast oscillations of defocus on visual quality in terms of contrast sensitivity, in young emmetropic individuals [Ghoushchi et al., 2022]. This effect was further investigated theoretically by calculating the MTF from the mean blurred PSF obtained by combining the effect of sinusoidal defocus fluctuations over various integration times.

This study can shed light on how the visual system processes instable, defocus-blurred images and provide more information on the defocus perception mechanism in the eye. Furthermore, induced defocus changes by focus tunable lenses have recently had applications in wearable optoelectronic spectacles for correcting presbyopia [Mompeán et al., 2020b] and instruments to simulate vision through multifocal contact lenses and IOLs [Akondi et al., 2018].

4.1.   Temporal domain of visual perception

The research examining the temporal domain of visual interpretation covers a vast array of topics, including visual perception in terms of image detection [Potter et al., 2014], facial expression discrimination [Milders et al., 2008], letter recognition [Bundesen & Harms, 1999; Petersen & Andersen, 2012], character orientation identification [Sawides et al., 2018], and picture comparison [Allan, 1975]. Studying the temporal domain of visual information has applications in many fields, such as 3D displays, augmented reality, virtual reality, and gaming.

These applications prompted studies on the flicker fusion frequency [Hoffman et al., 2011; Simonson & Brozek, 1952] and the visibility window, i.e., the spatial and temporal frequencies observable to human vision [Watson, 2013; Watson et al., 1986]. Davis et al. found that humans can detect flickers up to 500 Hz. [Davis et al., 2015]. Moreover, Sawides et al. found the minimum time required for letter orientation recognition to be as small as 5 ms [Sawides et al., 2018]. However, the mentioned studies investigated the temporal domain of vision on a static, fixed focal plane.

4.2. Experimental setup and controlling software

The optical arrangement employed in this experiment is shown in *Figure 4.1*. The HS sensor in the present system ran at 60 Hz. Defocus oscillations were induced by means of a tunable lens (EL-16-40-TC-VIS-20D, Optotune Switzerland AG) previously calibrated in both static and dynamic operation modes. The display for presenting the stimulus was an SXGA 60-Hz monitor (Dell UltraSharp 1704FPT 17" Flat Panel). Details on the apparatus, the tunable lens calibration process, and the monitor gamma correction protocol, can be found in the methods section.
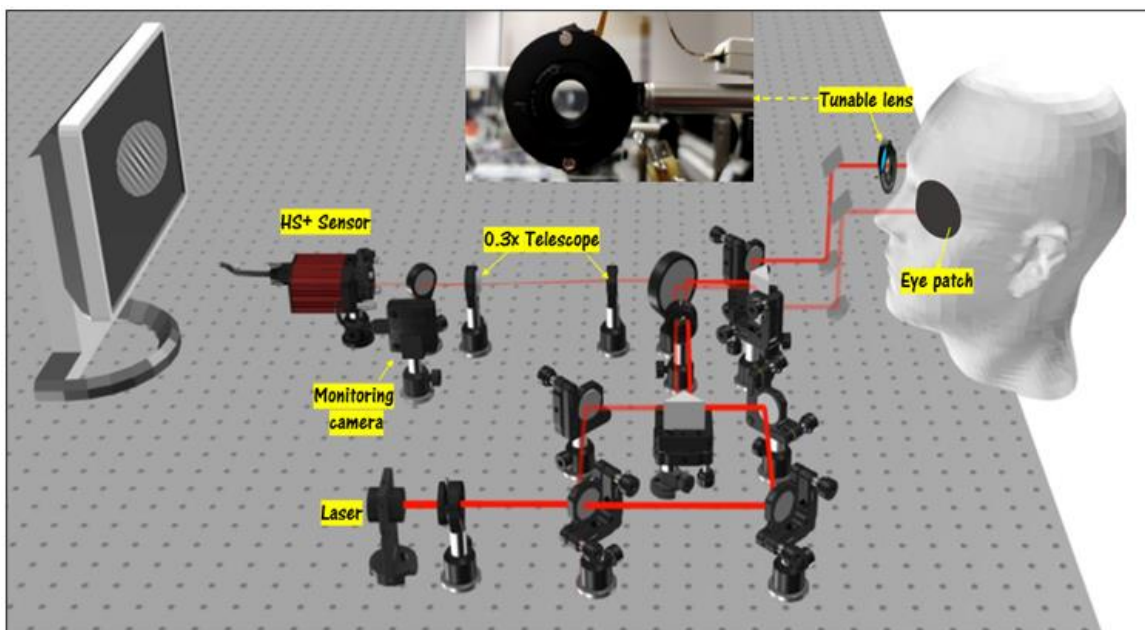
Figure 4.1. *The schematics of the optical setup. Measurements were monocular. The tunable lens was placed in front of the right eye and the left eye was occluded.*

The HS control software was updated for this experiment to drive the tunable lens. *Figure 4.2* shows a screenshot of the tunable lens control interface, in which various amplitudes and spatial

and temporal frequencies can be selected through the program. Also, the subject's objective refraction and pupil location are shown to the operator and recorded in real time.
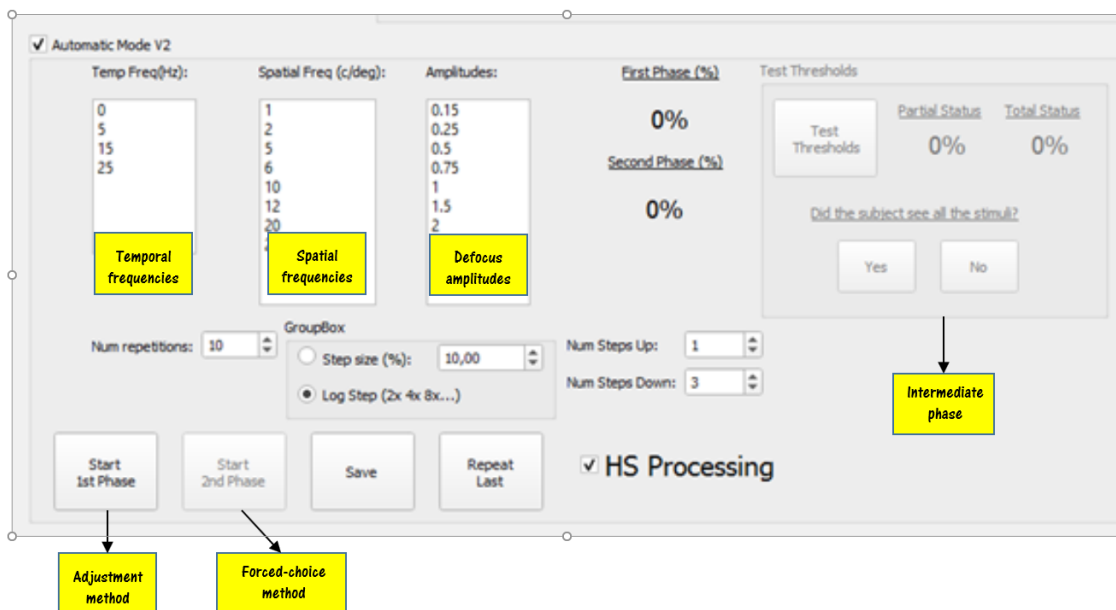
Figure 4.2. *Screenshot of the tunable lens control interface.*

4.3. Subjects

Five young emmetropic subjects (three men and two women, age $= 26.6 \pm 4.0$) with a mean refraction of -0.15 $\pm$ 0.24 D and a cylinder between 0 and -0.25 D participated in the experiment (*Table 4.1*). The subjects' objective and subjective refractive errors were measured with the adaptive optics visual simulator (VAO, Voptica SL, Murcia, Spain) before the experiment, to ensure they reached 20/20 or better VA. None of the individuals had visual impairments or had undergone prior surgery.

Before conducting the measurements, we informed the subjects of the experiment's procedure, purpose, and potential dangers and obtained their written consent. The study responds to the tenets of the Helsinki Declaration and the ethical guidelines of the University of Murcia.

Table 4.1. *Subjects' information.*

Subject	Sex	Age [years]	SE [D]
1	m	30	0.25
2	f	25	-0.38
3	m	29	-0.38
4	m	24	0.00
5	f	32	0.00

4.4. Experimental procedure

The subjects were centered with respect to the tunable lens with the aid of the pupil monitoring camera. A bite bar was employed to avoid the subjects' motion during the measurements (see *Figure 4.3*).
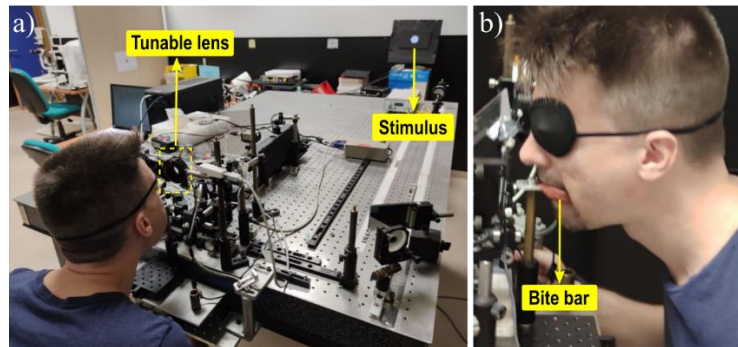
Figure 4.3. *Optical setup for measuring contrast sensitivity (a) General view. b) Detail of the bite bar.*

The experiment was conducted in a dark room. The visual stimulus was a 12-c/deg Gabor patch located at 3 meters and subtending 1 deg of the visual field. Contrast values were calculated with Michelson's formula (see Chapter 1). The stripes were tilted 10 degrees form the vertical in either direction. The measurements were carried out in monocular vision, and the subjects viewed the stimulus through the tunable lens with their right eye. The temporal frequencies of the applied sinusoidal waves were 5, 15, and 25 Hz, with peak-to-valley defocus values ranging from 0.15 to 3 D.

Prior to the experiment, a preliminary estimate of the contrast threshold for each condition was obtained by the adjustment method, which served as the starting point for the forced-choice method. In the adjustment protocol, the subject began with a high contrast value and changed it using the up and down arrow keys until reaching the Adjustment Contrast Threshold (ACT) value, which was the lowest visible contrast (*Figure 4.4 (a)*) [Richman et al., 2013]. The operator used the ACT values as a reference to calculate the 5 contrast values employed in the forced-choice phase, in a geometric progression: $C_1 = 2 \times ACT$, $C_2 = ACT$, $C_3 = ACT/2$, $C_4 = ACT/4$, and $C_5 = ACT/8$ (for each oscillation case). Before proceeding to the measurement round, the subject was shown the series of contrast values to check that it encompasses the actual contrast threshold. If the subject was able to see all or none of them, the sequence was halved or doubled, respectively. There were 10 trials per oscillation case, evenly divided in series with rest breaks between them. Each series was randomized across contrast, temporal
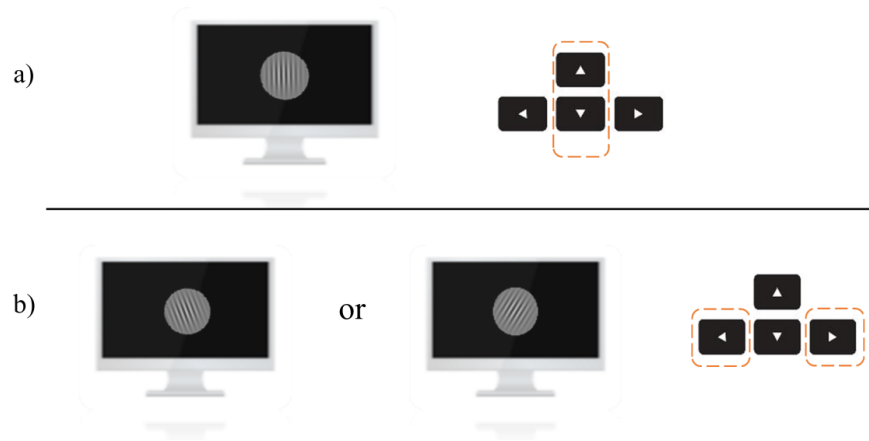
Figure 4.4. *Two step experimental protocol. a) Adjustment phase: The subject used up/down keys to choose the lowest visible contrast for each oscillation case. b) Forced-choice phase: The subject indicated the direction of the Gabor patch with left/right keys.*

frequency, and defocus peak-to-valley values. After each presentation, the subject was required to guess the tilt direction of the stripes and answer with the left and right arrow keys.

4.5. Data analysis

The probability of success, i.e., of selecting the right tilt direction, is theoretically 100% when the grid is visible for the subject (neglecting mistakes). If the contrast is so low that the Gabor patch is invisible, the subject would answer at random and the probability of success is 50%. The contrast value that gives the subject a 50% chance of seeing the grid is taken as the threshold. The compound probability of success at that point should be the average between these two values, i.e., 75%.

The success rates corresponding to each contrast value, C, were calculated from the subject's answers. For each frequency and peak-to-valley combination, the success rates as a function of C were fitted to a sigmoid curve and the Subjective Contrast Threshold (SCT) was estimated at the 75% success rate level (*Figure 4.5)*. If the subject's answers were inconsistent and the fitting was not successful, the SCT was left unspecified.

4.6. Experimental results

Each subject's contrast threshold as a function of peak-to-valley defocus oscillation is depicted in *Figure 4.6.* Except for a few outliers for one individual, the subjects were able to detect the correct direction of the Gabor patch with contrast as low as 0.2 for peak-to-valley
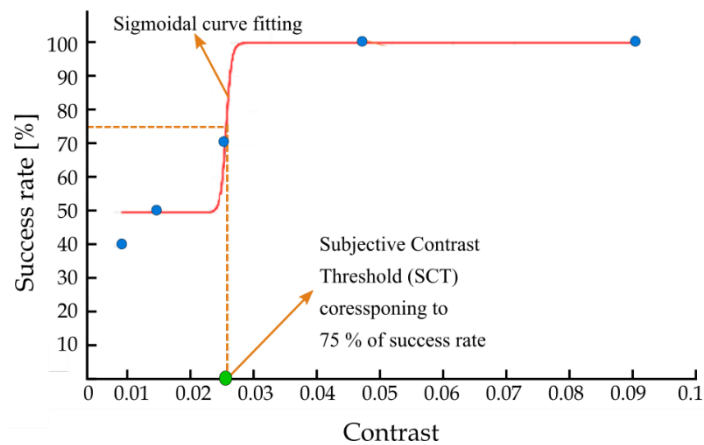
Figure 4.5. *Experimental success rates (blue dots) as a function of contrast and sigmoidal fitting (red line) for obtaining the subjective contrast threshold (green circle).*

values up to 2 D for all temporal frequencies. However, for 3 D peak-to-valley, individual contrast thresholds tended to be more variable.
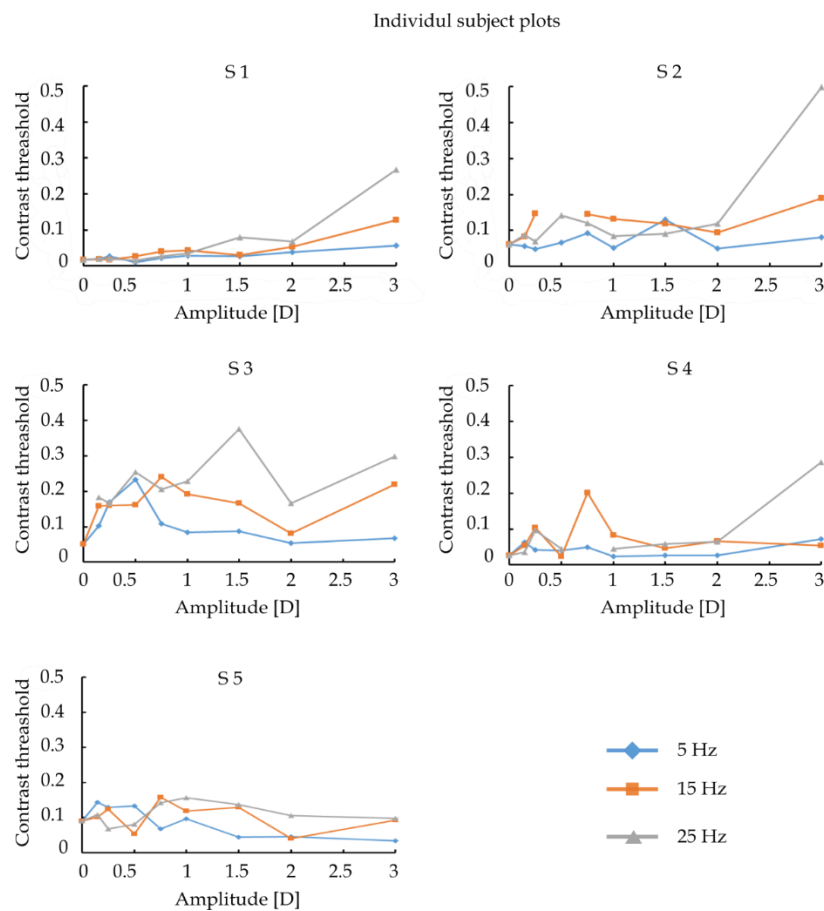
Figure 4.6. *Contrast threshold as a function of peak-to-valley of defocus oscillations in diopters. Each graph corresponds to a subject (S1 to S5). Each color represents a temporal frequency of fluctuation (see legend).*
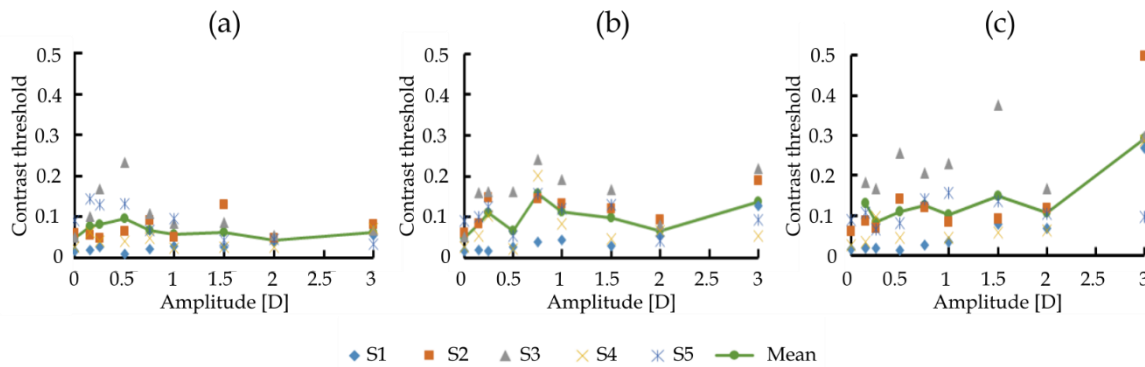
Figure 4.7. *Individual (symbols) and mean (line) contrast threshold as a function of peak-to-valley for defocus oscillations at 5 (a), 15 (b), and 25 Hz (c).*

Additionally, the mean contrast thresholds of all participants at each temporal frequency were examined. As shown in *Figure 4.7,* the mean contrast threshold line for 5 Hz remains fairly flat as the amplitude of the oscillation increases. For 15 Hz, the mean contrast threshold exhibits moderate deterioration and variability across different defocus powers. At 25 Hz, contrast degradation was more noticeable, with the most significant loss occurring at 3 D peak-to-valley defocus. *Figure 4.8* summarizes all mean contrast threshold charts. In general, the contrast threshold increases with temporal frequency. Furthermore, the inter-subject variability also increases with frequency, as can be appreciated by comparing the error bars, which correspond to one standard deviation across subjects.
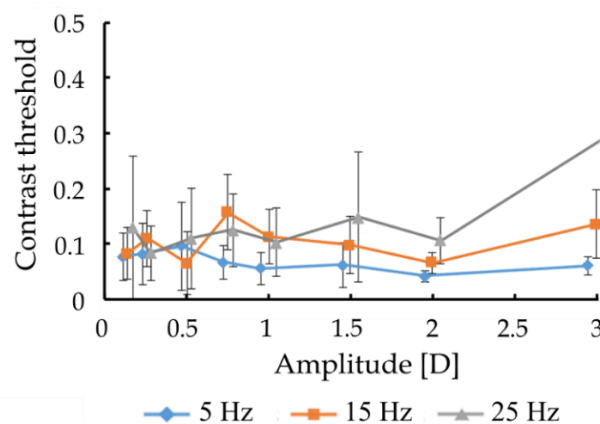
Figure 4.8. *Mean threshold values for 5-, 15-, and 25-Hz defocus oscillations as a function of peak-to-valley. Error bars denote 1 standard deviation across subjects.*

4.7. *Simulation method*

Defocus fluctuations produce a temporal evolution of the PSF. Assuming that the eye integrates retinal irradiance point by point over a period of time, the apparent PSF would be the average of the sequence of defocused PSFs over that period. The loss in contrast produced

by the ensuing blurring can be determined from the (combined) MTF obtained from this averaged PSF.

It is important to note that MTF computing is not a linear process. Therefore, the combined MTF does not coincide in general with the average of instantaneous MTFs, and the latter calculation, which is less computationally demanding, is not apt for our analysis. Conversely, if we consider the complex Optical Transfer Function (OTF), the OTF from the mean PSF is equivalent to the mean of individual OTFs, a fact that we exploit here. To further optimize the computation, instead of fixing a sampling step in time and computing the sequence of PSFs for each defocus oscillation condition, we precalculated a series of defocused PSFs and took the average of the ones from the stack closer to the instantaneous defocus values.

In summary, the simulation consisted of two computing loops. The first one consisted of producing the series of PSFs for defocus values between 0 and 3 D in 0.01 D steps. For such a small defocus difference, neighboring PSFs are practically indistinguishable, and the rounding errors are negligible. Additional parameters for the calculations were a 3-mm pupil diameter and a wavelength of 0.545 microns. Each PSF was Fourier transformed to obtain the OTF. Only the complex OTF value for 12 cpd (the spatial frequency selected for the experiment) was stored and flagged with the defocus value for future access.

The second loop was for temporal averaging over an integration time around the best focus case (0 D). For each oscillation condition (temporal frequency and defocus amplitude), a series of instantaneous defocus values were calculated in $5 \cdot 10^{-4}$ sec steps from 0 to half the integration time. These values, rounded to the hundredth of diopter, were used to select from the stack the OTF values to be averaged to obtain the integrated OTF. Since the defocused PSF does not depend on the sign of the defocus, each value (except for 0) was added twice, to cover both the positive and negative halves of the integration time.

Finally, the integrated MTF for each integration time and oscillation condition was obtained as the modulus of the averaged OTF. In each case, the modulation loss was calculated as the ration between the diffraction-limited (static 0 D defocus) MTF and the integrated MTF. With this protocol, the effect on image quality of the combined blur caused by variable defocus can be studied as a function of the dynamics of fluctuation and the integration time. This kind of

analysis will be used in the second part of this thesis in an attempt to shed some light on the behavior of the visual system under these conditions

4.7.1. *Simulation of linear defocus sweep around the best focus*

Figure 4.9 shows in orange the effect of a static defocus on the MTF at 12 c/deg. It is a well-known fact that the MTF initially drops with increasing defocus due to the blurring caused by the widening PSF, and then goes through a series of null values with phase reversals (alternating sign of the OTF) interspersed. On the other hand, the blue line represents the integrated MTF for a linear sweep of defocus around 0 D, computed by averaging the defocused PSFs in the range [-x, x].
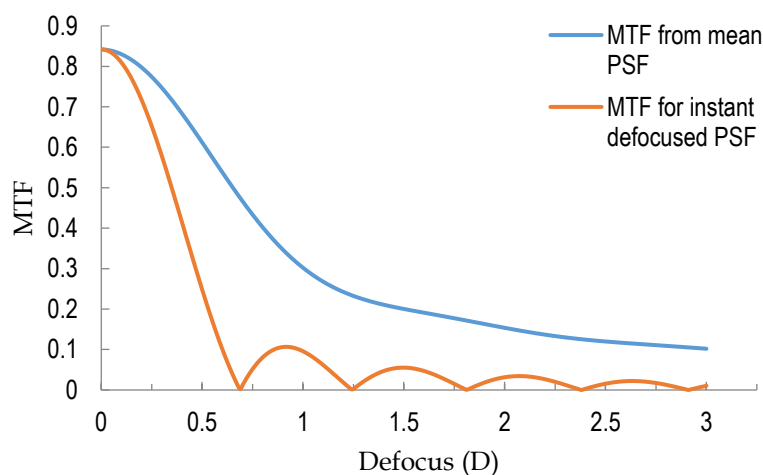
Figure 4.9. *MTF at 12 cpd for static and dynamic defocus. For the static case (orange line), the x-axis represents the amount of defocus introduced. For the dynamic case (blue line), the x-axis represents the maximum defocus in the sweep (the MTF comes from the average PSF in the range [-x, x] D)*

As would be expected, the drop in the MTF for a variable defocus is less marked that at the top of the range, as the evolving PSF goes through the best focus situation at some point. Actually, for defocus values up to 0.5 D (below the 1st phase reversal for the selected conditions), there is a constant scale factor between the curves close to 0.5, meaning that a defocus sweep produces a blurring effect analogous to half its amplitude of static defocus. *Figure 4.10*, displaying the amplitude of dynamic defocus that matches the MTF value obtained for each amount of static defocus, further illustrates this point. As a final comment, although *Figure 4.9* shows results for 12 cpd, the specific value used in this study, the ½ scaling factor is virtually independent of the spatial frequency, as the analysis for other lower and higher spatial frequencies produced graphs nearly identical to *Figure 4.10*
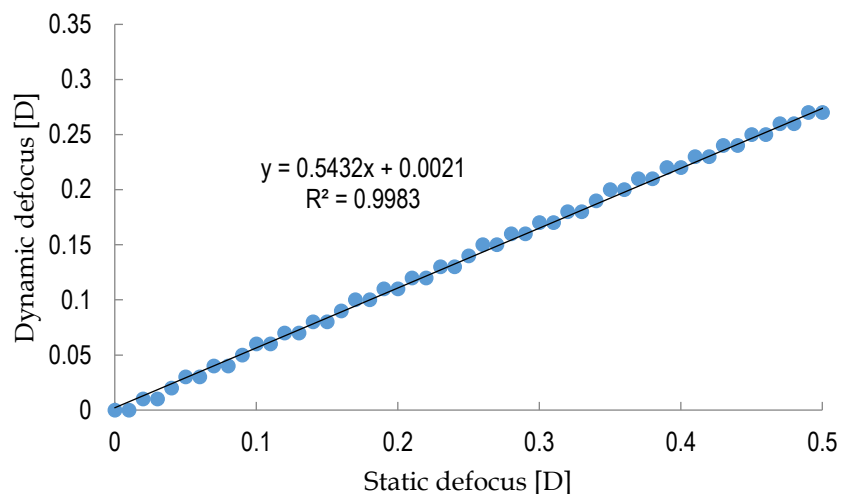
Figure 4.10. *Equivalence in blurring effects between static and dynamic defocus. Symbols: half-range of dynamic defocus (for a linear [-y, y] D fluctuation), producing an equivalent drop in the MTF to a x D static defocus. Line: regression line.*

4.7.2. *Simulation of sinusoidal defocus fluctuations*

Unlike the linear case, where the range suffices to evaluate the effects on the MTF, for sinusoidal defocus oscillations, an integration time must be defined in which to determine the instantaneous PSFs to be averaged.
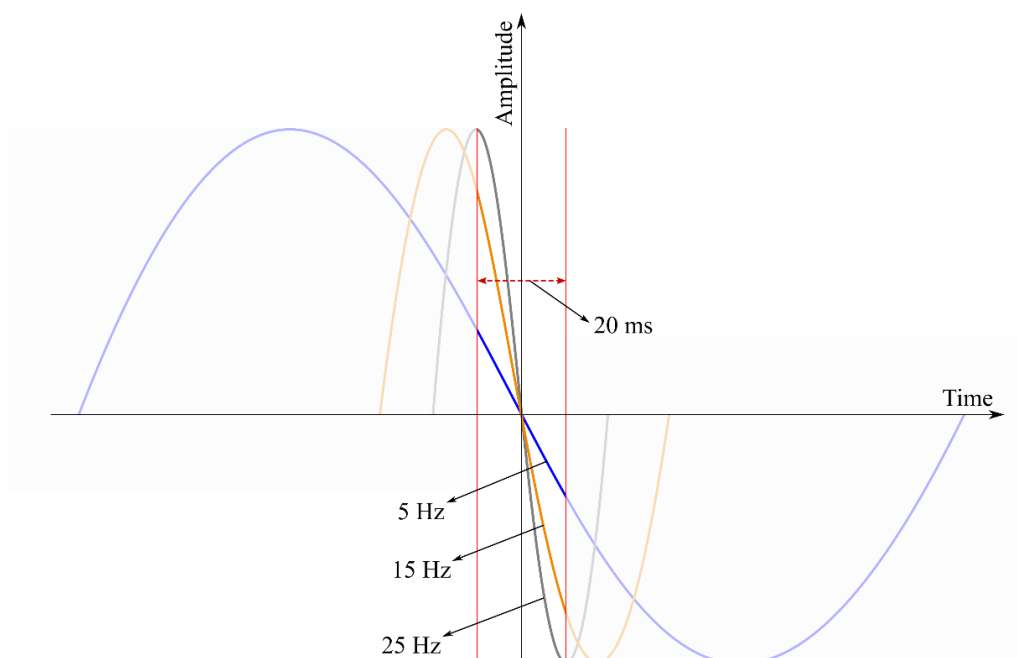
Figure 4.11. *An example of 20 ms integration time for 5, 15, and 25 Hz sinusoidal oscillations with identical amplitudes.*

An example of a 20 ms integration time for equal amplitude sinusoidal oscillations at 5, 15, and 25 Hz is illustrated in *Figure 4.11*.
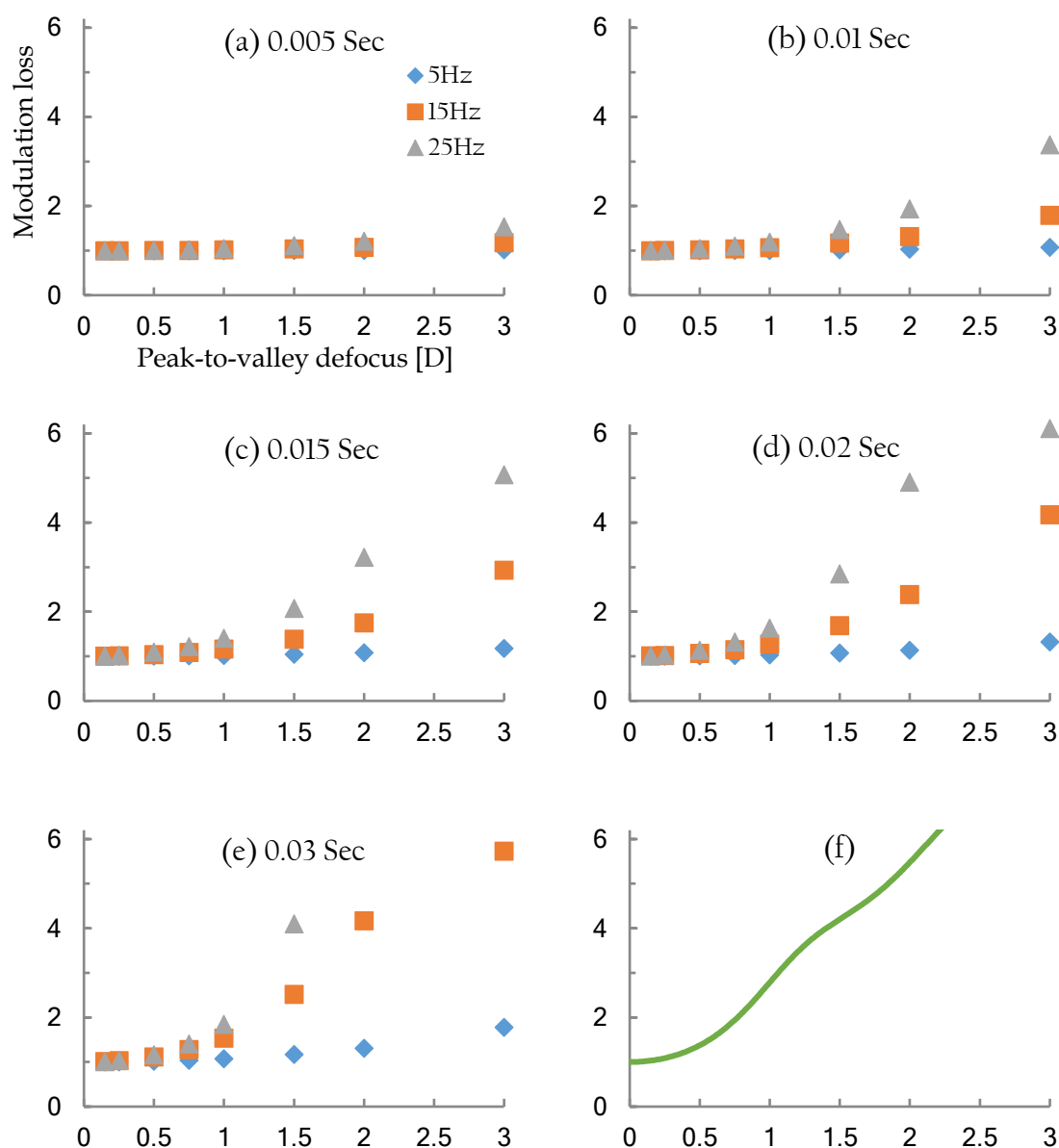
Figure 4.12. *(a) to (e) 12-c/deg modulation loss (diffraction limited MTF over integrated MTF) caused by defocus oscillations at 5 Hz (blue), 15 Hz (orange), and 25 Hz (gray), as a function of fluctuation peak-to-valley. Integration time on display. (f) Modulation loss caused by whole defocus range integration.*

The procedure described in the methods section was used to evaluate the modulation loss (ratio between the diffraction limited MTF and the integrated MTF for each condition) at 12 cpd. The modulation loss was calculated for defocus oscillations with the same temporal frequencies and amplitudes considered in the experiment, considering a range of integration times from 5 to 30 ms. Results are displayed in *Figure 4.12*, panels *(a)* to *(e)*. Panel *(f)* presents the modulation loss when the whole defocus range is integrated. This would be equivalent to averaging the blur over an extended period of time, at least equal to a cycle.

4.8. Discussion

Numerous studies have already investigated the temporal limits of the visual system; however, unlike the present study, almost all of them explored the temporal limits of visual perception with static and/or fixed defocus stimuli. To the best of our knowledge, there are no studies comparable to the present work in the literature. Only in one study, the stimulus focus was altered at low periodic sinusoidal oscillations (1 Hz), in order to examine the gain of the accommodation response and its phase lag. In that study, because stimuli oscillated at low temporal frequencies, accommodation was involved [Umemoto & Hirata, 2022]. Defocus fluctuations faster than 5 Hz are too swift to trigger ocular accommodation (accommodation takes more than 200 ms [Ghoushchi et al., 2021]), but they still can affect the retinal image quality and its PSF [Bharadwaj, 2017; Charman & Heron, 2015].

Instead of the VA, the contrast sensitivity was measured at a medium (12 c/deg) spatial frequency, since it is an optimal way to reduce the number of measured conditions and is sensitive to low defocus changes [Radhakrishnan et al., 2004]. Our initial hypothesis was that contrast sensitivity might be degraded dramatically with increasing temporal frequency and, especially, amplitude. This trend was not visible on average nor, in general, in individual cases, although data for some subjects was noisier. We found that human contrast sensitivity is resilient to induced periodic defocus. Even for a 25 Hz oscillation with 3 D peak-to-valley defocus, the individuals could discern the Gabor patch tilt direction if higher contrast was required. This means that the eye is resilient to fast oscillations of defocus, suggesting that the integration time for defocus is relatively short. In other words, the eye is able to interpret the visual stimulus if the retinal image is only focused for a short time.

The simulated MTF analysis with different defocus amplitudes and frequencies indicates that retinal image quality is negatively correlated with defocus integration time. Although the numerical comparison between experimental and simulated loss of modulation is unadvisable considering the small number of subjects, qualitative analysis suggests that the eye's integration time for defocus may be in the range of 1 hundredth of a second. For shorter intervals, the simulation predicts virtually no loss of image quality, while for much longer periods, an larger effect would be expected in the intermediate temporal frequency of fluctuation.

Accommodation microfluctuations, even the fast components, do not exceed the temporal frequencies studied here and the typical amplitudes are well below 1 D [Charman & Heron,

2015]. The eye's relative immunity to defocus variations, found in this work, suggests that microfluctuations should not greatly affect visual performance. In other words, not much of a gain would be expected if they were paralyzed or compensated.

.

Chapter 5

"It is not in doing what you like, but in liking what you do that is the secret of happiness."

J.M. Barrie, Peter Pan

Chapter 5.   Conclusions

The first part of this thesis studied the accommodation dynamics of subjects with various refractive errors in natural viewing conditions, to seek for some evidence of altered accommodative behavior in myopes as a first step in the search for a potential cause/effect relationship and the identification of hypothetical accommodation-related risk factors for myopia onset and/or progression. The second part of this thesis investigated the impact on vision of rapid defocus oscillations at various frequencies and amplitudes, with the aim of shedding some light on the resilience of the visual system when dealing with fluctuating blur around a fixed accommodative state.

The conclusions of this thesis are as follows:

1. Both the hardware and software of a preexisting binocular open-view HS sensor were improved to increase its light efficiency, speed, and dynamic range to measure higher myopic subjects. A previously developed software based on GPU processing was successfully implemented into the system, allowing the HS sensor to measure the accommodation dynamics in real time with no need for post-processing.

2. The open-view system was employed to study accommodation dynamics under realistic viewing conditions in myopic, and emmetropic young individuals. The three components of the accommodation reflex (i.e., convergence, accommodation, and pupillary response) were measured simultaneously in real time. Correlation analysis between refractive error and accommodation speed and of these two variables with various far-to-near response parameters was performed.

3. The correlation analysis refraction (SE) with accommodation dynamics parameters suggests that myopia mildly affects or is affected by accommodation. The lag of accommodation was found to be linked to refractive error ($R = -0.57$, $p = 0.01$). Moreover, the correlation between miosis speed and refractive error also had a p-value below 0.05 ($R = -0.49$, $p = 0.04$). In other words, myopes tend

to have slower pupil constriction and a larger lag of accommodation. The correlation coefficients between SE and the rest of accommodation-related parameters were small, with p-values well above 0.05.

4. A substantial, low-p-value correlation was found between accommodation speed and convergence speed (R = 0.48, p = 0.04). To the best of our knowledge, this finding has not been previously reported. Furthermore, the correlation was stronger between accommodation speed and convergence duration (R = 0.57, p = 0.01), which may reflect the differences in the dynamics of these two processes. In addition, there may be a correlation between accommodation speed and miosis amplitude since the p-value was below 0.05 (R = 0.47, p = 0.049). These analyses showed that slower accommodation might be a function of slow convergence and more evident pupil miosis.

5. For the second part of the thesis, a faster HS sensor with a refresh rate of 60 Hz and higher sensitivity to 1050 nm IR light was developed. This sensor was employed to characterize an optically tunable lens both in the typical static mode and, for the first time to our knowledge, in dynamic mode. After calibration, the tunable lens was used to apply defocus oscillations during contrast sensitivity measurements.

6. Contrast sensitivity was measured under the influence of these oscillations with different amplitudes and frequencies in five young emmetropes. It was found that contrast sensitivity is resilient to induced defocus oscillations. The data showed that only for fast, large variations (25 Hz, $\pm$ 1.5 D), there was a noticeable reduction in contrast sensitivity. This indicates that for the eye to clearly perceive visual stimuli, the retinal image only needs to be in focus for a short time.

7. A quantitative model was developed for predicting the deterioration in retinal image quality due to periodic defocus fluctuations. For the amplitudes and frequencies of oscillation used in the experiment, the average PSF was calculated for several integration times and the loss in the ensuing MTF was computed.

Comparison between experimental results and simulated data suggests that the eye may be integrating defocus blur at 10 to 20 ms intervals.

Acknowledgments

I would like to dedicate this thesis to my parents, Setareh and Habib, who always have supported me and respected my decisions. Their endless love and encouragement empowered me to overcome challenges in my life and advance in my academic career. Moreover, I would want to thank the compassion and care of my brothers and sisters who have been a huge source of motivation for me. Without the kind support of my beloved family, it would not have been possible for me to complete this long journey.

I would like to express my deepest and most sincere gratitude to my supervisor Prof. Pablo Artal who trusted me and gave me this wonderful opportunity to be part of his excellent group. He is a role model and created a world class research environment in LOUM. His dedication, self-discipline, hard work, and excellent problem solving were an inspiration for me. Under his supervision, I developed my research skills and deepened my knowledge of vision science. Even though he was extremely busy he always made time to listen to the problems and give feedback when it was needed.

My sincere and heartful thanks go to my co-supervisor Dr. Pedro Prieto for his substantial support from the first day I joined LOUM. He is a meticulous and knowledgeable vision scientist whose professionalism, honesty, and critical thinking are remarkable. His door was open to me whenever I needed to discuss any problem. He always corrected my errors and helped me with analysis and revisions. I learned a lot during our long discussions about experiments and various research topics. He was not just a supervisor but also a great friend.

Special thanks go to my colleague Juan who helped me a lot with programming and the software part of the project. He was ready to help with the measurements and without his generous assistance I would not have been able to complete this thesis. I am grateful to Juan Manuel, a brilliant academician with a fantastic sense of humor who helped me whenever I needed it. Moreover, I admire Josua's great personality and his fruitful academic and life comments which significantly helped me in many aspects. I would like to thank Carmen who

helped me with paperwork and bureaucracy. I would love to express my gratitude to my friends at LOUM: Raul, for being a real and sincere friend who has helped me numerous times and has assisted me in improving my Spanish, Esther whose advice, nice conversations, and good mood have been truly rewarding, my officemates Dibyendu and Consuelo for insightful conversations. I appreciate the friendship of Alba, Santi, Rosa, Adrian, Shoaib, Zhenghua, Pien, and Xinyu who were a part of my daily life and made my time so pleasant in Murcia. I would like to thank current and previous LOUM members during these years: Juan Tabernero, Eloy, Silvestre, Oscar, Luis, Antonio, Augusto, Dimitrios, Rahul, Nikolai, and Yiwei. Even though I was far away from my home country LOUM was my family in Spain.

I want to thank Prof. Siegfried Wahl and Dr. Arne Ohlendorf for hosting me in Zeiss vision lab in Tübingen, Germany. I am grateful to Pablo Sanz Diez who helped me a lot in the experiments during my stay in Tübingen. I appreciate Prof. Frank Schaeffel the coordinator of MYFUN and Dr. Christina Schwarz for her professional academic advice. My gratitude goes to all of my friends in the MYFUN network and our external advisors Prof. Donald Mutti and Porf. Christine Wildsoet. As an early stage researcher, I participated in many conferences, summer schools, and workshops with this incredible network and gained a lot of knowledge and experience.

I would like to thank all of my friends who made me enjoy my journey while studying for my Ph.D. I am grateful to Umut, who is a great friend with a humble personality, I really enjoyed our conversation and discussions. I want to thank my friends in the cycling club with whom I made a lot of long rides that kept me refreshed and sane and my friends in the dancing club for the enjoyable memories. In addition, I would like to thank our amazing lunch group at the university who created a lot of good moments, and the Iranian community in Murcia that helped me to feel good and enjoy my stay. In addition, I am grateful to all of my close friends who always listened to me, believed in me, encouraged me, and guided me during this long journey. Thank you all.

References

3doptix. (n.d.). *3DOptix simulation software*. 2022-09-26. https://3doptix.com.

A. Mark Smith. (n.d.). *Optics to the Time of Kepler*. Accessed 13 January 2023. Encyclopedia of the History of Science. https://doi.org/10.34758/9482-n985.

Abrahamsson, M., & Sjöstrand, J. (1986). Impairment of contrast sensitivity function (CSF) as a measure of disability glare. *Investigative Ophthalmology & Visual Science*, *27*(7), 1131–1136.

Adamson, P. (2016). *Philosophy in the Islamic World: A history of philosophy without any gaps, Volume 3*. Oxford University Press.

Aggarwala, K. R., Kruger, E. S., Mathews, S., & Kruger, P. B. (1995). Spectral bandwidth and ocular accommodation. *JOSA A*, *12*(3), 450–455.

Aggarwala, K. R., Nowbotsing, S., & Kruger, P. B. (1995). *Accommodation to Monochromatic and White-Light Targets*. *36*(13), 2695–2705.

Akondi, V., Sawides, L., Marrakchi, Y., Gambra, E., Marcos, S., & Dorronsoro, C. (2018). Experimental validations of a tunable-lens-based visual demonstrator of multifocal corrections. *Biomedical Optics Express*, *9*(12), 6302. https://doi.org/10.1364/boe.9.006302

Alió, J. L., & El Bahrawy, M. (2017). Laser refractive surgery. In *Handbook of Visual Optics, Volume Two* (pp. 233–251). CRC Press.

Allan, L. G. (1975). Temporal order psychometric functions based on confidence-rating data. *Perception & Psychophysics*, *18*(5), 369–372. https://doi.org/10.3758/BF03211214

Alpern, M. (1958). Variability of accommodation during steady fixation at various levels of illuminance. *JOSA*, *48*(3), 193–197.

Ang, M., Flanagan, J. L., Wong, C. W., Müller, A., Davis, A., Keys, D., Resnikoff, S., Jong, M., Wong, T. Y., & Sankaridurg, P. (2020). myopia control strategies recommendations from the 2018 WHO/IAPB/BHVI meeting on myopia. *British Journal of Ophthalmology*, *104*(11), 1482–1487.

ANSI. (2004). *Methods for reporting aberrations of eyes ANSI Z80.28*.

ANSI. (2007). ANSI Z136.1—2007. In *Laser Institute of America*. papers2://publication/uuid/D2E145A0-6015-4317-895E-3644589A4A40

Apple, D. J., & Sims, J. (1996). Harold Ridley and the invention of the intraocular lens. *Survey of Ophthalmology*, *40*(4), 279–292.

Arditi, A. (2005). Improving the design of the letter contrast sensitivity test. *Investigative Ophthalmology and Visual Science*, *46*(6), 2225–2229. https://doi.org/10.1167/iovs.04-1198

Armstrong, R. A. (2013). Statistical guidelines for the analysis of data obtained from one or both eyes. *Ophthalmic & Physiological Optics : The Journal of the British College of*

Ophthalmic Opticians (Optometrists), *33*(1), 7–14. https://doi.org/10.1111/OPO.12009

Armstrong, R. A. (2014). When to use the Bonferroni correction. *Ophthalmic and Physiological Optics*, *34*(5), 502–508. https://doi.org/10.1111/OPO.12131

Armstrong, R. A., Eperjesi, F., & Gilmartin, B. (2002). The application of analysis of variance (ANOVA) to different experimental designs in optometry. *Ophthalmic & Physiological Optics : The Journal of the British College of Ophthalmic Opticians (Optometrists)*, *22*(3), 248–256. https://doi.org/10.1046/J.1475-1313.2002.00020.X

Artal, P., & Fernández, E. J. (2005). Study on the effects of monochromatic aberrations in the accommodation response by using adaptive optics. *JOSA A, Vol. 22, Issue 9, Pp. 1732-1738*, *22*(9), 1732–1738. https://doi.org/10.1364/JOSAA.22.001732

Artal, P., & Navarro, R. (1994). Monochromatic modulation transfer function of the human eye for different pupil diameters: an analytical expression. *JOSA A*, *11*(1), 246–249.

Atchison, D. A., & Charman, W. N. (2010). Thomas Young's contribution to visual optics: The Bakerian lecture "On the mechanism of the eye." *Journal of Vision*, *10*(12), 16. https://doi.org/10.1167/10.12.16

Atchison, D. A., Pritchard, N., & Schmid, K. L. (2006). Peripheral refraction along the horizontal and vertical visual fields in myopia. *Vision Research*, *46*(8–9), 1450–1458.

Atchison, D. A., Smith, G., & Smith, G. (2000). *Optics of the human eye* (Vol. 35). Butterworth-Heinemann Oxford.

Babinsky, E., & Candy, T. R. (2013). Why Do Only Some Hyperopes Become Strabismic? *Investigative Opthalmology & Visual Science*, *54*(7), 4941. https://doi.org/10.1167/iovs.12-10670

Baker, D. B. (2012). *The Oxford handbook of the history of psychology: Global perspectives*. Oxford University Press.

Barten, P. G. J. (1999). Contrast sensitivity of the human eye and its effects on image quality. In *SPIE press*. SPIE press. https://doi.org/10.1117/3.353254

Beekes, R. (2009). Etymological dictionary of Greek (2 vols.). In *Etymological Dictionary of Greek (2 vols.)*. Brill.

Beers, A. P. A., & Van Der Heijde, G. L. (1994). In vivo determination of the biomechanical properties of the component elements of the accommodation mechanism. *Vision Research*, *34*(21), 2897–2905. https://doi.org/10.1016/0042-6989(94)90058-2

Beers, A. P., & Van der Heijde, G. L. (1996). Age-related changes in the accommodation mechanism. *Optometry and Vision Science: Official Publication of the American Academy of Optometry*, *73*(4), 235–242.

Benjamin, W. J. (2006). *Borish's Clinical Refraction-E-Book*. Elsevier Health Sciences.

Berggren, L. (2001). Studies of vision by Leonardo da Vinci. *Svensk Medicinhistorisk Tidskrift*, *5*(1), 171–185. http://www.ncbi.nlm.nih.gov/pubmed/11824410

Bharadwaj, S. R. (2017). Accommodation mechanisms. In *Handbook of Visual Optics, Volume One* (pp. 363–376). CRC Press.

Bieganowski, L. (2004). Ophthalmic aspects in Celsus' work de medicina libri octo. In *Klinika Oczna* (Vol. 106, Issue 3, pp. 376–381). Klin Oczna. https://pubmed.ncbi.nlm.nih.gov/15515329/

Biographyonline.net. (n.d.). *Newton's prism experiment*. Accessed 18-01-2023. https://www.biographyonline.net/ideas-that-changed-the-world/newton/

Bundesen, C., & Harms, L. (1999). Single-letter recognition as a function of exposure duration. *Psychological Research*, *62*(4), 275–279. https://doi.org/10.1007/s004260050057

Campbell, F. W., & Green, D. G. (1965a). Monocular versus binocular visual acuity. *Nature*, *208*(5006), 191–192.

Campbell, F. W., & Green, D. G. (1965b). Optical and retinal factors affecting visual resolution. *The Journal of Physiology*, *181*(3), 576.

Campbell, F. W., & Gubisch, R. W. (1966). Optical quality of the human eye. *The Journal of Physiology*, *186*(3), 558–578.

Campbell, F. W., & Robson, J. G. (1968). Application of Fourier analysis to the visibility of gratings. *The Journal of Physiology*, *197*(3), 551.

Campbell, F. W., Robson, J. G., & Westheimer, G. (1959). Fluctuations of accommodation under steady viewing conditions. *The Journal of Physiology*, *145*(3), 579.

Campbell, F. W., & Westheimer, G. (1960). Dynamics of accommodation responses of the human eye. *The Journal of Physiology*, *151*(2), 285–295. https://doi.org/10.1113/jphysiol.1960.sp006438

Carr, B. J., & Stell, W. K. (n.d.). *The science behind myopia*. Accessed 20-01-20233, WEBVISION. https://webvision.med.utah.edu/book/part-xvii-refractive-errors/the-science-behind-myopia-by-brittany-j-carr-and-william-k-stell/

Cassin, B., Solomon, S., & Rubin, M. L. (1990). *Dictionary of eye terminology*. Triad Publishing Company Gainesville.

Charman, W. N. (1979). Effect of refractive error in visual tests with sinusoidal gratings. *The British Journal of Physiological Optics*, *33*(2), 10–20.

Charman, W. N. (2005). Aberrations and myopia. *Ophthalmic & Physiological Optics : The Journal of the British College of Ophthalmic Opticians (Optometrists)*, *25*(4), 285–301. https://doi.org/10.1111/j.1475-1313.2005.00297.x

Charman, W. N., & Heron, G. (2015). Microfluctuations in accommodation: An update on their characteristics and possible role. In *Ophthalmic and Physiological Optics* (Vol. 35, Issue 5, pp. 476–499). https://doi.org/10.1111/opo.12234

Charman, W. N., & Radhakrishnan, H. (2009). Accommodation, pupil diameter and myopia. *Ophthalmic and Physiological Optics*, *29*(1), 72–79. https://doi.org/10.1111/j.1475-1313.2008.00611.x

Charman, W. N., & Tucker, J. (1977). Dependence of accommodation response on the spatial frequency spectrum of the observed object. *Vision Research*, *17*(1), 129–139.

Charman, W. N., & Tucker, J. (1978). Accommodation and color. *Journal of the Optical Society of America*, *68*(4), 459–471. https://doi.org/10.1364/JOSA.68.000459

Chen, L., Ghilardi, M., Busfield, J. J. C., & Carpi, F. (2021). Electrically Tunable Lenses: A Review. In *Frontiers in Robotics and AI* (Vol. 8). Frontiers Media S.A. https://doi.org/10.3389/frobt.2021.678046

Chen, L., Kruger, P. B., Hofer, H., Singer, B., & Williams, D. R. (2006). Accommodation with higher-order monochromatic aberrations corrected with adaptive optics. *Journal of the Optical Society of America A*, *23*(1), 1. https://doi.org/10.1364/josaa.23.000001

Cheng, X., Bradley, A., Hong, X., & Thibos, L. N. (2003). Relationship between refractive error and monochromatic aberrations of the eye. *Optometry and Vision Science : Official*

Publication of the American Academy of Optometry, *80*(1), 43–49. https://doi.org/10.1097/00006324-200301000-00007

Cheng, X., Xu, J., & Brennan, N. A. (2019). Accommodation and its role in myopia progression and control with soft contact lenses. *Ophthalmic and Physiological Optics*, *39*(3), 162–171. https://doi.org/10.1111/opo.12614

Chin, S. S., Hampson, K. M., & Mallen, E. A. H. (2008). Binocular correlation of ocular aberration dynamics. *Optics Express*, *16*(19), 14731–14745. https://doi.org/10.1364/OE.16.014731

Chin, S. S., Hampson, K. M., & Mallen, E. A. H. (2009a). Role of ocular aberrations in dynamic accommodation control. *Clinical and Experimental Optometry*, *92*(3), 227–237. https://doi.org/10.1111/j.1444-0938.2009.00361.x

Chin, S. S., Hampson, K. M., & Mallen, E. A. H. (2009b). Effect of correction of ocular aberration dynamics on the accommodation response to a sinusoidally moving stimulus. *Optics Letters*, *34*(21), 3274. https://doi.org/10.1364/OL.34.003274

Chin, S. S., Mallen, E. A. H., & Hampson, K. M. (2010). Effect of temporal location of correction of monochromatic aberrations on the dynamic accommodation response. *Biomedical Optics Express, Vol. 1, Issue 3, Pp. 879-894*, *1*(3), 879–894. https://doi.org/10.1364/BOE.1.000879

Chirre, E. (2017a). Design of an open-view binocular sensor for the study of accommodation [Universidad de Murcia]. In *Proyecto de investigación*. https://digitum.um.es/digitum/handle/10201/55727

Chirre, E. (2017b). *Design of an open-view binocular sensor for the study of accommodation*. https://digitum.um.es/digitum/handle/10201/55727

Chirre, E., Prieto, P. M., & Artal, P. (2014). Binocular open-view instrument to measure aberrations and pupillary dynamics. *Optics Letters*, *39*(16), 4773. https://doi.org/10.1364/OL.39.004773

Chirre, E., Prieto, P. M., & Artal, P. (2015). Dynamics of the near response under natural viewing conditions with an open-view sensor. *Biomedical Optics Express*, *6*(10), 4200. https://doi.org/10.1364/BOE.6.004200

Choh, V., & Sivak, J. G. (2017). Anatomy and embryology of the eye: An overview. In P. Artal (Ed.), *Handbook of Visual Optics, Volume One* (pp. 129–141). CRC Press.

Chua, S. Y. L., & Foster, P. J. (2020). The Economic and Societal Impact of Myopia and High Myopia. *Updates on Myopia: A Clinical Perspective*, 53–63.

Ciuffreda, K. J., & Kruger, P. B. (1988). Dynamics of human voluntary accommodation. In *Optometry and Vision Science* (Vol. 65, Issue 5, pp. 365–370). https://doi.org/10.1097/00006324-198805000-00010

Collins, G. (1939). The electronic refractionometer. *Clinical and Experimental Optometry*, *22*(2), 122–132. https://doi.org/10.1111/j.1444-0938.1939.tb01569.x

Collins, M., Davis, B., & Wood, J. (1995). Microfluctuations of steady-state accommodation and the cardiopulmonary system. *Vision Research*, *35*(17), 2491–2502.

Collins, M. J., Wildsoet, C. F., & Atchison, D. A. (1995). Monochromatic aberrations and myopia. *Vision Research*, *35*(9), 1157–1163. https://doi.org/10.1016/0042-6989(94)00236-F

Congdon, N., Burnett, A., & Frick, K. (2019). The impact of uncorrected myopia on

individuals and society. *Community Eye Health*, *32*(105), 7–8.
http://www.ncbi.nlm.nih.gov/pubmed/31409943

Craik, E. (2014). *The 'Hippocratic' corpus: Content and context*. Routledge.

CUDA. (n.d.). *Nvidia Cublas library*. 2017-06-05.
https://docs.nvidia.com/cuda/cublas/index.html

Culhane, H. M., & Winn, B. (2000). Dynamic accommodation and myopia. *Journal of American Association for Pediatric Ophthalmology and Strabismus*, *4*(1), 63–64.
https://doi.org/10.1016/S1091-8531(00)90021-1

Curtis Sparks. (n.d.). *Anatomy of the eye and ear*. Accessed 20-01-20233.
https://slideplayer.com/slide/8955946/

Czepita, D., Mojsa, A., Ustianowska, M., Czepita, M., & Lachowicz, E. (2010). Reading, writing, working on a computer or watching television, and myopia. *Klinika Oczna*, *112*(10–12), 293–295. http://www.ncbi.nlm.nih.gov/pubmed/21469524

Davis, J., Hsieh, Y. H., & Lee, H. C. (2015). Humans perceive flicker artifacts at 500 Hz. *Scientific Reports*, *5*, 7861. https://doi.org/10.1038/srep07861

Day, M., Gray, L. S., Seidel, D., & Strang, N. C. (2009). The relationship between object spatial profile and accommodation microfluctuations in emmetropes and myopes. *Journal of Vision*, *9*(10), 5.

De Valois, R. L., Morgan, H., & Snodderly, D. M. (1974). Psychophysical studies of monkey vision-III. Spatial luminance contrast sensitivity tests of macaque and human observers. *Vision Research*, *14*(1), 75–81.

Deng, G., & Cahill, L. W. (1994). Adaptive Gaussian filter for noise reduction and edge detection. *IEEE Nuclear Science Symposium & Medical Imaging Conference*, *pt 3*, 1615–1619. https://doi.org/10.1109/NSSMIC.1993.373563

Dogru, M., Chen, M., Shimmura, S., & Tsubota, K. (2009). *Chapter 4 - Corneal epithelium and stem cells* (F. S. Brightbill, P. J. McDonnell, A. A. Farjo, C. N. J. McGhee, O. N. Serdarevic, & C. L. B. T.-C. S. (Fourth E. Laurel (eds.); pp. 25–31). Mosby.
https://doi.org/https://doi.org/10.1016/B978-0-323-04835-4.50010-0

Dolgin, E. (2015). The myopia boom. *Nature*, *519*(7543), 276–278.
https://doi.org/10.1038/519276a

Doughty, M. J., & Zaman, M. L. (2000). Human Corneal Thickness and Its Impact on Intraocular Pressure Measures: A Review and Meta-analysis Approach. *Survey of Ophthalmology*, *44*(5), 367–408. https://doi.org/https://doi.org/10.1016/S0039-6257(00)00110-7

Edmund Optics. (n.d.). *Datasheets for Hot Mirrors and Cold Mirrors*. Accessed 13-01-2023.
https://datasheets.globalspec.com/ds/2155/EdmundOptics

Fahrbach, F. O., Gurchenkov, V., Alessandri, K., Nassoy, P., & Rohrbach, A. (2013). Light-sheet microscopy in thick media using scanned Bessel beams and two-photon fluorescence excitation. *Optics Express*, *21*(11), 13824.
https://doi.org/10.1364/OE.21.013824

Falco, C. M. (2007). Ibn al-Haytham and the origins of modern image analysis. *2007 9th International Symposium on Signal Processing and Its Applications*, 1–2.

Fercher, A. F., Drexler, W., Hitzenberger, C. K., & Lasser, T. (2003). Optical coherence tomography-principles and applications. *Reports on Progress in Physics*, *66*(2), 239.

Fernández, E. J., & Artal, P. (2008). Ocular aberrations up to the infrared range: from 6328 to 1070 nm. *Optics Express*, *16*(26), 21199. https://doi.org/10.1364/oe.16.021199

Fielder, A. R., & Moseley, M. J. (1996). Does stereopsis matter in humans? *Eye*, *10*(2), 233–238.

Fincham, E. F. (1951). The accommodation reflex and its stimulus. *The British Journal of Ophthalmology*, *35*(7), 381.

Finger, S. (1994). *Origins of neuroscience : a history of explorations into brain function*. 462.

Fischler, M. A., & Bolles, R. C. (1981). Random sample consensus. *Communications of the ACM*, *24*(6), 381–395. https://doi.org/10.1145/358669.358692

Fisher, R. F. (1986). The ciliary body in accommodation. *Transactions of the Ophthalmological Societies of the United Kingdom*, *105 (Pt 2*, 208–219. http://europepmc.org/abstract/MED/3467496

Fledelius, H. C., & Stubgaard, M. (1986). Changes in refraction and corneal curvature during growth and adult life: a cross-sectional study. *Acta Ophthalmologica*, *64*(5), 487–491.

Flitcroft, D. I. (2014). Emmetropisation and the aetiology of refractive errors. *Eye*, *28*(2), 169–179. https://doi.org/10.1038/eye.2013.276

Flitcroft, D. I., He, M., Jonas, J. B., Jong, M., Naidoo, K., Ohno-Matsui, K., Rahi, J., Resnikoff, S., Vitale, S., & Yannuzzi, L. (2019). IMI – Defining and Classifying Myopia: A Proposed Set of Standards for Clinical and Epidemiologic Studies. *Investigative Opthalmology & Visual Science*, *60*(3), M20. https://doi.org/10.1167/iovs.18-25957

Freedman, R. D., & Thibos, L. N. (1975). Contrast sensitivity in humans with abnormal visual experience. *The Journal of Physiology*, *247*(3), 687–710.

Fry, G. A. (1963). Retinal image formation: review, summary, and discussion. *JOSA*, *53*(1), 94–97.

Furukawa, H., Hiro-Oka, H., Satoh, N., Yoshimura, R., Choi, D., Nakanishi, M., Igarashi, A., Ishikawa, H., Ohbayashi, K., & Shimizu, K. (2010). Full-range imaging of eye accommodation by high-speed long-depth range optical frequency domain imaging. *Biomedical Optics Express*, *1*(5), 1491. https://doi.org/10.1364/BOE.1.001491

G. Morgan, I., Ohno-Matsui, K., & Saw, S.-M. (2012). Myopia. *The Lancet*, *379*, 1739–1748. https://doi.org/10.1016/S0140-6736(12)60272-4

Gambra, E., Sawides, L., Dorronsoro, C., & Marcos, S. (2009). Accommodative lag and fluctuations when optical aberrations are manipulated. *Journal of Vision*, *9*(6), 4–4. https://doi.org/10.1167/9.6.4

Geary, J. M. (2015). Introduction to wavefront sensors. *Syria Studies*, *7*(1), 37–72. https://www.researchgate.net/publication/269107473_What_is_governance/link/548173 090cf22525dcb61443/download%0Ahttp://www.econ.upf.edu/~reynal/Civil wars_12December2010.pdf%0Ahttps://think-asia.org/handle/11540/8282%0Ahttps://www.jstor.org/stable/41857625

Gellrich, M.-M. (2014). History of the slit lamp. In *The Slit Lamp* (pp. 189–210). Springer.

Ghoushchi, V. P. (2015). Opto-Mechanical Design And Development of an Optodigital Confocal Microscope. In *Optoelectronics & Photonics Engineering*. https://doi.org/10.1007/978-3-540-69000-9_100362

Ghoushchi, V. P., Aas, M., Ulusoy, E., & Ürey, H. (2017). Effect of spatial coherence of

LED sources on image resolution in holographic displays. *Advances in Display Technologies VII*, *10126*, 101260A. https://doi.org/10.1117/12.2252413

Ghoushchi, V. P., Mompeán, J., Prieto, P. M., & Artal, P. (2021). Binocular dynamics of accommodation, convergence, and pupil size in myopes. *Biomedical Optics Express*, *12*(6), 3282. https://doi.org/10.1364/boe.420334

Ghoushchi, V. P., Mompeán, J., Prieto, P. M., & Artal, P. (2022). Effect of periodic defocus oscillations on contrast sensitivity. *Investigative Ophthalmology & Visual Science*, *63*(7), 3060 – F0532-3060 – F0532.

Gilmartin, B. (1986). A review of the role of sympathetic innervation of the ciliary muscle in ocular accommodation. *Ophthalmic and Physiological Optics*, *6*(1), 23–37.

Goldberg, D. B. (2011). Computer-animated model of accommodation and theory of reciprocal zonular action. *Clinical Ophthalmology (Auckland, N.Z.)*, *5*, 1559–1566. https://doi.org/10.2147/OPTH.S25983

Goodman, J. W., & Sutton, P. (1996). Introduction to Fourier optics. *Quantum and Semiclassical Optics-Journal of the European Optical Society Part B*, *8*(5), 1095.

Goss, D. (1995). Ocular accommodation, convergence and Disparity Fixation: a manual of clinical analysis. In *Editorial Butterworth-Heinemann*. Elsevier Health Sciences.

Goss, D. A. (2000). Nearwork and myopia. *The Lancet*, *356*(9240), 1456–1457. https://doi.org/10.1016/S0140-6736(00)02864-6

Goss, D. A., & Wickham, M. G. (1995). Retinal-image mediated ocular growth as a mechanism for juvenile onset myopia and for emmetropization - A literature review. *Documenta Ophthalmologica*, *90*(4), 341–375. https://doi.org/10.1007/BF01268122

Guirao, A. (2017). Optical and visual metrics. In P. Artal (Ed.), *Handbook of Visual Optics, Volume Two* (pp. 275–295). CRC Press.

Guirao, A., & Williams, D. R. (2003). A method to predict refractive errors from wave aberration data. *Optometry and Vision Science*, *80*(1), 36–42.

Gwiazda, J. E., Hyman, L., Norton, T. T., Hussein, M. E. M., Marsh-Tootle, W., Manny, R., Wang, Y., & Everett, D. (2004). Accommodation and Related Risk Factors Associated with Myopia Progression and Their Interaction with Treatment in COMET Children. *Investigative Opthalmology & Visual Science*, *45*(7), 2143. https://doi.org/10.1167/iovs.03-1306

Gwiazda, J., Grice, K., Held, R., McLellan, J., & Thorn, F. (2000). Astigmatism and the development of myopia in children. *Vision Research*, *40*(8), 1019–1026.

Haarman, A. E. G., Enthoven, C. A., Tideman, J. W. L., Tedja, M. S., Verhoeven, V. J. M., & Klaver, C. C. W. (2020). The complications of myopia: a review and meta-analysis. *Investigative Ophthalmology & Visual Science*, *61*(4), 49.

Hampson, K. M., Chin, S. S., & Mallen, E. A. H. (2008). Binocular Shack–Hartmann sensor for the human eye. *Journal of Modern Optics*, *55*(4–5), 703–716.

Harb, E., Thorn, F., & Troilo, D. (2006). *Characteristics of accommodative behavior during sustained reading in emmetropes and myopes &. 46*, 2581–2592. https://doi.org/10.1016/j.visres.2006.02.006

Hartmann, J. (1904). Objektivuntersuchungen. *Zeitschrift Für Instrumentenkunde*, *24*, 1–25, 33–47, 97–117. https://archive.org/details/zeitschriftfrin09gergoog

Hartwig, A., & Atchison, D. A. (2012). Analysis of higher-order aberrations in a large clinical population. *Investigative Ophthalmology & Visual Science*, *53*(12), 7862–7870. https://doi.org/10.1167/iovs.12-10610

Hazel, C. A., Cox, M. J., & Strang, N. C. (2003). Wavefront aberration and its relationship to the accommodative stimulus-response function in myopic subjects. *Optometry and Vision Science : Official Publication of the American Academy of Optometry*, *80*(2), 151–158. https://doi.org/10.1097/00006324-200302000-00011

He, J. C., Sun, P., Held, R., Thorn, F., Sun, X., & Gwiazda, J. E. (2002). Wavefront aberrations in eyes of emmetropic and moderately myopic school children and young adults. *Vision Research*, *42*(8), 1063–1070. https://doi.org/10.1016/S0042-6989(02)00035-4

He, Z., Sui, X., Jin, G., & Cao, L. (2019). Progress in virtual reality and augmented reality based on holographic display. *Applied Optics*, *58*(5), A74–A81. https://doi.org/10.1364/AO.58.000A74

Heath, G. G. (1956). Components of accommodation. *Optometry and Vision Science*, *33*(11), 569–579.

Hecht, E. (2017). *Optics* (5th ed.). Pearson Education Limited.

Hendrickson, A. E., & Yuodelis, C. (1984). The morphological development of the human fovea. *Ophthalmology*, *91*(6), 603–612.

Heron, G., Charman, W. N., & Gray, L. S. (2002). *Accommodation dynamics as a function of age*. 389–396.

Hervella, L., Villegas, E. A., Prieto, P. M., & Artal, P. (2019). Assessment of subjective refraction with a clinical adaptive optics visual simulator. *Journal of Cataract & Refractive Surgery*, *45*(1), 87–93. https://doi.org/10.1016/j.jcrs.2018.08.022

Hodge, W. G., Whitcher, J. P., & Satariano, W. (1995). Risk factors for age-related cataracts. *Epidemiologic Reviews*, *17*(2), 336–346. https://doi.org/10.1093/oxfordjournals.epirev.a036197

Hofer, H., Artal, P., Singer, B., Aragón, J. L., & Williams, D. R. (2001). Dynamics of the eye's wave aberration. *Journal of the Optical Society of America A*, *18*(3), 497. https://doi.org/10.1364/josaa.18.000497

Hoffman, D. M., Girshick, A. R., Akeley, K., & Banks, M. S. (2008). Vergence–accommodation conflicts hinder visual performance and cause visual fatigue. *Journal of Vision*, *8*(3), 33.

Hoffman, D. M., Karasev, V. I., & Banks, M. S. (2011). Temporal presentation protocols in stereoscopic displays: Flicker visibility, perceived motion, and perceived depth. *Journal of the Society for Information Display*, *19*(3), 271. https://doi.org/10.1889/jsid19.3.271

Holden, B. A., Fricke, T. R., Wilson, D. A., Jong, M., Naidoo, K. S., Sankaridurg, P., Wong, T. Y., Naduvilath, T. J., & Resnikoff, S. (2016). Global Prevalence of Myopia and High Myopia and Temporal Trends from 2000 through 2050. *Ophthalmology*, *123*(5), 1036–1042. https://doi.org/10.1016/j.ophtha.2016.01.006

Holden, B., Sankaridurg, P., Smith, E., Aller, T., Jong, M., & He, M. (2014). Myopia, an underrated global challenge to vision: Where the current data takes us on myopia control. *Eye (Basingstoke)*, *28*(2), 142–146. https://doi.org/10.1038/eye.2013.256

Home, R. (1978). Binocular summation: a study of contrast sensitivity, visual acuity and

recognition. *Vision Research*, *18*(5), 579–585.

Hope, D. (n.d.). Macula. *Accessed: 14-01-2023, from Wikipedia*. https://en.wikipedia.org/wiki/Macula

Howland, H. C., Dobson, V., & Sayles, N. (1987). Accommodation in infants as measured by photorefraction. *Vision Research*, *27*(12), 2141–2152. https://doi.org/10.1016/0042-6989(87)90128-3

Huang, D., Swanson, E. A., Lin, C. P., Schuman, J. S., Stinson, W. G., Chang, W., Hee, M. R., Flotte, T., Gregory, K., & Puliafito, C. A. (1991). Optical coherence tomography. *Science*, *254*(5035), 1178–1181.

Huang, H. M., Chang, D. S. T., & Wu, P. C. (2015). The association between near work activities and myopia in children - A systematic review and meta-analysis. *PLoS ONE*, *10*(10), 1–15. https://doi.org/10.1371/journal.pone.0140419

Hughes, R. P., Vincent, S. J., Read, S. A., & Collins, M. J. (2020). Higher order aberrations, refractive error development and myopia control: a review. *Clinical and Experimental Optometry*, *103*(1), 68–85. https://doi.org/10.1111/cxo.12960

Hung, G. K., & Ciuffreda, K. J. (1988). Dual-mode behaviour in the human accommodation system. *Ophthalmic & Physiological Optics : The Journal of the British College of Ophthalmic Opticians (Optometrists)*, *8*(3), 327–332. https://doi.org/10.1111/j.1475-1313.1988.tb01062.x

Hung, G. K., Ciuffreda, K. J., & Rosenfield, M. (1996). Proximal contribution to a linear static model of accommodation and vergence. *Ophthalmic and Physiological Optics*, *16*(1), 31–41.

Hunt, R. W. G. (1995). *The reproduction of colour* (Vol. 4). Wiley Online Library.

Ingram, R. M., & Barr, A. (1979). Changes in refraction between the ages of 1 and 3 1/2 years. *British Journal of Ophthalmology*, *63*(5), 339–342.

Ip, J. M., Saw, S.-M., Rose, K. A., Morgan, I. G., Kifley, A., Wang, J. J., & Mitchell, P. (2008). Role of near work in myopia: findings in a sample of Australian school children. *Investigative Ophthalmology & Visual Science*, *49*(7), 2903–2910.

ISO. (n.d.). *ISO 24157: 2008*. Accessed 20-01-2023. https://www.iso.org/obp/ui/#iso:std:iso:24157:ed-1:v1:en

Jabbour, J. M., Malik, B. H., Olsovsky, C., Cuenca, R., Cheng, S., Jo, J. a, Cheng, Y.-S. L., Wright, J. M., & Maitland, K. C. (2014). Optical axial scanning in confocal microscopy using an electrically tunable lens. *Biomedical Optics Express*, *5*(2), 645–652. https://doi.org/10.1364/BOE.5.000645

Jiang, B. C., & White, J. M. (1999). Effect of accommodative adaptation on static and dynamic accommodation in emmetropia and late-onset myopia. *Optometry and Vision Science : Official Publication of the American Academy of Optometry*, *76*(5), 295—302. https://doi.org/10.1097/00006324-199905000-00017

Johnson, M. A. (1986). Color Vision in the Peripheral Retina. *Optometry and Vision Science*, *63*(2). https://journals.lww.com/optvissci/Fulltext/1986/02000/Color_Vision_in_the_Peripheral _Retina.3.aspx

Jonas, J. B., Ang, M., Cho, P., Guggenheim, J. A., He, M. G., Jong, M., Logan, N. S., Liu, M., Morgan, I., Ohno-Matsui, K., Pärssinen, O., Resnikoff, S., Sankaridurg, P., Saw, S.-

M., Smith, E. L., Tan, D. T. H., Walline, J. J., Wildsoet, C. F., Wu, P.-C., … Wolffsohn, J. S. (2021). IMI Prevention of Myopia and Its Progression. *Investigative Opthalmology & Visual Science*, *62*(5), 6. https://doi.org/10.1167/iovs.62.5.6

Jong, M. (2021). *IMI Pathologic Myopia*.

Jong, M., & Ian Flitcroft, D. (2019). Defining and Classifying Myopia Report IMI. *The International Myopia Institut*, 1–4.

Joubert, C., & Bedell, H. E. (1990). Proximal vergence and perceived distance. *Optometry and Vision Science*, *67*(1), 29–35. https://doi.org/10.1097/00006324-199001000-00007

Jung, S.-K., Lee, J. H., Kakizaki, H., & Jee, D. (2012). Prevalence of Myopia and its Association with Body Stature and Educational Level in 19-Year-Old Male Conscripts in Seoul, South Korea. *Investigative Opthalmology & Visual Science*, *53*(9), 5579. https://doi.org/10.1167/iovs.12-10106

Kaphle, D., Varnas, S. R., Schmid, K. L., Suheimat, M., Leube, A., & Atchison, D. A. (2022a). Accommodation lags are higher in myopia than in emmetropia: Measurement methods and metrics matter. *Ophthalmic and Physiological Optics*, *42*(5), 1103–1114. https://doi.org/10.1111/opo.13021

Kaphle, D., Varnas, S. R., Schmid, K. L., Suheimat, M., Leube, A., & Atchison, D. A. (2022b). Accommodation lags are higher in myopia than in emmetropia: Measurement methods and metrics matter. *Ophthalmic and Physiological Optics*, *42*(5), 1103–1114. https://doi.org/10.1111/opo.13021

Keele, K. D. (1955). *Leonardo da Vinci on vision*. SAGE Publications.

Keele, K. D. (1963). Galen: On Anatomical Procedures: the Later Books. *Medical History*, *7*(1), 85. https://www.ncbi.nlm.nih.gov/pmc/articles/PMC1034789/

Keeler, C. R. (2002). The ophthalmoscope in the lifetime of Hermann von Helmholtz. *Archives of Ophthalmology*, *120*(2), 194–201. https://doi.org/10.1001/archopht.120.2.194

King, L. S. (1969). Galen: On the Usefulness of the Parts of the Body. *JAMA: The Journal of the American Medical Association*, *207*(12), 2288. https://doi.org/10.1001/jama.1969.03150250118036

Kobayashi, H., & Kohshima, S. (1997). Unique morphology of the human eye. *Nature*, *387*(6635), 767–768.

Kobayashi, M., Nakazawa, N., Yamaguchi, T., Otaki, T., Hirohara, Y., & Mihashi, T. (2008). Binocular open-view Shack-Hartmann wavefront sensor with consecutive measurements of near triad and spherical aberration. *Applied Optics*, *47*(25), 4619–4626. https://doi.org/10.1364/AO.47.004619

Koelbing, H. M. (1990). [Felix Platter (1536-1614) as ophthalmologist]. *Gesnerus*, *47 Pt 1*, 21–30. http://europepmc.org/abstract/MED/2184100

Kotulak, J. C., Morse, S. E., & Billock, V. A. (1995). Red-green opponent channel mediation of control of human ocular accommodation. *The Journal of Physiology*, *482*(3), 697–703.

Kruger, P. B., Mathews, S., Katz, M., Aggarwala, K. R., & Nowbotsing, S. (1997). Accommodation without feedback suggests directional signals specify ocular focus. *Vision Research*, *37*(18), 2511–2526.

Kruger, P. B., & Pola, J. (1986). Stimuli for accommodation: blur, chromatic aberration and

size. *Vision Research*, *26*(6), 957–971.

Kruger, P. B., & Pola, J. (1987). Dioptric and non-dioptric stimuli for accommodation: target size alone and with blur and chromatic aberration. *Vision Research*, *27*(4), 555–567.

Kruger, P. B., Stark, L. R., & Nguyen, H. N. (2004). Small foveal targets for studies of accommodation and the Stiles–Crawford effect. *Vision Research*, *44*(24), 2757–2767. https://doi.org/10.1016/J.VISRES.2004.06.013

Labhishetty, V., & Bobier, W. R. (2017). Are high lags of accommodation in myopic children due to motor deficits? *Vision Research*, *130*, 9–21. https://doi.org/10.1016/j.visres.2016.11.001

Lamb, T. D. (2016). Why rods and cones? *Eye*, *30*(2), 179–185. https://doi.org/10.1038/eye.2015.236

Laurie O'Keefe. (n.d.). *Astigmatism*. Accessed 18-01-2023, Allaboutvision.Com. https://www.allaboutvision.com/conditions/astigmatism.htm

Leahy, C., Leroux, C., Dainty, C., & Diaz-Santana, L. (2010). Temporal dynamics and statistical characteristics of the microfluctuations of accommodation: Dependence on the mean accommodative effort. *Optics Express*, *18*(3), 2668–2681.

Leek, M. R. (2001). Adaptive procedures in psychophysical research. *Perception & Psychophysics*, *63*(8), 1279–1292.

Leffler, C. T., Hadi, T. M., Udupa, A., Schwartz, S. G., & Schwartz, D. (2016). A medieval fallacy: The crystalline lens in the center of the eye. In *Clinical Ophthalmology* (Vol. 10, pp. 649–662). Dove Press. https://doi.org/10.2147/OPTH.S100708

Leung, T.-W., Lam, A. K.-C., Deng, L., & Kee, C.-S. (2012). Characteristics of astigmatism as a function of age in a Hong Kong clinical population. *Optometry and Vision Science*, *89*(7), 984–992.

Li, Y., Tan, O., Brass, R., Weiss, J. L., & Huang, D. (2012). Corneal epithelial thickness mapping by Fourier-domain optical coherence tomography in normal and keratoconic eyes. *Ophthalmology*, *119*(12), 2425–2433.

Liang, C., Yen, E., Su, J., Liu, C., Chang, T., Park, N., Wu, M., Lee, S., Flynn, J. T., & Juo, S. H. (2004). Impact of Family History of High Myopia on Level and Onset of Myopia. *Investigative Opthalmology & Visual Science*, *45*(10), 3446. https://doi.org/10.1167/iovs.03-1058

Lin, L. L. K., Shih, Y. F., Hsiao, C. K., & Chen, C. J. (2004). Prevalence of myopia in Taiwanese schoolchildren: 1983 to 2000. *Annals of the Academy of Medicine, Singapore*, *33*(1), 27–33. http://www.ncbi.nlm.nih.gov/pubmed/15008558

Lin, Z., Duarte-Toledo, R., Manzanera, S., Lan, W., Artal, P., & Yang, Z. (2020). Two-dimensional peripheral refraction and retinal image quality in orthokeratology lens wearers. *Biomedical Optics Express*, *11*(7), 3523–3533. https://doi.org/10.1364/BOE.397077

Lin, Z., Vasudevan, B., Mao, G. Y., Ciuffreda, K. J., Jhanji, V., Li, X. X., Zhou, H. J., Wang, N. L., & Liang, Y. B. (2016). The influence of near work on myopic refractive change in urban students in Beijing: a three-year follow-up report. *Graefe's Archive for Clinical and Experimental Ophthalmology*, *254*, 2247–2255.

Liu, T., & Thibos, L. N. (2017). Compensation of corneal oblique astigmatism by internal optics: a theoretical analysis. *Ophthalmic and Physiological Optics*, *37*(3), 305–316.

https://doi.org/10.1111/opo.12364

Logan, N. S., Radhakrishnan, H., Cruickshank, F. E., Allen, P. M., Bandela, P. K., Davies, L. N., Hasebe, S., Khanal, S., Schmid, K. L., Vera-Diaz, F. A., & Wolffsohn, J. S. (2021). IMI accommodation and binocular vision in myopia development and progression. *Investigative Ophthalmology and Visual Science*, *62*(5). https://doi.org/10.1167/iovs.62.5.4

Lundström, L., Gustafsson, J., Svensson, I., & Unsbo, P. (2005). Assessment of objective and subjective eccentric refraction. *Optometry and Vision Science : Official Publication of the American Academy of Optometry*, *82*(4), 298–306. https://doi.org/10.1097/01.OPX.0000159366.61943.62

Maddock, R. J., Millodot, M., Leat, S., & Johnson, C. A. (1981). Accommodation responses and refractive error. *Investigative Ophthalmology & Visual Science*, *20*(3), 387–391. http://www.ncbi.nlm.nih.gov/pubmed/7203882

Mahabadi, N., & Al Khalili, Y. (n.d.). *Neuroanatomy, Retina*. Accessed: 15-01-2023. StatPearls [Internet]. Treasure Island (FL): StatPearls Publishing. https://www.ncbi.nlm.nih.gov/books/NBK545310/

Maiello, G., Kerber, K. L., Thorn, F., Bex, P. J., & Vera-Diaz, F. A. (2018). Vergence driven accommodation with simulated disparity in myopia and emmetropia. *Experimental Eye Research*, *166*, 96–105. https://doi.org/10.1016/j.exer.2017.10.004

Major, R. H. (1930). The Papyrus Ebers. *Annals of Medical History*, *2*(5), 547.

Marcos, S. (2001). Refractive Surgery and Optical Aberrations. *Optics and Photonics News*, *12*(1), 22. https://doi.org/10.1364/OPN.12.1.000022

Marcos, S., Pérez-Merino, P., & Dorronsoro, C. (2017). Monochromatic aberrations. In *Handbook of Visual Optics, Volume One* (pp. 293–311). CRC Press. https://doi.org/10.1201/9781315373034

Martin, H., Guthoff, R., Terwee, T., & Schmitz, K. (2005). *Comparison of the accommodation theories of Coleman and of Helmholtz by finite element simulations*. *45*, 2910–2915. https://doi.org/10.1016/j.visres.2005.05.030

Mathews, S., & Kruger, P. B. (1994). Spatiotemporal transfer function of human accommodation. *Vision Research*, *34*(15), 1965–1980. https://doi.org/10.1016/0042-6989(94)90026-4

McBrien, N. A., & Millodot, M. (1987). The relationship between tonic accommodation and refractive error. *Investigative Ophthalmology & Visual Science*, *28*(6), 997–1004. http://www.ncbi.nlm.nih.gov/pubmed/3583639

McKillup, S. (2005). Statistics explained: An introductory guide for life scientists. In *Statistics Explained: An Introductory Guide for Life Scientists*. Cambridge University Press. https://doi.org/10.1017/CBO9780511815935

Metlapally, S., Tong, J. L., Tahir, H. J., & Schor, C. M. (2014). The impact of higher-order aberrations on the strength of directional signals produced by accommodative microfluctuations. *Journal of Vision*, *14*(12), 25.

Milders, M., Sahraie, A., & Logan, S. (2008). Minimum presentation time for masked facial expression discrimination. *Cognition and Emotion*, *22*(1), 63–82. https://doi.org/10.1080/02699930701273849

Miller, P. E. (2008). Structure and Function of the Eye. In D. J. Maggs, P. E. Miller, & R. B.

T.-S. F. of V. O. (Fourth E. Ofri (Eds.), *Slatter's Fundamentals of Veterinary Ophthalmology* (pp. 1–19). Elsevier. https://doi.org/10.1016/B978-072160561-6.50004-6

Mira-Agudelo, A., Lundström, L., & Artal, P. (2009). Temporal dynamics of ocular aberrations: monocular vs binocular vision. *Ophthalmic and Physiological Optics*, *29*(3), 256–263. https://doi.org/https://doi.org/10.1111/j.1475-1313.2009.00655.x

Mitchell, D. E. (1966). A review of the concept of "Panum's fusional areas." *Optometry and Vision Science*, *43*(6), 387–401.

Moisseiev, E., & Yiu, G. (2017). Clinical Picture Retinal detachment in severe myopia. *The Lancet*, *389*(10074), 1133. https://doi.org/10.1016/S0140-6736(16)31407-6

Mompeán, J., Aragón, J. L., & Artal, P. (2020a). Portable device for presbyopia correction with optoelectronic lenses driven by pupil response. *Scientific Reports*, *10*(1). https://doi.org/10.1038/s41598-020-77465-5

Mompeán, J., Aragón, J. L., & Artal, P. (2020b). Portable device for presbyopia correction with optoelectronic lenses driven by pupil response. *Scientific Reports*, *10*(1), 1–9. https://doi.org/10.1038/s41598-020-77465-5

Mompeán, J., Aragón, J. L., Prieto, P. M., & Artal, P. (2019). GPU-based processing of Hartmann–Shack images for accurate and high-speed ocular wavefront sensing. *Future Generation Computer Systems*, *91*, 177–190. https://doi.org/10.1016/j.future.2018.09.010

Moore, B. D., Augsburger, A. R., Ciner, E. B., Cockrell, D. A., Fern, K., & Harb, E. (1997). Optometric clinical practice guideline: care of the patient with hyperopia. *American Optometric Association*, 1–29.

Morgan, I. G., Rose, K. A., Ellwein, L. B., & Group, R. E. S. in C. S. (2010). Is emmetropia the natural endpoint for human refractive development? An analysis of population-based data from the refractive error study in children (RESC). *Acta Ophthalmologica*, *88*(8), 877–884.

Morgan, I. G., Wu, P. C., Ostrin, L. A., Tideman, J. W., Yam, J. C., Lan, W., Baraas, R. C., He, X., Sankaridurg, P., Saw, S. M., French, A. N., Rose, K. A., & Guggenheim, J. A. (2021). IMI risk factors for myopia. *Investigative Ophthalmology and Visual Science*, *62*(5), 12–15. https://doi.org/10.1167/iovs.62.5.3

Morris, D. (1985). *Bodywatching: A field guide to the human species*. Outlet.

Moulakaki, A. I., Del Águila-Carrasco, A. J., Esteve-Taboada, J. J., & Montés-Micó, R. (2017). Effect of even and odd-order aberrations on the accommodation response. *International Journal of Ophthalmology*, *10*(6), 955–960. https://doi.org/10.18240/ijo.2017.06.19

Murdoch, I. E., Morris, S. S., & Cousens, S. N. (1998). People and eyes: statistical approaches in ophthalmology. *The British Journal of Ophthalmology*, *82*(8), 971–973. https://doi.org/10.1136/BJO.82.8.971

Mutti, D. O., Jones, L. A., Moeschberger, M. L., & Zadnik, K. (1996). *AC / A Ratio , Age , and Refractive Error in Children*.

Mutti, D. O., Mitchell, G. L., Hayes, J. R., Jones, L. A., Moeschberger, M. L., Cotter, S. A., Kleinstein, R. N., Manny, R. E., Twelker, J. D., Zadnik, K., & Group, S. (2006). *Accommodative Lag before and after the Onset of Myopia*. *47*(3).

https://doi.org/10.1167/iovs.05-0888

Mutti, D. O., Mitchell, G. L., Jones-Jordan, L. A., Cotter, S. A., Kleinstein, R. N., Manny, R. E., Twelker, J. D., & Zadnik, K. (2017). The response AC/A ratio before and after the onset of myopia. *Investigative Ophthalmology and Visual Science*, *58*(3), 1594–1602. https://doi.org/10.1167/iovs.16-19093

Mutti, D. O., Mitchell, G. L., Jones, L. A., Friedman, N. E., Frane, S. L., Lin, W. K., Moeschberger, M. L., & Zadnik, K. (2005). Axial growth and changes in lenticular and corneal power during emmetropization in infants. *Investigative Ophthalmology & Visual Science*, *46*(9), 3074–3080.

Mutti, D. O., & Zadnik, K. (1995). *The Utility of Three Predictors of Childhood Myopia : a Bayesian Analysis*. *35*(9), 1345–1352.

MYFUN. (n.d.). *MyFun: Myopia Fundamental Understanding Needed*. Accessed 13-01-2023, Commission 3–5 (2017). https://cordis.europa.eu/project/id/675137

Nakatsuka, C. (2003). Accommodative Lag Under Habitual Seeing Conditions: Comparison Between Adult Myopes and Emmetropes. *Japanese Journal of Ophthalmology*, *47*(3), 291–298. https://doi.org/10.1016/S0021-5155(03)00013-3

Neal, D. R., Copland, J., & Neal, D. A. (2002). Shack-Hartmann wavefront sensor precision and accuracy. *Advanced Characterization Techniques for Optical, Semiconductor, and Data Storage Components*, *4779*(November 2002), 148. https://doi.org/10.1117/12.450850

Nejabat, M., Maleki, B., Nimrouzi, M., Mahbodi, A., & Salehi, A. (2012). Avicenna and cataracts: a new analysis of contributions to diagnosis and treatment from the canon. *Iranian Red Crescent Medical Journal*, *14*(5), 265.

Norton, T. T., & Siegwart, J. T. (2013). Light levels, refractive development, and myopia – A speculative review. *Experimental Eye Research*, *114*, 48–57. https://doi.org/10.1016/j.exer.2013.05.004

Ogle, K. N. (1952). On the limits of stereoscopic vision. *Journal of Experimental Psychology*, *44*(4), 253.

Onural, L. (2016). *Holographic True-3D Displays : Basic Principles*. *September*.

Optotune. (2022). *Electrically tunable large aperture lens EL-16-40-TC-VIS-20D*. https://www.optotune.com/s/Optotune-EL-16-40-TC-VIS-20D.pdf

Otsu, N. (1979). THRESHOLD SELECTION METHOD FROM GRAY-LEVEL HISTOGRAMS. *IEEE Trans Syst Man Cybern*, *SMC-9*(1), 62–66. https://doi.org/10.1109/tsmc.1979.4310076

Ovenseri-Ogbomo, G. O., & Oduntan, O. A. (2015). Mechanism of accommodation: A review of theoretical propositions. *African Vision and Eye Health*, *74*(1), 1–6. https://doi.org/10.4102/aveh.v74i1.28

Owsley, C. (2003). Contrast sensitivity. *Ophthalmology Clinics of North America*, *16*(2), 171–177. https://doi.org/10.1016/S0896-1549(03)00003-8

Owsley, C., Sekuler, R., & Siemsen, D. (1983). Contrast sensitivity throughout adulthood. *Vision Research*, *23*(7), 689–699.

Pan, C.-W., Ramamurthy, D., & Saw, S.-M. (2012). Worldwide prevalence and risk factors for myopia. *Ophthalmic and Physiological Optics*, *32*(1), 3–16. https://doi.org/10.1111/j.1475-1313.2011.00884.x

Pelli, D. G., & Bex, P. (2013). Measuring contrast sensitivity. *Vision Research*, *90*, 10–14. https://doi.org/10.1016/j.visres.2013.04.015

Petersen, A., & Andersen, T. S. (2012). The effect of exposure duration on visual character identification in single, whole, and partial report. *Journal of Experimental Psychology: Human Perception and Performance*, *38*(2), 498–514. https://doi.org/10.1037/a0026728

Philipson, B. (1973). Changes in the lens related to the reduction of transparency. *Experimental Eye Research*, *16*(1), 29–39. https://doi.org/https://doi.org/10.1016/0014-4835(73)90234-0

Platt, B. C., & Shack, R. (2001). History and Principles of Shack-Hartmann Wavefront Sensing. *Journal of Refractive Surgery*, *17*(5). https://doi.org/10.3928/1081-597X-20010901-13

Platt, B. C., & Shack, R. (2003). *Wavefront Sensing*. *17*(October 2001).

Potter, M. C., Wyble, B., Hagmann, C. E., & McCourt, E. S. (2014). Detecting meaning in RSVP at 13 ms per picture. *Attention, Perception, and Psychophysics*, *76*(2), 270–279. https://doi.org/10.3758/s13414-013-0605-z

Prieto, P. M., Vargas-Martín, F., Goelz, S., & Artal, P. (2000). Analysis of the performance of the Hartmann–Prieto, P. M., Vargas-Martín, F., Goelz, S., & Artal, P. (2000). Analysis of the performance of the Hartmann–Shack sensor in the human eye. Journal of the Optical Society of America A, 17(8), 1388. https://doi. *Journal of the Optical Society of America A*, *17*(8), 1388. https://doi.org/10.1364/josaa.17.001388

Prince, J. D. (1904). *The code of Hammurabi*. University of Chicago Press.

Purves, D., Augustine, G. J., Fitzpatrick, D., Hall, W., LaMantia, A.-S., & White, L. (2019). *Neurosciences*. De Boeck Supérieur.

Pusti, D., Benito, A., Madrid-Valero, J. J., Ordoñana, J. R., & Artal, P. (2020). Inheritance of Refractive Error in Millennials. *Scientific Reports*, *10*(1), 8173. https://doi.org/10.1038/s41598-020-65130-w

Quigley, H. A., Brown, A. E., Morrison, J. D., & Drance, S. M. (1990). The size and shape of the optic disc in normal human eyes. *Archives of Ophthalmology*, *108*(1), 51–57.

Radhakrishnan, H., Allen, P. M., & Charman, W. N. (2007). *Dynamics of Accommodative Facility in Myopes*. *48*(9). https://doi.org/10.1167/iovs.07-0269

Radhakrishnan, H., Pardhan, S., Calver, R. I., & O'Leary, D. J. (2004). Effect of positive and negative defocus on contrast sensitivity in myopes and non-myopes. *Vision Research*, *44*(16), 1869–1878. https://doi.org/https://doi.org/10.1016/j.visres.2004.03.007

Ramamurthy, D., Lin Chua, S. Y., & Saw, S.-M. (2015). A review of environmental risk factors for myopia during early life, childhood and adolescence. *Clinical and Experimental Optometry*, *98*(6), 497–506. https://doi.org/10.1111/cxo.12346

Randall S. Barton. (n.d.). *Triumph of Gilgamesh*. Accessed 13-01-2023. https://www.reed.edu/reed_magazine/june2013/articles/eliot_circular/gilgamesh.html

Read, S. A., Collins, M. J., Carney, L. G., & Franklin, R. J. (2006). The Topography of the Central and Peripheral Cornea. *Investigative Ophthalmology & Visual Science*, *47*(4), 1404–1415. https://doi.org/10.1167/iovs.05-1181

Read, S. A., Vincent, S. J., & Collins, M. J. (2014). The visual and functional impacts of astigmatism and its clinical management. *Ophthalmic and Physiological Optics*, *34*(3), 267–294. https://doi.org/10.1111/opo.12128

Reichelt, S., Häussler, R., Fütterer, G., & Leister, N. (2010). Depth cues in human visual perception and their realization in 3D displays. In B. Javidi, J.-Y. Son, J. T. Thomas, & D. D. Desjardins (Eds.), *Three-Dimensional Imaging, Visualization, and Display 2010 and Display Technologies and Applications for Defense, Security, and Avionics IV* (Vol. 7690, Issue May 2010, p. 76900B). https://doi.org/10.1117/12.850094

Reichenbach, M., Seidler, R., Pfundt, B., & Fey, D. (2014). Fast image processing for optical metrology utilizing heterogeneous computer architectures. *Computers and Electrical Engineering*, *40*(4), 1158–1170. https://doi.org/10.1016/j.compeleceng.2013.09.008

Reinstein, D. Z., Archer, T. J., & Gobbe, M. (2012). The History of LASIK. *Journal of Refractive Surgery*, *28*(4), 291–298. https://doi.org/10.3928/1081597X-20120229-01

Renima, A., Tiliouine, H., & Estes, R. J. (2016). The Islamic Golden Age: A Story of the Triumph of the Islamic Civilization. In *The State of Social Progress of Islamic Societies* (pp. 25–52). Springer, Cham. https://doi.org/10.1007/978-3-319-24774-8_2

Retief, F., Stulting, A., & Cilliers, L. (2008). The eye in antiquity: history of medicine: SAMJ forum. *South African Medical Journal*, *98*(9), 697–700.

Reymond, A. (1927). *History of the sciences in Greco-Roman antiquity* (Vol. 5). Methuen & Company Limited.

Richman, J., Spaeth, G. L., & Wirostko, B. (2013). Contrast sensitivity basics and a critique of currently available tests. *Journal of Cataract and Refractive Surgery*, *39*(7), 1100–1106. https://doi.org/10.1016/j.jcrs.2013.05.001

Ridley, H. (1952). Intra-ocular acrylic lenses: a recent development in the surgery of cataract. *The British Journal of Ophthalmology*, *36*(3), 113.

Roberts, T. L., Anderson, H. A., & Stuebing, K. K. (2015). Accommodative Gain in Relation to Perceived Target Clarity. *Optometry and Vision Science*, *92*(11), 1092–1102. https://doi.org/10.1097/OPX.0000000000000711

Rosen, E. (1956). The invention of eyeglasses. *Journal of the History of Medicine and Allied Sciences*, *11*(1), 13–46.

Rosenfield, M., Ciuffreda, K. J., Hung, G. K., & Gilmartin, B. (1993). Tonic accommodation: a review I. Basic aspects. *Ophthalmic and Physiological Optics*, *13*(3), 266–283.

Rosenfield, M., Ciuffreda, K. J., Hung, G. K., & Gilmartin, B. (1994). Tonic accommodation: a review. II. Accommodative adaptation and clinical aspects. *Ophthalmic and Physiological Optics*, *14*(3), 265–277.

Rosenfield, M., Desai, R., & Portello, J. K. (2002). Do progressing myopes show reduced accommodative responses? *Optometry and Vision Science : Official Publication of the American Academy of Optometry*, *79*(4), 268–273. https://doi.org/10.1097/00006324-200204000-00014

Rosenfield, M., & Gilmartin, B. (1999). Accommodative error, adaptation and myopia. *Ophthalmic and Physiological Optics*, *19*(2), 159–164. https://doi.org/10.1046/j.1475-1313.1999.00419.x

Rucker, F. J., & Kruger, P. B. (2004). Accommodation responses to stimuli in cone contrast space. *Vision Research*, *44*(25), 2931–2944.

Ruffieux, P., Scharf, T., Herzig, H. P., Völkel, R., & Weible, K. J. (2006). On the chromatic aberration of microlenses. *Optics Express*, *14*(11), 4687. https://doi.org/10.1364/oe.14.004687

Sahoo, P. K., Soltani, S., & Wong, A. K. C. (1988). A survey of thresholding techniques. *Computer Vision, Graphics and Image Processing*, *41*(2), 233–260. https://doi.org/10.1016/0734-189X(88)90022-9

Salmon, T. O., & van de Pol, C. (2006). Normal-eye Zernike coefficients and root-mean-square wavefront errors. *Journal of Cataract & Refractive Surgery*, *32*(12), 2064–2074.

Salmon, T. O., West, R. W., Gasser, W., & Kenmore, T. (2003). Measurement of refractive errors in young myopes using the COAS Shack-Hartmann aberrometer. *Optometry and Vision Science*, *80*(1), 6–14.

Sankaridurg, P., Tahhan, N., Kandel, H., Naduvilath, T., Zou, H., Frick, K. D., Marmamula, S., Friedman, D. S., Lamoureux, E., Keeffe, J., Walline, J. J., Fricke, T. R., Kovai, V., & Resnikoff, S. (2021). IMI impact of myopia. *Investigative Ophthalmology and Visual Science*, *62*(5). https://doi.org/10.1167/iovs.62.5.2

Sanz Diez, P., Ohlendorf, A., Schaeffel, F., & Wahl, S. (2019). Effect of spatial filtering on accommodation. *Vision Research*, *164*, 62–68. https://doi.org/10.1016/j.visres.2019.07.005

Sanz Diez, P., Yang, L.-H., Lu, M.-X., Wahl, S., & Ohlendorf, A. (2019). Growth curves of myopia-related parameters to clinically monitor the refractive development in Chinese schoolchildren. *Graefe's Archive for Clinical and Experimental Ophthalmology*, *257*(5), 1045–1053. https://doi.org/10.1007/s00417-019-04290-6

Saw, S.-M. (2003). A synopsis of the prevalence rates and environmental risk factors for myopia. *Clinical and Experimental Optometry*, *86*(5), 289–294. https://doi.org/10.1111/j.1444-0938.2003.tb03124.x

Saw, S.-M., Hong, C.-Y., Chia, K.-S., Stone, R. A., & Tan, D. (2001). Nearwork and myopia in young children. *The Lancet*, *357*(9253), 390.

Sawides, L., Gambín-Regadera, A., de Castro, A., & Artal, P. (2018). High speed visual stimuli generator to estimate the minimum presentation time required for an orientation discrimination task. *Biomedical Optics Express*, *9*(6), 2640. https://doi.org/10.1364/boe.9.002640

Schade, O. H. (1956). Optical and photoelectric analog of the eye. *JoSA*, *46*(9), 721–739.

Schaeffel, F., Glasser, A., & Howland, H. C. (1988). Accommodation, refractive error and eye growth in chickens. *Vision Research*, *28*(5), 639–657.

Schaeffel, F., Wilhelm, H., & Zrenner, E. (1993). Inter-individual variability in the dynamics of natural accommodation in humans: relation to age and refractive errors. *The Journal of Physiology*, *461*(1), 301–320. https://doi.org/10.1113/jphysiol.1993.sp019515

Schmid, K. L., & Strang, N. C. (2015a). Differences in the accommodation stimulus response curves of adult myopes and emmetropes: A summary and update. *Ophthalmic and Physiological Optics*, *35*(6), 613–621. https://doi.org/10.1111/opo.12255

Schmid, K. L., & Strang, N. C. (2015b). Differences in the accommodation stimulus response curves of adult myopes and emmetropes: a summary and update. *Ophthalmic and Physiological Optics*, *35*(6), 613–621. https://doi.org/10.1111/opo.12255

Schor, C. M. (1992). A dynamic model of cross-coupling between accommodation and convergence: simulations of step and frequency responses. *Optometry and Vision Science*, *69*(4), 258–269.

Schor, C. M., Alexander, J., Cormack, L., & Stevenson, S. (1992). Negative feedback control

model of proximal convergence and accommodation. *Ophthalmic and Physiological Optics*, *12*(3), 307–318.

Schwarz, C. (2013). Influencia de las aberraciones en visión binocular mediante el uso de sistemas de óptica adaptativa= Influence of aberrations on binocular vision by means of adaptive optics instruments. *Proyecto de Investigación:*

Schwiegerling, J. (2014). History of the Shack Hartmann wavefront sensor and its impact in ophthalmic optics. *Fifty Years of Optical Sciences at The University of Arizona*, *9186*(520), 91860U. https://doi.org/10.1117/12.2064536

Seidemann, A., & Schaeffel, F. (2002). *Effects of longitudinal chromatic aberration on accommodation and emmetropization*. *42*, 2409–2417.

Shibata, T., Kim, J., Hoffman, D. M., & Banks, M. S. (2011). Visual discomfort with stereo displays: effects of viewing distance and direction of vergence-accommodation conflict. *Stereoscopic Displays and Applications XXII*, *7863*, 222–230.

Siegwart, J. T., & Norton, T. T. (2011). Perspective: How Might Emmetropization and Genetic Factors Produce Myopia in Normal Eyes? *Optometry and Vision Science*, *88*(3), E365–E372. https://doi.org/10.1097/OPX.0b013e31820b053d

Simonson, E., & Brozek, J. (1952). Flicker Fusion Frequency: Background and Applications. *Physiological Reviews*, *32*(3), 349–378. https://doi.org/10.1152/physrev.1952.32.3.349

Smith, W. J. (2008). *Modern Optical Engineering* (Fourth). McGraw-Hill.

Stark, L. R., & Atchison, D. A. (1997). Pupil size, mean accommodation response and the fluctuations of accommodation. *Ophthalmic and Physiological Optics*, *17*(4), 316–323.

Stark, L., & Takahashi, Y. (1965). Absence of an Odd-Error Signal Mechanism in Human Accommodation. *IEEE Transactions on Biomedical Engineering*, *BME-12*(3 and 4), 138–146. https://doi.org/10.1109/TBME.1965.4502370

Stevens, R. E., Jacoby, T. N. L., Aricescu, I. Ș., & Rhodes, D. P. (2017). A review of adjustable lenses for head mounted displays. *Https://Doi.Org/10.1117/12.2276677*, *10335*, 160–178. https://doi.org/10.1117/12.2276677

Stevenson, A. (2010). *Oxford dictionary of English*. Oxford University Press, USA.

Strang, N. C., Schmid, K. L., & Carney, L. G. (1998). Hyperopia is predominantly axial in nature. *Current Eye Research*, *17*(4), 380–383. https://doi.org/10.1080/02713689808951218

Sunness, J. S., Rubin, G. S., Applegate, C. A., Bressler, N. M., Marsh, M. J., Hawkins, B. S., & Haselwood, D. (1997). Visual function abnormalities and prognosis in eyes with age-related geographic atrophy of the macula and good visual acuity. *Ophthalmology*, *104*(10), 1677–1691.

Suryakumar, R., Meyers, J. P., Irving, E. L., & Bobier, W. R. (2007a). Application of video-based technology for the simultaneous measurement of accommodation and vergence. *Vision Research*, *47*(2), 260–268. https://doi.org/10.1016/j.visres.2006.10.003

Suryakumar, R., Meyers, J. P., Irving, E. L., & Bobier, W. R. (2007b). Vergence accommodation and monocular closed loop blur accommodation have similar dynamic characteristics. *Vision Research*, *47*(3), 327–337. https://doi.org/10.1016/j.visres.2006.10.006

Tan, G. J., Ng, Y. P., Lim, Y. C., Ong, P. Y., Snodgrass, A., & Saw, S. M. (2000). Cross-sectional study of near-work and myopia in kindergarten children in Singapore. *Annals*

of the Academy of Medicine, Singapore, 29(6), 740–744.

Tarrant, J., Severson, H., & Wildsoet, C. F. (2008). Accommodation in emmetropic and myopic young adults wearing bifocal soft contact lenses. *Ophthalmic and Physiological Optics*, 28(1), 62–72. https://doi.org/10.1111/j.1475-1313.2007.00529.x

Tbakhi, A., & Amr, S. S. (2007). Ibn Al-Haytham: Father of Modern Optics. *Annals of Saudi Medicine*, 27(6), 464. https://doi.org/10.5144/0256-4947.2007.464

Tedja, M. S., Haarman, A. E. G., Meester-Smoor, M. A., Kaprio, J., Mackey, D. A., Guggenheim, J. A., Hammond, C. J., Verhoeven, V. J. M., & Klaver, C. C. W. (2019). IMI – Myopia genetics report. *Investigative Ophthalmology and Visual Science*, 60(3), M89–M105. https://doi.org/10.1167/iovs.18-25965

Thibos, L. N., Applegate, R. A., Schwiegerling, J. T., & Webb, R. (2002). Standards for reporting the optical aberrations of eyes. *Journal of Refractive Surgery*, 18(5). https://doi.org/10.3928/1081-597x-20020901-30

Thibos, L. N., Hong, X., Bradley, A., & Applegate, R. A. (2004). Accuracy and precision of objective refraction from wavefront aberrations. *Journal of Vision*, 4(4), 9. https://doi.org/10.1167/4.4.9

Thibos, L. N., Wheeler, W., & Horner, D. (1997). Power vectors: an application of Fourier analysis to the description and statistical analysis of refractive error. *Optometry and Vision Science*, 74(6), 367–375.

Thorlabs. (n.d.-a). *High-sensitivity CMOS camera DCC3240*. Accessed 15-12-2022. https://www.thorlabs.com/thorproduct.cfm?partnumber=DCC3240N&pn=DCC3240N#14746

Thorlabs. (n.d.-b). *Longpass dichroic mirror DMLP950*. Accessed 15-12-2022. https://www.thorlabs.com/thorproduct.cfm?partnumber=DMLP950

Tombran-Tink, J., & Barnstable, C. J. (2007). *Retinal degenerations: biology, diagnostics, and therapeutics*. Springer Science & Business Media.

Torres-Sepúlveda, W., Henao, J., Morales-Marín, J., Mira-Agudelo, A., & Rueda, E. (2020). Hysteresis characterization of an electrically focus-tunable lens. *Optical Engineering*, 59(04), 1. https://doi.org/10.1117/1.oe.59.4.044103

Tower, P. (1956). Notes on the Life and Work of George Bartisch. *Archives of Ophthalmology*, 56(1), 57–70. https://doi.org/10.1001/archopht.1956.00930040063009

Tsutsui, K.-I., Taira, M., & Sakata, H. (2005). Neural mechanisms of three-dimensional vision. *Neuroscience Research*, 51(3), 221–229.

Tucker, J., & Charman, W. N. (1979). Reaction and response times for accommodation. *Optometry and Vision Science*, 56(8), 490–503. https://doi.org/10.1097/00006324-197908000-00003

Umemoto, S., & Hirata, Y. (2022). Temporal changes in accommodative responses to periodic visual motion. *Vision Research*, 191(May 2021), 107969. https://doi.org/10.1016/j.visres.2021.107969

Unesco. (n.d.). *International Year of Light: Ibn al Haytham, pioneer of modern optics celebrated at UNESCO*. https://www.unesco.org/en/articles/international-year-light-ibn-al-haytham-pioneer-modern-optics-celebrated-unesco

Vilupuru, A. S., & Glasser, A. (2002). Dynamic accommodation in rhesus monkeys. *Vision Research*, 42(1), 125–141. https://doi.org/10.1016/S0042-6989(01)00260-7

Vitale, S., Ellwein, L., Cotch, M. F., Iii, F. L. F., & Sperduto, R. (2008). *Prevalence of Refractive Error in the United States, 1999-2004. 126*(8), 1999–2004.

Vitale, S., Sperduto, R. D., & Ferris, F. L. (2009). Increased prevalence of myopia in the United States between 1971-1972 and 1999-2004. *Archives of Ophthalmology*, *127*(12), 1632–1639.

Von Helmholtz, H., & Southall, J. P. C. (1924). *Mechanism of accommodation.*

Wagner, S., Zrenner, E., & Strasser, T. (2019). Emmetropes and myopes differ little in their accommodation dynamics but strongly in their ciliary muscle morphology. *Vision Research*, *163*(May), 42–51. https://doi.org/10.1016/j.visres.2019.08.002

Walsh, G., & Charman, W. N. (1988). Visual sensitivity to temporal change in focus and its relevance to the accommodation response. *Vision Research*, *28*(11), 1207–1221. https://doi.org/10.1016/0042-6989(88)90037-5

Wang, M., Schaeffel, F., Jiang, B., & Feldkaemper, M. (2018). Effects of Light of Different Spectral Composition on Refractive Development and Retinal Dopamine in Chicks. *Investigative Opthalmology & Visual Science*, *59*(11), 4413. https://doi.org/10.1167/iovs.18-23880

Watson, A. B. (2013). High frame rates and human vision: A view through the window of visibility. *SMPTE Motion Imaging Journal*, *122*(2), 18–32. https://doi.org/10.5594/j18266XY

Watson, A. B. (2018). The field of view, the field of resolution, and the field of contrast sensitivity. *Electronic Imaging*, *2018*(14), 1–11.

Watson, A. B., Ahumada, A., & Farrell, J. E. (1986). Window of visibility: a psychophysical theory of fidelity in time-sampled visual motion displays. *JOSA A, Vol. 3, Issue 3, Pp. 300-307*, *3*(3), 300–307. https://doi.org/10.1364/JOSAA.3.000300

Weizhong, L., Zhikuan, Y., Wen, L., Xiang, C., & Jian, G. (2008). A longitudinal study on the relationship between myopia development and near accommodation lag in myopic children. *Ophthalmic and Physiological Optics*, *28*(1), 57–61. https://doi.org/10.1111/j.1475-1313.2007.00536.x

Wikipedia. (n.d.). *Emission theory*. 12-01-2023. https://en.wikipedia.org/wiki/Emission_theory_(vision)

Williams, D. R. (1985). Aliasing in human foveal vision. *Vision Research*, *25*(2), 195–205. https://doi.org/https://doi.org/10.1016/0042-6989(85)90113-0

Wilson, B. J., Decker, K. E., & Roorda, A. (2002). Monochromatic aberrations provide an odd-error cue to focus direction. *Journal of the Optical Society of America A*, *19*(5), 833. https://doi.org/10.1364/JOSAA.19.000833

Wolffsohn, J. S., Flitcroft, D. I., Gifford, K. L., Jong, M., Jones, L., Klaver, C. C. W., Logan, N. S., Naidoo, K., Resnikoff, S., Sankaridurg, P., Smith, E. L., Troilo, D., & Wildsoet, C. F. (2019). IMI – Myopia Control Reports Overview and Introduction. *Investigative Opthalmology & Visual Science*, *60*(3), M1. https://doi.org/10.1167/iovs.18-25980

Woods, A. J. (2012). Crosstalk in stereoscopic displays: a review. *Journal of Electronic Imaging*, *21*(4), 40902.

Wu, J. F., Bi, H. S., Wang, S. M., Hu, Y. Y., Wu, H., Sun, W., Lu, T. L., Wang, R., & Jonas, J. B. (2013). *Refractive Error , Visual Acuity and Causes of Vision Loss in Children in Shandong , China . The Shandong Children Eye Study*. *8*(12).

https://doi.org/10.1371/journal.pone.0082763

Wyszecki, G., & Stiles, W. S. (1982). *Color science* (Vol. 8). Wiley New York.

Xu, L., Wang, Y., Li, Y., Wang, Y., Cui, T., Li, J., & Jonas, J. B. (2006). Causes of Blindness and Visual Impairment in Urban and Rural Areas in Beijing. *Ophthalmology*, *113*(7), 1134.e1-1134.e11. https://doi.org/10.1016/j.ophtha.2006.01.035

Yamada, T., & Ukai, K. (1997). Amount of defocus is not used as an error signal in the control system of accommodation dynamics. *Ophthalmic and Physiological Optics*, *17*(1), 55–60. https://doi.org/10.1016/S0275-5408(96)00021-X

Yanoff, M., & Sassani, J. W. (2018). *Ocular pathology*. Elsevier Health Sciences.

Yaraş, F., Kang, H., & Onural, L. (2010). State of the Art in Holographic Displays: A Survey. *Journal of Display Technology*, *6*(10), 443–454. https://doi.org/10.1109/JDT.2010.2045734

Young, T. (1801). II. The Bakerian Lecture. On the mechanism of the eye. *Philosophical Transactions of the Royal Society of London*, *91*, 23–88.

List of figures

List of tables